Universitat de Lleida

Escola Politècnica Superior

Màster en Ciències Aplicades a l'Enginyeria

Treball de final de màster

Compact thermal storage: A-state-of-the-art review of experimental results

Autor/a: Jaume Cot Gores
Director/s: Dr. Albert Castell Casol
Dr. Luisa F. Cabeza
Setembre 2011

Contents

List of Tables

List of Figures

1 Introduction

The increased demand for energy, the rise in the price of fuel associated with the depletion of fossil fuels, and the growth of CO_2 emissions all require the development of more energy-efficient processes and a shift from non-renewable energy sources to renewable energy sources. In this sense, thermal energy storage (TES) can increase the thermal energy efficiency of a process by reusing the waste heat from industrial processes, solar energy or other sources. Furthermore, considering that in 2004 the heating and cooling demands of the industrial, commercial and domestic sector accounted for between 40-50 % of the total global 320 EJ (7,639 Mtoe[1]) final energy demand [1], TES could contribute to substantial energy savings and a reduction in CO_2 emissions [2].

Heat is the form of energy most widely used in industry and power plants for driving the processes or producing electricity, either through steam or in fired furnaces. As a consequence of the work produced, most of this heat is degraded to a lower level and is released to the environment through cooling water, cooling towers, flue gases or other means. This waste heat is left unused due to its relatively low grade. Thermal energy storage not only allows the waste heat to be re-used, it also allows the heat to be upgraded by means of a chemical heat pump. Furthermore, when the thermal demand is located at a distance from the supply, this heat could be transported.

Even in the transport sector, TES can be used to recover the waste heat lost through the radiator or the exhaust. In both cases, the waste heat accounts for less than 30 % of the fuel energy [3]. In fact, only 20 % of fuel energy is used to power the vehicle, (see Figure 1.1). Therefore, recovering this heat and reusing it for heating or cooling applications would significantly increase the efficiency of the process.

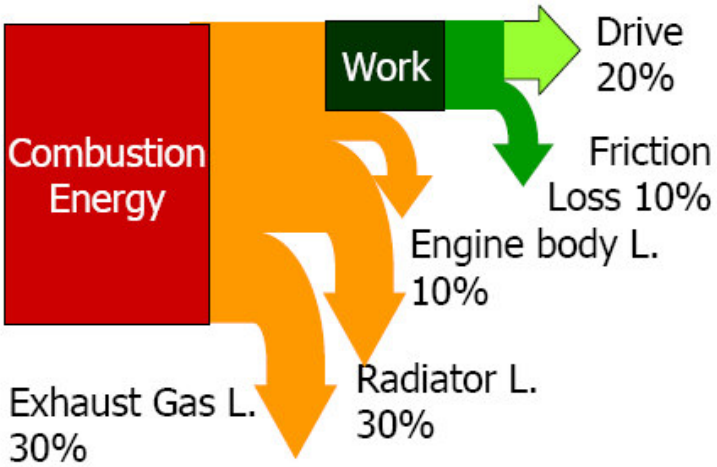

Figure 1.1: Automobile waste heat potential – 20 % of the fuel energy used to drive the vehicle [3].

TES may also be able to increase the potential of solar energy. TES can be used to eliminate the time gap between energy supply and energy demand. This is between seasons, between day-time and night-time or even between sunny and cloudy days. For instance, for space heating and domestic hot water in households and offices, the surplus of energy generated during the summer period could be stored and used in the winter, when the demand exceeds the solar supply, see Figure 1.2, or, in a solar power plant, the surplus of thermal energy generated during the day could be stored and used at night or on cloudy days to produce electricity.

[1] Million tonnes of oil equivalent

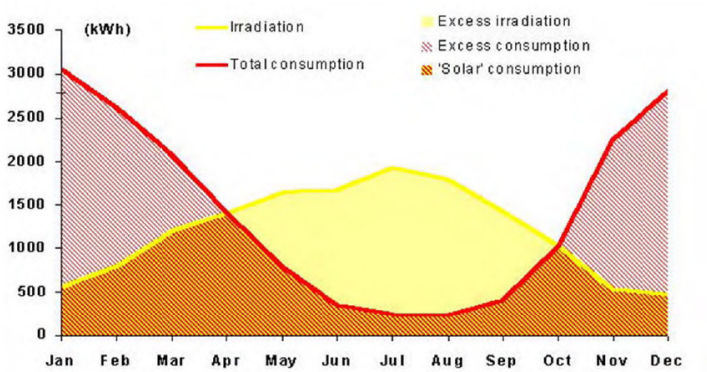

Figure 1.2: Annual energy demand – Excess of solar heat in summer months, deficit in winter months [4].

1.1 Types of Thermal Energy Storage

Thermal energy can be stored by sensible heat, by latent heat, by sorption process or by chemical reaction.

1.1.1 Sensible Heat

In sensible heat storage, heat is stored by increasing the temperature of the material such as water, rock, sand and molten salts. The storage density is related to the product of the specific heat of the material and the temperature change [5].

The research on thermal energy storage by sensible heat is mainly focused in the built environment and in solar power plants.

1.1.1.1 Built environment

Traditionally, water is used in households for storing solar heat for short periods of time. However, for a longer period (seasonal heat storage), the storage tank is too large to be placed inside a single family house. A roughly estimation of this volume for a low-energy house in mid-Europe, would require a water tank of 34 m^3 to meet the heating demand in the winter period (10 GJ[2]) [6], see Figure 1.3. Therefore, this type of storage technique can then only be economical if applied on a large scale (> 100 houses) [5,7].

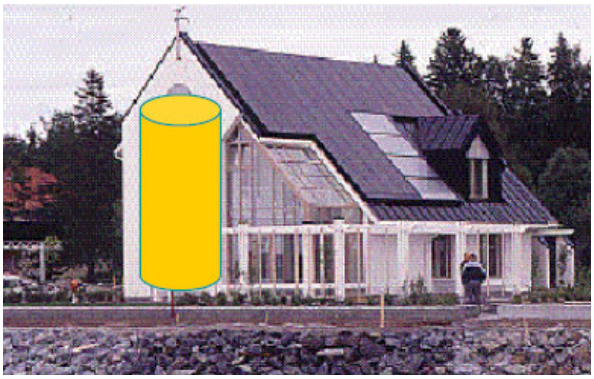

Figure 1.3: Hypothetical size of storage tank for low-energy house [8].

[2] Heat to be stored 1850 kWh + 25 % unavoidable heat losses = 10 GJ $\Rightarrow$ 34 m^3 water at ΔT = 70 ºC.

There are four main technologies for large-scale seasonal thermal storage, which have been developed, tested and monitored over recent decades [9] see Figure 1.4. Background information on those technologies as well as the existing demonstration plants can be found elsewhere [5,9-12]; however, a brief description is given now.

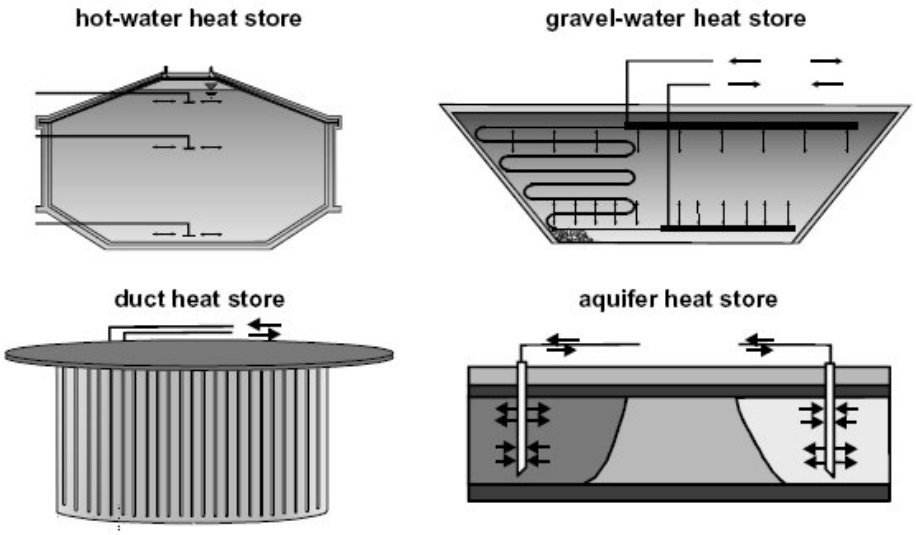

Figure 1.4: Four main technologies for seasonal heat storage by means of sensible heat [10].

The decision to use a certain technology mainly depends on the local conditions and, primarily, on the geological and hydro-geological situation in the ground below the respective construction site [10].

Hot-water heat storage

Hot-water tanks have the most widespread use. Because of the high specific heat of water and the high capacity rates for charging and discharging, it is the most favourable of the four storage types from the thermodynamic point of view [10]. Furthermore, the storage efficiency of the tank can be improved by ensuring optimum stratification [5,6].

Water tanks are usually made of reinforced concrete and are partially embedded in the ground. The roof and the walls of the tanks are heat insulated, see Figure 1.5.

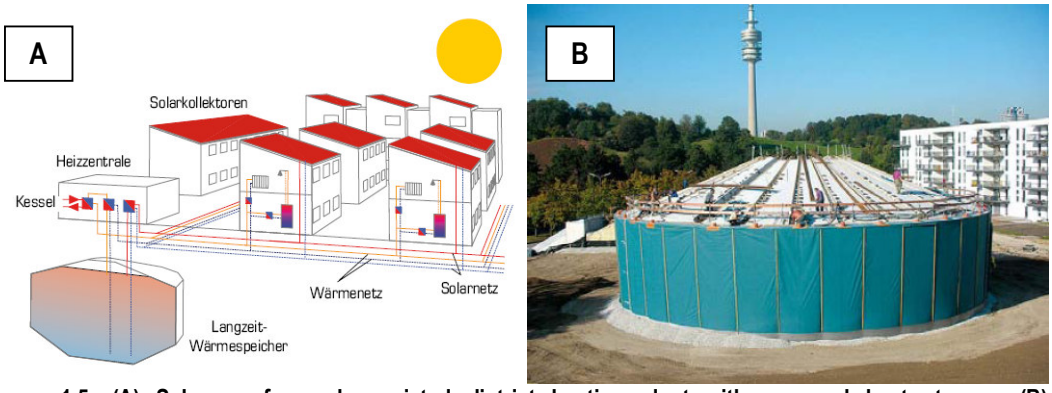

Figure 1.5: (A) Scheme of a solar-assisted district heating plant with seasonal heat storage. (B) Demonstration plant in Munich, 5700 m³, 2007 [13].

To avoid water vapour transfer through the concrete wall, and thus also protect the insulation from moisture and to reduce heat losses, an inner stainless steel liner is added to the wall. Over the last few years, fibreglass-reinforced plastic has been studied as an alternative to concrete to reduce the specific costs [10].

Gravel/water heat store

Gravel/water heat store is simply a pit with a watertight plastic liner which separates the storage material from the surrounding soil. The storage material is usually a mixture of gravel and water, but also sand and water, soil and water, or even layer combinations with these mixtures, see Figure 1.6. Heat is charged into and discharged out of the store either by direct water exchange or by plastic pipes installed in different layers inside the store [10]. Side-walls and roof are normally heat insulated.

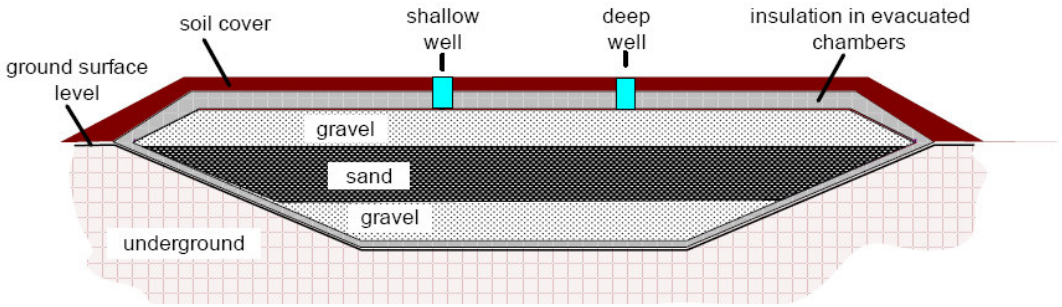

Figure 1.6: Newest generation of gravel/water TES in Eggenstein [14].

This technology appears as an alternative to reduce the construction costs of water tanks. However, since gravel/water mixtures have a lower specific heat capacity than water alone, the volume of the store has to be approximately 50% higher than a hot-water store to obtain the same heat capacity for the whole store.

Duct heat store or borehole storage

Duct heat store consists of vertical heat exchangers installed inside a borehole, which ensures the transfer of thermal energy to and from the ground (clay, sand or rock). There are several types of heat exchanger and they are normally installed at a depth of between 30 and 100 meters, see Figure 1.7.

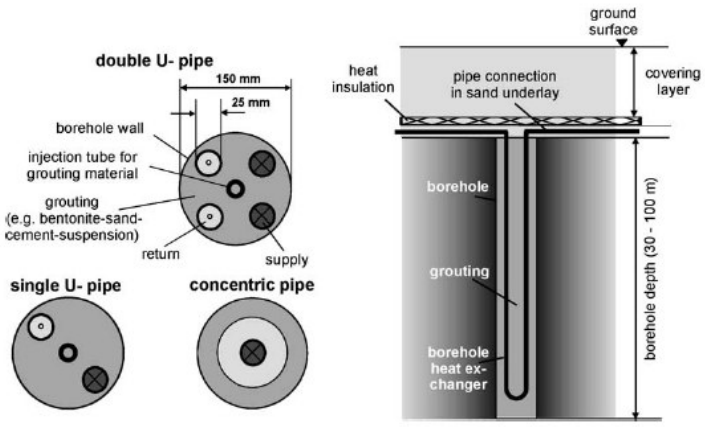

Figure 1.7: Types of borehole heat exchangers (left side) and sample installation [10].

A duct store requires less effort for construction than hot water or gravel-water heat stores, and it allows for modular design. Additional boreholes can be connected easily and the store can grow with e.g. the size of a housing district. However, the size of a duct store has to be between three to five times higher than that of a hot-water store to provide the same heat capacity. Besides, an additional buffer store is often required due to the lower capacity for charging and discharging [10].

Aquifer heat store

An aquifer heat store uses water-saturated and permeable underground layers as storage medium. Thermal energy is transferred by extracting groundwater from the cold well and by re-injecting it into the hot well when it has been heated, see Figure 1.8.

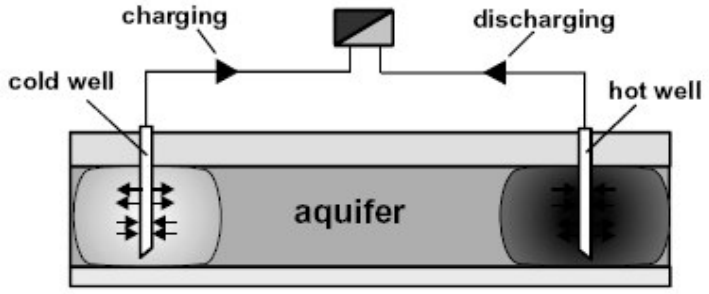

Figure 1.8: Scheme of an aquifer heat store [10].

A typical aquifer heat store works in the temperature range of 10 - 40 ºC. Storing at higher temperatures (e.g., up to about 150 ºC) was shown to cause many problems in experimental and pilot plants in the 1980s [5].

1.1.1.2 Solar Power Plants

As mentioned in the introduction, TES can be beneficial in a solar concentrator plant to store the excess solar energy generated during the daytime and use it at night or on cloudy days. This is the case of the current solar plant Andasol [15,16], installed in the province of Granada, Spain, see Figure 1.9.

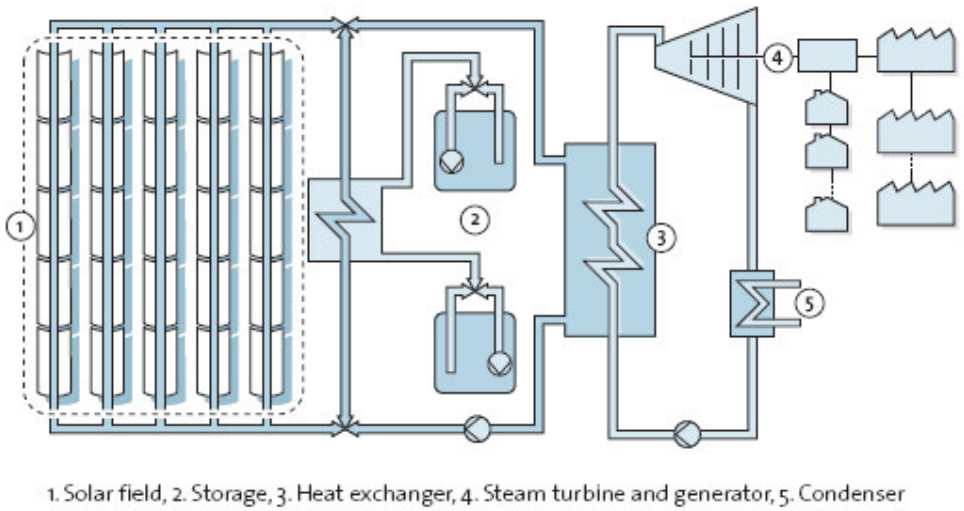

1. Solar field, 2. Storage, 3. Heat exchanger, 4. Steam turbine and generator, 5. Condenser

Figure 1.9: Scheme of the solar thermal power plant, Andasol [15].

The plant uses a mixture of molten salts ($NaNO_3$ and KNO_3) as heat storage medium. This salt mixture is kept as a liquid in a cold storage tank at approximately 290 ºC. When the heat supply exceeds the demand, the salt is heated to 390 ºC and pumped to a hot storage tank. Heat stored can then provide the necessary heat to operate the plant at night or during overcast periods.

1.1.2 Latent heat

Another means of storing energy is by using phase change materials (PCM) or latent heat materials. When the PCM undergoes the phase change, it absorbs or releases a large amount of energy as latent heat. In fact, the energy density in the form of latent heat is much larger than in the form of sensible heat, which means lower volumes of materials need to be used. The phase change could be solid/liquid or liquid/gas: however, liquid/gas changes are not practical due to the large volume changes or high pressures required to store the materials in the gas phase.

Initially, the solid-liquid PCM behaves like sensible heat storage, i.e. heat is stored by raising the temperature of the material. When the temperature reaches the phase change the process becomes isothermal until all the material is transformed to the liquid phase. This makes latent heat especially useful for applications which operate in a narrow temperature range.

There are different classes of phase change materials involving inorganic and organic substances (Figure 1.10). Common substances are salts, hydrates, paraffins and fatty acids. A complete review of these materials and their properties can be found in Abhat [17], Lane [18,19], Kenisarin [20], Dinçer and Rosen [5], Zalba et al. [21], Farid [22], and Tyagi and Buddhi [23]. Based on these references among others, a full inventory of PCMs is given in Cabeza et al. [24] and H. Mehling and Cabeza, [25]. More recent reviews have been carried out by Cabeza et al. [26] and Gil et al. [27].

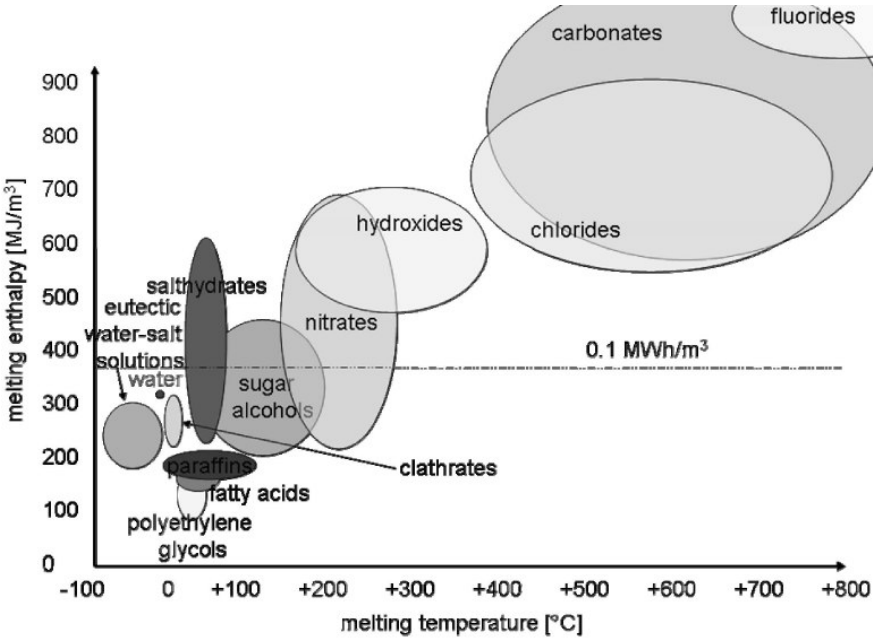

Figure 1.10: Classes of phase change materials at different temperature ranges [25].

The main advantages and disadvantages of organic and inorganic PCMs are reported in Table 1.1, [21].

Table 1.1: Comparison of organic and inorganic material for heat storage [21].

Organics	Inorganics
Advantages	Advantages
Non corrosives	Greater phase change enthalpy
Little or none undercooling	
Chemical and thermal stability	
Disadvantages	Disadvantages
Lower phase change enthalpy	Undercooling
Low thermal conductivity	Corrosion
Inflammability	Phase separation
	Phase segregation, lack of thermal stability

So far the most studied and developed technology using PCMs is the incorporation of these materials into the building components such as walls, roofs and floors [21,28]. By incorporating the PCM into the building material, the thermal inertia (thermal mass) of the building material can be increased, thereby smoothing the temperature fluctuations and reducing the heating and cooling demands. Other successful applications of PCM are reported in Zalba et al. [21]. However, its uses as TES like replacing water tanks or in solar plants is still being investigated and no large demonstration plant has been built [16,27]. In addition, the cost of these PCM systems is substantially higher than the cost of sensible heat systems. Moreover, the long term stability of these materials is another important aspect for their application.

1.1.3 Sorption processes

1.1.3.1 Definition

In sorption processes heat is not stored directly as sensible or latent heat but by way of a reversible physical or chemical process. Figure 1.11 shows a schematic overview of the working principle.

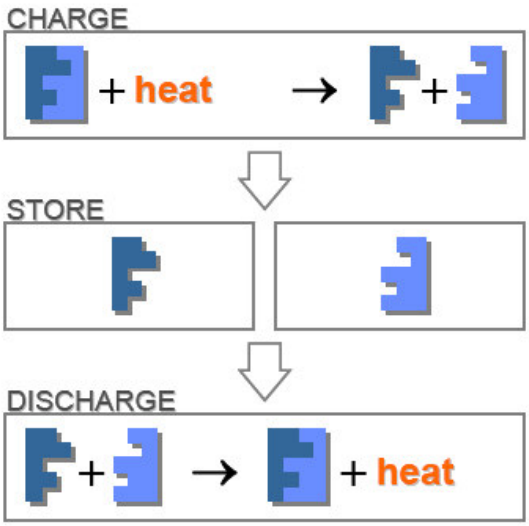

Figure 1.11: Working principle of a thermal storage system based on sorption process [29].

During the charging mode, heat is supplied and the thermochemical material dissociates into two components, which can be stored separately at ambient temperature. In the reverse step of storage

discharge, the two components are associated to form the original thermochemical material, thus releasing the stored heat.

Materials used in sorption storage have a much higher energy density than phase change materials or sensible heat materials. However, the relevance of storage systems based on sorption phenomena lies not only in their high energy density, but also in their negligible thermal loss, since as long as the two components are stored separately no reaction will occur. Therefore, it allows for effective long-term heat storage or even for heat transportation.

Storage systems based on sorption phenomena can be divided into open and closed systems, see Figure 1.12. On the one hand, in open systems the gaseous working fluid is directly released to the environment and thereby the entropy is released; therefore only water is a possible candidate as working fluid. On the other hand, in closed systems, not the working fluid itself but the entropy is released to the environment via a heat exchanger (condensation) [6]. An advantage of a closed system is that it can be used as a chemical heat pump for heating and cooling applications, or it can even be used to upgrade waste heat (e.g. industrial process) when it acts as a heat transformer (chemical heat pump) [30-39].

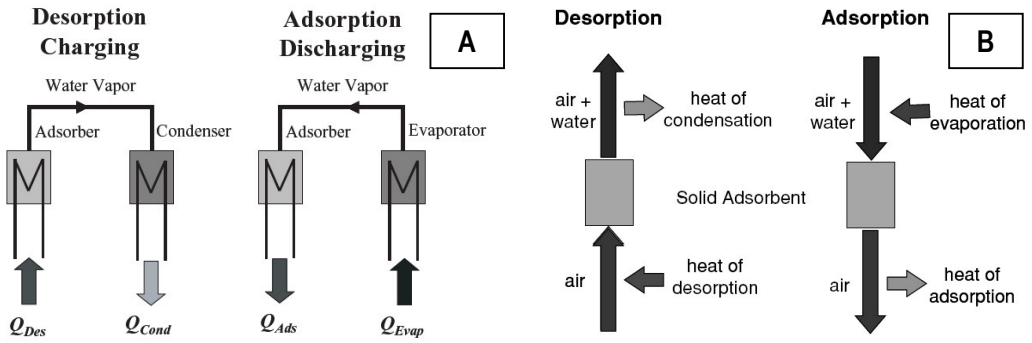

Figure 1.12: (A) Closed sorption system. (B) Open sorption storage system using a packed bed of solid adsorbent [40].

The sorption process can be carried out with adsorption, absorption, and composite materials.

1.1.3.2 Adsorption process

Adsorption means the binding of a gaseous or liquid phase of a component on the inner surface of a porous material [40]. Depending on the nature of the bonding the process is classified as physisorption or chemisorption. The former involves only relative weak intermolecular forces (van der Waals forces) whereas the latter involves, essentially, the formation of a chemical bond between the sorbate molecule and the surface of the adsorbent. Although chemisorption has a higher heat of sorption than physisorption, the former may be irreversible [41].

Physisorption

In physisorption, the most common classes of solid adsorbents are zeolites, silicagels and activated carbon. These materials are products of large-tonnage production (mainly for the needs of the chemical industry), and therefore, they are available, cheap, well-studied, and non-toxic [35]. The main difference between these materials is the way they are built. Silicagels and activated carbon have a micropore size distribution whereas zeolites have a crystalline structure and there is virtually no distribution of pore size [41]. A detailed description of these and other adsorbents is given by Dąbrowski [42]. The most important property affecting the application of these adsorbents as thermal energy storages media is the amount of water that can be adsorbed [40].

As adsorbates, water, ammonia and methanol are generally used. The main advantages of water are its high heat of vaporization, it is non-toxic and environmentally friendly, and its disadvantages are the low water pressure and the high freezing point. Ammonia has a low freezing point and a high pressure, but lower heat of vaporization than water. Finally, methanol is characterized by intermediate values of these characteristics [35].

Adsorption heat pumps have been widely studied for heating and cooling applications, and most of these studies are discussed in reviews [30-39]. However, until recently only adsorption water chillers have become commercially available [35]. The main problems so far are the poor heat and mass transfer in the solid adsorbent, and the low thermal conductivity of the absorbent. These problems lead to low COP (coefficient of performance) and to a reduced energy density of the absorbent. Besides, vacuum leakages, deterioration of the adsorbent, and cycle times are also problems to be solved [36].

For long-term heat storage, the most studied working pairs are zeolite-water and silicagel-water. Several international research programmes have been carried out in the last 10 years to show the feasibility and the relevance of long-term energy storage (solar energy in particular) by adsorption, [6,40,43]:

- HYDES (High Energy Density Sorption Heat Storage for Solar Space Heating) from 1998 to 2001.
- MODESTORE (modular high energy density heat storage) from 2003 to 2007.
- Monosorp (a seasonal adsorption storage integrated to a building ventilation system) from 2003 to 2007.

The demonstration projects showed the technical feasibility of the proposed systems. However, the current materials are a limitation for the processes studied. Silicagels can not reach the entire theoretical adsorption capacity (< 20 %), and so the energy density of the material is reduced considerably. Zeolite, on the other hand, requires a high desorption temperature (180 ºC), which makes the use of solar heat difficult with this material [40,43-45].

In the last few years, new classes of adsorbents have been developed with a high capacity for water uptake, such as aluminaphosphate (ALPO), silica-aluminaphosphate (SAPO) and metal organic framework (MOF). However, most of these novel materials are too expensive, especially for long-term storage [46].

Chemisorption

Over the last few decades, the formation of metal hydrides by the combination of hydrogen and metal or metal alloy has gained importance not only for hydrogen storage but also for effective utilization and storage of industrial waste heat and solar energy. Since the process involves chemisorption, the energy density of metal hydrides is much greater than that of the previous adsorbents. In addition, the condensation of hydrogen is so low that the conventional heat exchanger-reactor configuration cannot be realized [34]. Therefore, there are usually two metal hydride reactors connected with the heat and cold sources, instead of a reactor and evaporator/condenser as in the conventional systems.

The common metal hydrides used are AB_5, AB, A_2B type of alloys with the major compounds of La, Lm or Ni, or with part of the Ni replaced by Al, Mn, Cu, etc. For high-temperature applications the elemental metal hydride MgH_2 (usually Ni doped) is a good candidate [47]. An important advantage of metal hydrides is that the properties of the alloys can be modified by changing the alloy composition. Therefore, a large number of metal hydrides can be synthesized to meet the requirements of specific applications.

The first heat storage system using metal hydride was proposed and patented by Winshe [48] at the Atomic energy commission (USA) in 1970. The storage system aimed to produce high energy steam

power from a low energy isotope source using MgCu as the high-temperature hydride and Ti_2Fe as the low-temperature hydride. During the charging period, the low energy isotope source was used for desorbing hydrogen from the MgCu while heat was released from the low-temperature reactor to allow absorbing the hydrogen onto Ti_2Fe. On the other hand, during the discharging period, hydrogen is desorbed from the Ti_2Fe and absorbed onto MgCu and the heat of absorption is used to produce steam at high-temperature. In 1975, Gruen and Sheft [49] proposed a double metal hydride heat pump system sing solar heat or any other appropriate energy source for space heating and cooling, refrigeration and power production. Also, a concept of a double metal hydride heat pump was patented by Terry [50] in 1977. However, was from this year when Gruen [51,52] built the first demonstration unit named Argonne HYCSOS at the Argonne National Laboratory (USA) which was then first tested using the $CaNi_5$ (high-temperature hydride) and $LiNi_5$ (low-temperature hydride). The HYCSOS was further tested with other metal hydrides in accordance with Sheft et al. [53].

During the 80th, the experimental research on thermally-driven heat pump under practical conditions gained much attention. Especially in Japan, several projects were carried out to demonstrate the feasibilities of such system. Most of this research in Japan is reviewed by Suda [54]. Besides Japan, a further review at world scale and extended until 2002 was carried out by Murphy [55].

Recently, Muthukumar and Groll [47] carried out an extensively review on the research of metal hydrides heat pumps for thermal applications. The review has a detailed explanation on the research for selecting metal hydride alloys, for improving heat and mass transfer of the metal hydride beds by the formation of composite materials as well as the research on the performance of thermally-driven and compressor-driven metal hydrides heat pumps based on theoretical analysis, models, simulations and experiments.

Based on the previous review [47] as the starting point the experimental research on thermally-driven heat pump under practical conditions over the last two decades is summarized in Table 1.2.

Table 1.2: State of the art on the experimental research of thermally-driven metal hydride heat pumps (1990-2011). Based on Muthukumar and Groll et al. [47] and updated.

Korea Advanced Institute of Science and Technology (Korea)		
Lee et al. [56]	$Zr_{0.9}Ti_{0.1}Cr_{0.9}Fe_{1.1}$/ $Zr_{0.9}$ $Ti_{0.1}Cr_{0.6}Fe_{1.4}$	1993
New Material Research Center & Sanyo Electric Co. (Japan)		
Imoto et al. [57]	$LaNi_{4.6}Mn_{0.3}Al_{0.1}$/ $La_{0.6}Y_{0.4}Ni_{4.8}Mn_{0.2}$	1995
Indian Institute of Technology (India)		
Ram Gopal and Srinivasa Murthy [58]	ZrMnFe / $MmNi_{4.5}Al_{0.5}$	1999
Air Conditioning and Environmental Control Lab. (Korea)		
Kang et al. [59]	$LaNi_{4.7}Al_{0.3}$ / $MmNi_{4.15}Fe_{0.85}$	1996
State Research Institute of Scientific and Industrial Association 'Lutch' (Russia)		
Chernikov et al [60]	$MmNi_{4.15}Fe_{0.85}$ / $LaNi_{4.6}Al_{0.4}$	2002
(IKE), University of Stuttgart (Germany)		
Klein et al. [61,62]	$LmNi_{4.91}Sn_{0.15}$ / $LaNi_{4.1}Al_{0.52}Mn_{0.38}$ / $Ti_{0.99}Zr_{0.01}V_{0.43}Fe_{0.09}Cr_{0.05}Mn_{1.5}$	2001
Linder et al. [63]	$LmNi_{4.91}Sn_{0.15}$ / $Ti_{0.99}Zr_{0.01}V_{0.43}Fe_{0.09}Cr_{0.05}Mn_{1.5}$	2010
Willers and Groll [64]	$LmNi_{4.85}Sn_{0.15}$ + $LmNi_{4.49}Co_{0.1}Mn_{0.205}Al_{0.205}$ + $LmNi_{4.08}Co_{0.2}Mn_{0.62}Al_{0.1}$	1999
Willers et al. [65,66]	Several hydrides	1999
Trane Air Conditioning and Shanghai Maritime University		
Ni and Liu [67]	$LaNi_{4.61}Mn_{0.26}Al_{0.13}$ / $La_{0.6}Y_{0.4}Ni_{4.8}Mn_{0.2}$	2006
Shanghai Jiatong University, Chinese Academy of Sciences and Zhejiang Yinlun Machinery Co. Ltd. (Japan)		
Qin et al. [68]	$LaNi_{4.61}Mn_{0.26}Al_{0.13}$ / $La_{0.6}Y_{0.4}Ni_{4.8}Mn_{0.2}$	2007

1.1.3.3 Absorption process

Absorption is a process in which atoms, molecules, or ions enter the bulk of a solid or liquid. In contrast to the surface phenomenon of adsorption, one substance penetrates into the inner structure of the other [42,69].

Generally, absorption heat storage is based on solid-gas and liquid-gas phase systems but some three-phase systems have also been studied.

Liquid-vapor absorption

The use of liquid-gas absorption as heat pump is a well developed technology that has been introduced to the market, especially for cooling and refrigeration applications. The working pairs used are ammonia-water and lithium bromide-water [33]. For the purposes of thermal energy storage, however, research is still being carried out to find an optimum working pair. Some projects have attempted to demonstrate the feasibility and potential of liquid-vapor absorption processes for long-term solar heat storage [70-72].

At EMPA (Swiss Federal Laboratories for Materials Testing and Research), Weber and Dorer [70] developed a prototype based on the absorption of water by sodium hydroxide solution (caustic soda, NaOH) to fulfill the heating demand with 100 % solar fraction in a low-energy family house. The results showed that the heat capacity compared to a water storage system is about 3 times better for domestic hot water and about 6 times better for space heating. As the next step, EMPA plans to build a double-stage system.

ZAE Bayern [71] developed a solar-driven liquid desiccant based on a concentrated lithium chloride salt solution ($LiCl$-H_2O) for cooling and dehumidification of the air in an office building in Germany (5700 m^2). The system was designed for a total air conditioning capacity of 150 kW (80 kW cooling demand and 70 kW dehumidification demand), requiring 10 m^3 of desiccant solution. An important drawback of LiCl is the high cost of the salt, about 3600 €/m^3.

Finally, at the University of Minnesota, Quinell et al. [72] aimed to develop a prototype based on a concentrated solution of calcium chloride salt ($CaCl_2$-H_2O) for space heating. The material density of this system is more than double that of sensible storage with water.

Absorption solid-liquid-vapor

The energy density of the salt solution can be increased by allowing the solution to reach the crystallization point. On the other hand, however, the complexity of the system is also increased.

ClimateWell developed a TCA (Thermo-Chemical Accumulator) based on LiCl solution, which has been commercialized. The storage density for the store is roughly 5 times greater than for water for cold whereas it is only 1.5 times greater for heat [73].

PROSSIS (*PROcédé de Stockage Solaire Inter Saisonnier*) is a project coordinated by the LOCIE (*Laboratoire Optimisation de la Conception et Ingénierie de l'Environnement*, Chambéry) in France and the *Université de Savoie* which aims to develop a prototype based on $LiBr$-H_2O solution for house heating. The couple $LiBr$-H_2O was chosen after some static simulation on some potential working pairs. The next step is to develop a detailed model for a dynamic simulation and to carry out experiments in a prototype, N'Tsoukpoe et al. [43,74,75], Hui et al. [76] and Pierrès et al. [77]. Further research is also aimed to identify new working pairs based on static calculations, Hui et al. [78].

Solid-gas absorption

Over the last few years, a lot of research has been carried out on absorption solid-gas processes as a very promising system for effective utilization and storage of industrial waste heat and solar energy. It provides high energy density, greater than liquid-gas absorption, and a wide range of working temperatures (low temperature < 100ºC, and middle temperature 100 to 400 ºC). Although it is expected to have more promising prospects in the future, more efforts are needed today to solve many theoretical and practical problems such as complicated chemical kinetics, safety and low system efficiency [34]. One of the major problems with salt hydrates is the swelling (or changing of volume) and agglomeration, which are critical to heat and mass transfer [79-82].

The research on solid-gas absorptions has been mainly focused on hydration and ammoniation of solid salts (alkaline, alkaline-earth or metallic nitrates, sulfates, sulfides, chlorides, etc). Over the last decade, the hydration process has been intensively studied for long-term storage of solar heat in the built environment. At ECN (Netherlands), Visscher et al. [83] examined theoretically a large number of materials, including salt hydrates, and identified magnesium sulfate heptahydrate ($MgSO_4.7H_2O$) as the most promising material for heat storage, which was then further investigated by Essen et al. [84]. However, with the deepening of the research, other potential candidates were identified such as the hydrates of aluminum sulfate ($Al_2(SO_4)_3.18H_2O$) and, calcium and magnesium chlorides ($CaCl_2.6H_2O$ and $MgCl_2.7H_2O$), the last being the most suitable material, Essen el at. [85] and Zondag et al. [77]. $MgSO_4.7H_2O$ was also investigated by Bertsch et al. [78], at ITW (Germany), who also investigated copper sulfate pentahydrate ($CuSO_4.5H_2O$) as heat storage material. At the Virginia Polytechnic Institute and State University (USA), Balasumbramanian et al. [86] modeled a thermochemical energy storage based on the reversible hydration of $MgSO_4$.

The hydration reaction has also been studied for other purposes than only long-term heat storage. Also at ECN, de Boer et al. [87,88] investigated a storage system based on sodium sulfide and water (Na_2S-H_2O) for cooling in buildings and industrial applications. A chemical heat pump based on the reversible hydration of $CaSO_4$ was studied at Chiba University (Japan) by Ogura et al. [89] for heating and cooling applications. In a common project between the Osaka university and the Shinsei Cooling Water System Company, Yoshino et al. [90] carried out a fundamental study on the reversible hydration of $CaCl_2$ to develop a multipurpose chemical heat pumps for cold-heat generation. Later Fujioka et al. [91] proposed a reaction model for the hydration of $CaCl_2$. Finally, there is also some research on reversible hydration reactions of chloride and sulfate salts hosted on different porous matrix (composite materials).

Unlike hydration processes, the systems based on ammoniation processes are designed for use only in industrial applications because of safety considerations. Goetz et al. [92] pointed out that probably chloride salts are probably the most suitable materials for heat transformers or chemical heat pumps. Chen and Tan [93] reached a similar conclusion from their experiments [94]. However, even though most of the studies concern the ammoniation of chloride salts, the current research is mainly focused on improving heat and mass transfer by using composite materials. There are only a few studies concerning to the ammoniation of bulk salts. Trudel et al. [95] studied the equilibrium of the NH_3-$CoCl_2$ system in a chemical heat pump. A double-effect chemical heat pump with $MnCl_2(6/2)NH_3$ and $NiCl_2(6/2)NH_3$ systems was analyzed theoretically by Nevau and Castaing [96]. Fadhel et al. [97] investigated the performance of a solar-assisted heat pump drier using the $CaCl_2(8/2)NH_3$ system under meteorological conditions of Malaysia. Rivera et al. [98] studied a thermo-chemical refrigerator using the $BaCl_2(8/0)NH_3$ system. Finally, Wang et al. [99] investigated the sorption characteristics of various alkaline-earth metal chlorides and composites of $CaCl_2/CaSO_4$ and of $SrCl_2/CaSO_4$.

To overcome the high pressure problem in the ammonia system, other researchers have been recommended methanol (CH_3OH) or methylamine (CH_3NH_2) as alternative working fluid to ammonia because of their lower vapour pressure. The research based on methanol as working fluid was

investigated with $CaCl_2$ at Yantai University (China), by Sun et al [100,101], at Beijing Institute of Chemical Technology, by Lai et al. [94,102] and by Zhang et al. [103], and at Xi'an Jiaotong University, by Song et al. [104]. On the other hand, the research based on methylamine as the working fluid has also been investigated with composites materials, as in the case of ammonia.

1.1.3.4 Composite sorbent materials

Composite materials are mainly aimed to improve heat and mass transfer of the absorption solid materials. These materials are made up by the combination of a salt hydrate (absorbent) and an additive with a porous structure and high thermal conductivity, which may or may not be an adsorbent, such as expanded graphite, metal foam, activated carbon or activated carbon fiber [31-39]. For instance the thermal conductivity of calcium chloride is only 0.1-0.5 W/(m ºC); but that of a consolidated composite with 20 % of expanded graphite is 7.1-9.2 $W \cdot m^{-1}K^{-1}$ [105], and if it is impregnated with 30 % expanded graphite the conductivity is 11.1-15.2 $W \cdot m^{-1}K^{-1}$ [106]. Also zeolites and silicagels can be mixed with expanded graphite and metallic foams to increase their conductivity (circa 0.09 $Wm^{-1}K^{-1}$). In addition, composite materials are also used, such as the combination of a salt hydrate and an adsorbent with poor thermal conductivity like zeolites or silicagels. However, in that case the aim is to increase the sorption capacity of the adsorbent. Therefore, the aim of composite materials can be understood in two ways. On the one hand, to increase the heat and mass transfer of the salt hydrate, and on the other hand, to increase the sorption capacity of adsorbents.

The composite of chloride or bromide salts with expanded graphite has been studied the most. In 1986, Coste et al. [107] patented the first method of combining chloride salt with expanded graphite, which was further developed and named the IMPEX method, in 1994, by Mauran et al. [108] and, in 1999, by Bou et al. [109]. Over the last two decades, several methods and preparation procedures for manufacturing composite materials of chloride salts with expanded graphite were developed as well as new composite materials of chloride salts with other host matrixs such activated carbon, carbon fibers, vermiculite, y-alummina and Sibunit. In general, the methods used to produce composites materials are: simple mixture, impregnation, or mixture or impregnation and consolidation. The studies based on the manufacture of composite materials have been summarized in Table 1.3. In addition, Table 1.3 includes studies concerning to the characterization and properties of some composite materials

Table 1.3: Research on the manufacturing, characterization and properties of the composite materials over the last two decades.

Societe Nationale Elf Aquitaine (France)			
Chloride salts	Expanded graphite	-	Coste et al. [107] Mauran et al. [108] and Bou et al. [109]
CNRS (France)			
$MnCl_2$	Expanded graphite	NH_3	Mauran et al. [81], Olives et al. [110]
$CaCl_2$	Expanded graphite	CH_3NH_2	Mauran et al. [81]
$MnCl_2$	Carbon fibers	NH_3	Dellero et al. [111,112]
Shangai Jiao University (China)			
$CaCl_2$	Expanded graphite	NH_3	Oliveira et al [113,114], K. Wank et al. [115], S.L. Li et al. [116,117]
$MnCl_2$	Expanded graphite	NH_3	T.X. Li et al. [118]
$SrCl_2$	Expanded graphite	NH_3	Zhang et al. [119]
$CaCl_2$	Activated carbon	NH_3	L.W. Wang et al. [120,121]
Phohang University of Science and Technology and, Seoul National University (South Korea)			
$CaCl_2$, $MnCl_2$, $BaCl_2$	Expanded graphite	NH_3	Han and Lee [106,122], Han et al. [123]
ECN (Netherlands)			
$MgCl_2$ + LiCl	Metal foam	NH_3	Haije et al. [124]

CanmetENERGY (Canada)			
$CoCl_2$	Activated carbon	NH_3	Aidoun and Ternan [125]
Borestov Institute of Catalysis (Russia)			
$BaCl_2$	Vermiculite	NH_3	Zhong et al. [126,127], Sharonov et al. [128], Veselovskaya et al. [129]
$CaCl_2$	Vermiculite	NH_3	Sharonov et al. [130]
$CaCl_2$	γ-Al_2O_3	NH_3	Sharonov et al. [130]
$BaCl_2$	γ-Al_2O_3	NH_3	Veselovskaya et al. [129]
$BaCl_2$	Sibunit	NH_3	Veselovskaya et al. [129]
Luikov Heat & Mass Transfer Institute (Belarus)			
$CaCl_2$, $NiCl_2$, $MnCl_2$	Busofit	NH_3	Vasiliev et al. [131]
Shinsei Cooling Water System Co. and Osaka University (Japan)			
$CaCl_2$	Expanded graphite	CH_3OH	Hirata et al. [132], Fujioka et al. [133]
$CaCl_2$	Active carbon	CH_3OH	Fujioka et al. [133]
$CaCl_2$	Expanded graphite	CH_3NH_2	Fujioka et al. [133-135]
Korea University, Samsung Advanced Institute of Technology and Seonam University (Republic of Korea)			
$MnCl_2$ + $NiCl_2$	Expanded graphite	NH_3	Lee et al. [136]
Wroclaw University of Technology and the Polish Academy of Sciences in Wroclaw (Poland)			
$CaCl_2$	Expanded graphite + active carbon	NH_3	Zajaczkowski et al. [137]
Nanjing University of Technology (China)			
$CaCl_2$	Attapulgite	H_2O	Chen et al. [138]
LiCl	Attapulgite	H_2O	Chen et al. [139]
Bauhaus-University Weimar (Germany)			
$MgSO_4/MgCl_2$	Attapulgite	H_2O	Posern and Kaps [140]

Based on the previous studies, the performance of the composite materials in a chemical heat pump was investigated experimentally and theoretically under practical conditions. Table 1.4 summarizes these experimental, modelling and simulation research carried out over the last two decades

Table 1.4: Experimental, modelling and simulation research on composite materials in chemical heat pumps.

CNRS (France)			
$BaCl_2$ + $MnCl_2$	Expanded graphite	NH_3	Lépinasse et al. [141-143]
$BaCl_2$ + $NiCl_2$	Expanded graphite	NH_3	Goetz et al. [144]
$PbCl_2$ + $MnCl_2$	Expanded graphite	NH_3	Lépinasse et al. [145]
$SrCl_2$ + $CoCl_2$	Expanded graphite	NH_3	Llobet et al. [146]
$SrBr_2$ + $NiCl_2$	Expanded graphite	NH_3	Nevau et al. [147]
$MnCl_2$ + $NiCl_2$	Expanded graphite	NH_3	Wagner et al. [148]
$BaCl_2$	Expanded graphite	NH_3	Le Pierrès et al. [149-152]
$MnCl_2$	Expanded graphite	NH_3	Mazet et al. [153], Mazet and Amouroux [154], Goetz and Marty [155], Nevau and Castaing-Lasvignottes [156], Castaing-Lasvignottes and Nevau [157], Lu et al. [158], Lu and Mazet [159], Stitou et al. [160]
$SrCl_2$, $ZnCl_2$, $MnCl_2$, $FeCl_2$, $MgCl_2$ $NiCl_2$	Expanded graphite	NH_3	Goetz et al. [161]
$CaCl_2$	Expanded graphite	CH_3NH_2	Balat and Spinner [80], Lebrun and Spinner [162], Lebrun [163]
$MnCl_2$	Expanded graphite	H_2O	Stitou et al. [164]
$SrBr_2$	Expanded graphite	H_2O	Lahmidi et al. [165] Mauran et al. [166]
Université Pau Sabatier, CNRS and Université-site de Tarbes (France)			
$MnCl_2$	Expanded graphite	NH_3	Dutour et al. [167]

East China University of Science and Technology and CNRS (France)			
$SrCl_2$	Expanded graphite	NH_3	Huang et al. [168]
Shangai Jiao University (China)			
$BaCl_2 + MnCl_2$	Expanded graphite	NH_3	T.X. Li et al. [169-172]
$MnCl_2 + NH_4Cl_2$	Expanded graphite	NH_3	Bao et al. [173,174] and Xu et al. [175]
NaBr	Expanded graphite	NH_3	Oliveira et al. [176]
$NaBr + MnCl_2$	Expanded graphite	NH_3	Oliveira et al. [176]
$CaCl_2 + MnCl_2$	Expanded graphite	NH_3	C. Wang et al. [177,178], Zhang P. et al. [119]
$CaCl_2$	Expanded graphite	NH_3	Oliveira et al [113,114], S.L. Li et al. [179], Xia et al. [180]
$MnCl_2$	Expanded graphite	NH_3	T.X. Li et al. [118]
LiCl	Expanded graphite	NH_3	Kliplagat et al. [181]
$SrCl_2$	Expanded graphite	NH_3	Chen et al. [182]
$BaCl_2$	Expanded graphite	NH_3	Chen et al. [183]
$CaCl_2$	Activated carbon	NH_3	L.W. Wang et al. [184,185], Lu et al. [186,187] and T.X. Li et al. [188,189]
Phohang University of Science and Technology and, Seoul National University (South Korea)			
$MnCl_2$	Expanded graphite	NH_3	Han and Lee [190]
ECN (Netherlands)			
$MgCl_2 + LiCl$	Metal foam	NH_3	Spoelstra et al. [191] Haije et al. [124], van der Paal et al. [192,193]
University of Ljubljana (Slovenia), Zae Bayern (Germany) and CNRS (France)			
$NiCl_2$	Expanded graphite	NH_3	Cerknenik et al. [194]
CanmetENERGY (Canada)			
$CoCl_2$	Activated carbon	NH_3	Aidoun and Ternan [125,195-197]
$MnCl_2$	Expanded graphite	NH_3	Mbaye et al. [198]
Luikov Heat & Mass Transfer Institute (Belarus)			
$CaCl_2$, $NiCl_2$ and $MnCl_2$	Busofit	NH_3	Vasiliev et al. [131,199-202], Aristov et al. [203]
Borestov Institute of Catalysis (Russia)			
$BaCl_2$	Vermiculite	NH_3	Veselovskaya et al. [204,205]

Finally, most of the research based on composite materials using zeolites and silicagels is well discussed in reviews [30-39] and in other papers [4,206].

1.1.4 Chemical reactions

Heat can also be stored by means of a reversible thermo-chemical reaction. The working principle is similar to that of the sorption process:

$A + HEAT \Leftrightarrow B + C$

First, in the charging period, chemical A is transformed into two new chemicals, B and C, because of heat absorption (endothermic reaction). Subsequently, the two new chemicals must be stored in separate vessels at ambient temperature. Second, in the discharging period, chemical B reacts with chemical C to form the original chemical A while releasing the stored heat (exothermic reaction).

The energy of thermo-chemical reactions is the highest of all the systems discussed here, and so it is the most compact way to store thermal energy. In addition, chemical reactions extend the temperature range for heat storage, allowing us to store high grade heat (>400 ºC) besides low and medium grade heat. Therefore it allows for important energy savings as the waste heat lost from many industrial applications and power plants is medium and high grade heat [207].

Research has mainly focused in solid-vapour and liquid-vapour reactions, however there is also some research on gas reactions, on solid-liquid reactions and on solid-liquid-vapour reactions.

Solid-gas reactions

Over the last two decades, much of the research on chemical heat pump based on solid-vapour reactions has been conducted in Japan. So far, the reactions studied the most are reversible hydration of magnesium oxide (MgO) and of calcium oxide (CaO) and the reversible carbonation of CaO and of lead (II) oxide (PbO). However, the first studies were discussed by Ervin [208] in 1977 with the reaction of magnesium oxide and calcium oxide with water, which was also pointed out in 1981 by Kanzawa et al. [209]. The reaction of CaO with carbon dioxide was also proposed by Baker et al. [210] in 1973.

At the Tokyo Institute of Technology (Tokyo Tech., Japan), the system $MgO/H_2O/Mg(OH)_2$ was widely studied by Kato et al. [211-222], Ryu et al. [223] and Kim et al. [224] to recover waste heat from the exhaust gas of combustion engines (gas and diesel) such as cogeneration systems, vehicles, fuel cells, micro-gas turbines, etc. Besides this, a twin chemical reaction type of heat pump using CaO/CO_2 and PbO/CO_2 was proposed and studied by Kato et al. [225-228] to store the heat output from a high temperature gas-reactor.

The system $CaO/H_2O/Ca(OH)_2$ was studied at the Tokyo Institute of Technology (Tokyo Tech., Japan) in cooperation with the Kyushu Institute of Technology (Kyutech, Japan) by Ogura et al. [229-246] for effective thermal energy utilization in domestic use and industrial use such as electric power or drying. In addition, Fujimoto et al. [247,248] modelled and simulated the $CaO/H_2O/Ca(OH)_2$ heat pump at the Ecole Polytechnique (Canada) in cooperation with the Kyutech. The same type of system was also modelled and simulated by Schaube et al. [249] at the German Aerospace Centre (DLR, Germany), who also simulated the $CaO/CO_2/CaCO_3$ heat pump. The studies on the reversible hydration of CaO were also carried out at the National Institute of Advanced Industrial Science and Technology (AIST, Japan) by Lin et al. [250,251] to supply or transport heat and at the Nottingham Trent University by Darkwa [252,253] for energy reduction from automobile engines during cold starting. Cerkvenik et al. [254-256] studied the $Ca(OH)_2/H_2O/CaO$ heat pump for refrigeration applications in a common project between the university of Ljublijana (Slovenia), ZAE Bayern (Germany) and the Tokyo Institute of Technology (Japan). Finally, Fujii et al. [257] investigated the behaviour during the dehydration experiments of pellets of pure and sopped $Ca(OH)_2$ to be used in chemical heat pump for solar heat storage.

Furthermore, the reversible reaction of BaO with CO_2 was studied by Kubota et al. [258] at the Magoya University (Japan) to store and upgrade the heat output from a high temperature gas-reactor.

Liquid-gas reactions

So far, liquid-vapour reactions are related to organic substances. Several reversible hydrogenation reactions were proposed during the 1980s, mainly to recover low-grade heat from industrial process. Prevost and Bugarel [259] proposed the system acetone/2-propanol/hydrogen in 1981, which was further studied by Kato and Kameyama [260], Saito et al. [261], and recently by KlinSoda and Piumsomboom [262]. In 1982, Shinji et al. [243] proposed the system benzene/cyclohexane/hydrogen and, finally, in 1984, Tanisho et al. [263] proposed the system acetaldehyde/ethanol/hydrogen, which was further studied by Wakao et al. [244] (middle-grade heat recovery) and Fahim et al. [264]. Later, during the 1990s, Kato et al. [265] proposed the hydration/dehydration of isobutene/*tert*-butanol and Kawasaki et al. [266] proposed the polymerization and depolymerization of acetaldehyde and paraldehyde.

However, the main obstacle to the application of liquid-gas reactions is the complexity of these reactions:

- They require a catalyst and a solvent.

- Selectivity is limited by the formation of by-products.
- Good temperature control (pressurization).
- Temperature below the decomposition temperature of organic compounds.
- The system requires a separation unit (usually, a distillation column) to separate the product from the reactant.
- When there is a large variation of heat duty or a long time gap between heat supply and demand, the amount of hydrogen to be stored becomes a limiting factor.

In fact, Spoelstra et al. [191] evaluated the economical feasibility of the system acetone/2-propanol/hydrogen. They found a negative Internal Rate of Return [267] and concluded that this type of heat pump has no economic prospect for an application in Western Europe. In addition, they remarked that the major drawback of such a system is the formation of by-products.

Gas reactions

Some gas phase reactions are currently used to store and transport high-grade heat from concentrated solar plants and/or nuclear plants. The reforming of methane with steam is used to store and transport the heat produced by nuclear reaction, and that with carbon dioxide is used for conversion and transportation of concentrated solar energy. Dissociation and synthesis of ammonia is used for concentrated solar energy storage and transportation. A review of these technologies among other less developed technologies, such as methanol decomposition and synthesis, can be found in Ma et al. [268] and Gil et al. [27].

Solid-Liquid-Gas

Azpiazu et al. [269] studied also the reversible hydration of CaO with water, however the hydration reaction was carried out with water in the liquid phase instead of the vapour phase.

1.2 Scope of this report

The objective of this report is to provide a state-of-the-art review on material research and development for compact heat storage applications. Consequently, the study is focused on processes based on chemisorption (metal hydrides), as well as solid-gas absorption and chemical reactions, since the materials involved in such processes have the highest energy density of all the materials examined. In addition, these processes can cover a wide range of working temperatures and allow for long-term storage due to the negligible heat loss, thereby increasing the potential for energy saving in many applications.

The main advantages and drawbacks of the current material research are presented in this study, as well as possible future applications. The study is focused solely on experimental research under practical conditions, and provides the results and conclusions from small and pilot scale test rigs. It concludes with a summary of the main challenges and the outlook for future research.

Finally, it should be pointed out that a small amount of relevant research in this field is reported in languages other than English. Unfortunately, this work will only be cited or a summary given when the English abstracts are available or when relevant information can be extrapolated from them.

2 State-of-the-art review

Compact thermal storage involves processes based on a chemical reaction, absorption and chemisorption between a solid and a gas.

2.1 Solid-gas chemical reactions

As discussed in the introduction, the research on solid-gas chemical reactions has been focused on the formation and decomposition of hydroxides and carbonates.

2.1.1 Hydroxides

Magnesium hydroxide and calcium hydroxide are the state-of-the-art hydroxides for compact heat storage.

2.1.1.1 $Mg(OH)_2$

The decomposition and subsequent formation of magnesium hydroxide, $Mg(OH)_2$, from the oxide is as follows:

$$MgO(s) + H_2O(g) \Leftrightarrow Mg(OH)_2(s) \qquad \Delta Hr = -81.02\ kJ \cdot mol^{-1} \qquad (1)$$

$$H_2O(g) \Leftrightarrow H_2O\ (l) \qquad \Delta Hv = -40.02\ kJ/mol^{-1} \qquad (2)$$

This reversible chemical reaction has been extensively studied by Kato et al. [211-220] and Ryu et al. [223] over the last two decades for heat storage sources at medium temperature (200-400 ºC). The chemical heat pump is intended to recover waste heat from the exhaust gas of combustion engines (gas and diesel) such as cogeneration systems, vehicles, fuel cells, micro-gas turbines, etc. The hydration rate of magnesium oxide was measured by a gravimetric analysis and a kinetic model was proposed as a preliminary stage [211]. The study showed that the heat pump could be used as a heat amplifier to transform a heat source at 70-90 ºC to one at 100-150 ºC by storing heat at a temperature of 350 ºC. Furthermore, the authors suggested that the hydration of MgO has four reaction regimes with water:

1.- Containment of water as fixed structural water.
2.- Physical adsorption of water.
3.- Chemical reaction with water producing $Mg(OH)_2$.
4.- Inert portion of water.

The feasibility and the thermal performance of the chemical heat pump were also studied experimentally using a type of packed bed reactor [212-216]. The dehydration temperature was usually kept at 400 ºC to ensure a high enough temperature distribution in the whole bed. Due to the low thermal conductivity of the reactant, there is a temperature gradient between the wall (400 ºC) and the inner part of the bed. However, lower dehydration temperatures (≤ 300 ºC) can be obtained if the heat conductivity in the bed is enhanced. The maximum conversion was 60 %, which was obtained after 2 hours. The hydration of MgO (average particle diameter 1.5 mm) was carried out at different water vapour pressures ranging from 30 kPa to 203 kPa at corresponding evaporation temperatures (dew points) ranging from 69 ºC to 121 ºC. Figure 2.1 shows the effect of the hydration pressure on the hydration temperature.

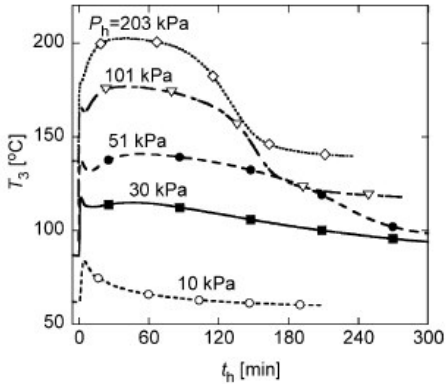

Figure 2.1: Effect of hydration pressure on the temperature profile inside the bed [215].

The temperature profiles show two peaks, one generated by physical adsorption at the former part and the other by the chemical reaction. The physical adsorption effect becomes indiscernible at higher vapour pressures, when hydration reactivity becomes more active. Table 2.1 shows the thermal performance of the heat pump for the 60 min hydration operation.

Table 2.1: Experimental thermal performance of the heat pump after 60 minutes of the hydration operation [216].

P_h (kPa)	T_{max} (ºC)	q_{60} (kJ·kg^{-1})	W_{60} (W·kg^{-1})
50	138	281	78
101	177	416	116
203	203	427	119

Ph, Tmax, q and w denotes the hydration pressure, maximum temperature, gross heat output and heat output rate respectively.

The maximum heat density is 427 kJ·kg^{-1} and is achieved at a water vapour pressure of 203 kPa. Higher vapour pressure can be obtained by using part of the heat output. The effect of the initial bed temperature was also measured for temperatures ranging from 100 to 130 ºC at fixed vapour pressure. The hydration reactivity was enhanced at lower reaction temperatures.

There are also several studies on the durability of MgO and $Mg(OH)_2$ in repetitive reactions [217-219]. A first study [217] was carried out to compare three types of magnesium oxide that were formed using the following precursors: ultra-fine magnesium oxide powder (average diameter 10 nm), common magnesium hydroxide and magnesium ethoxide. Ultra-fine powder (UFP) of MgO was more durable and had a higher heat output than the other two precursors. Following an initial decrease in the activity during the initial 5 cycles, the material showed a high rate of activity (50 % conversion) that was maintained during the next 19 cycles. The authors attributed the higher durability of the ultra-fine magnesium oxide to the fact that it was purer than the other materials. The hydration and dehydration of UPF-MgO entailed aggregation and cracking of the particles, which provides a fresh reaction surface for each hydration. However, the cracking of particles is inhibited in places where impurities are present. In addition, particles gradually become aggregated during the repetition, which results in larger particles. Consequently, it becomes more difficult to crack the particle.

In a further study [218], the reaction condition dependency on the repetitive hydration reactivity was explained by a nucleation mechanism. In other words, a higher reactivity condition leads to greater repetitive durability, because the higher reactivity causes greater nucleation during the repetition, and nucleation leads to a greater reaction surface area and higher diffusivity for the reaction. However, since the production of ultra-fine MgO powder (UFP) is expensive (=80-90 USD[3]·kg^{-1}), the material was

[3] United States Dollar ($)

compared to MgO obtained from conventional $Mg(OH)_2$ precipitated from seawater (<1 USD·kg^{-1}) and subjected to impurity reduction [219]. In addition, a molding method was introduced for material preparation to fit the multi-production process and, thus reduce cost. Similar to the previous results, the reactivity of the molded material made of UPF-MgO decreased during the initial 5 cycles, but remained relatively constant over the next 65 cycles. However, the impurity removal from the conventional $Mg(OH)_2$ was shown to be effective for durability enhancement. The decrease in reactivity was slightly higher than for UPF-MgO, but remained relatively constant from the 10th cycle until the 15th last cycle. Finally, the heat output density of the molded UPF-MgO was estimated to be 725 kJ·kg^{-1} at the 70th cycle, for a 60 min operation at a water vapour pressure of 48 kPa.

Ryu et al [223] also studied how mixing transition metal ions into magnesium hydroxide affects the dehydration and hydration reactivity. These materials were developed to shift the dehydration temperature of $Mg(OH)_2$ to lower temperatures (< 300 ºC). Nickel and cobalt were chosen as the additive material, because of the lower dehydration temperature:

$$CoO(s) + H_2O(g) \Leftrightarrow Co(OH)_2(s) \qquad \Delta Hr=-60 kJ\cdot mol^{-1} \qquad (3)$$

$$NiO(s) + H_2O(g) \Leftrightarrow Ni(OH)_2(s) \qquad \Delta Hr=-48\ kJ\cdot mol^{-1} \qquad (4)$$

The hydroxides mixed at atomic level, $Mg_\alpha M_{1-\alpha}O$ (M = Ni, Co; α = 0-1), were prepared by a precipitation method and the reactivity of the materials was measured via thermogravimetric analysis. The advantage of this method is that the mixed hydroxide forms a new phase with a unique thermal property. This is in contrast to simple physical mixtures in which the hydroxides would decompose independently.

The decomposition of $Mg(OH)_2$ started at about 310 ºC, and that of $Mg_\alpha Ni_{1-\alpha}O$ and $Mg_\alpha Co_{1-\alpha}O$ was shifted to lower temperatures, with an increase in Ni and Co content. However, $Co(OH)_2$ showed a relatively higher dehydration temperature than other lower content mixtures. The authors suggested that the dehydration of authentic $Co(OH)_2$ had a unique reaction mechanism, such as a multistep dehydration via Co_3O_4. The hydration experiments were performed using $Mg_{0.5}Ni_{1-0.5}O$ and $Mg_{0.5}Co_{1-0.5}O$ obtained after dehydration at 280 ºC. The thermal storage performance of the mixtures was estimated from the hydration measurements at an initial bed temperature of 110 ºC and a vapour water pressure of 57.8 kPa. The thermal storage capacity of $Mg_{0.5}Co_{1-0.5}O$ was estimated at 358 kJ·kg^{-1} and that of $Mg_{0.5}Ni_{1-0.5}O$ was estimated at 165 kJ·mol^{-1}.

Further experiments by Kato et al. [220] were performed only with $Mg_{0.5}Ni_{1-0.5}O$, using a packed bed reactor. The dehydration was carried out at 330 ºC to ensure a bed temperature of 280 ºC inside the bed. The effect of the hydration pressure on the temperature profile was measured for water vapour pressures of 57.8, 198 and 618 kPa and an initial bed temperature of 200 ºC, see Figure 2.2.

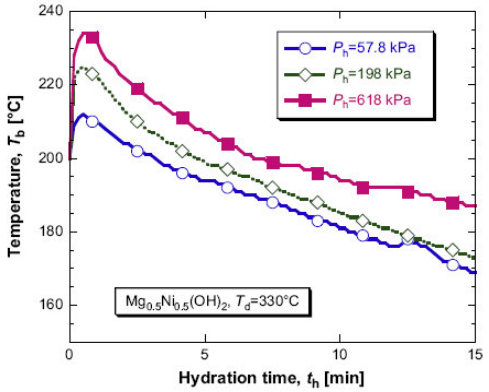

Figure 2.2: Effect of the hydration pressure on the temperature profile of the bed temperature, $Mg_{0.5}Ni_{1-0.5}O$ [220].

The authors suggest that the first peak is due to physical adsorption, but that the chemical reaction only proceeds in the temperature range from 170 to 210 ºC for a water vapour pressure of 57.8 and 198 kPa and in a temperature range from 185 to 200 ºC for a water vapour pressure of 618 kPa.

Finally, the latter studies at the Tokyo Institute of Technology were focused on the thermal conductivity enhancement in the bed. Kato [221] studied the use of a cupper fin for thermal conductivity enhancement and demonstrated the effectiveness in the improvement of the heat pump performance. However, the main drawbacks in the use of cupper fins were the corrosion of the material under high-temperature vapour and the difficulty of construction of heating fin structure. The current information was obtained from a further investigation by Kato et al. [222], since the previous study was not available. In this further investigation the use of a carbon fiber sheet was examined for heating because of its high-chemical durability under vapour atmosphere, high-thermal conductivity and easy construction handling in accordance with the author.

The thermal performance of the system was demonstrated in a 500 W chemical heat pump test rig under practical conditions. The reactor bed was packed in a basket vessel made of stainless steel mesh with an inside diameter of 360 mm and a height of 140 mm. The amount of $Mg(OH)_2$ used for the experiment was 6.8 kg with an average particle diameter of 1.5 mm. Quadrilateral carbon fiber fin (12 cm of height x 16 or 11 cm of width x 0.2 mm of thickness) of 28 sheets were set crossing at right angles to a spiral heating tube in the bed. Averaged interval between the fins was 2 cm.

The dehydration experiments were carried out at a subjective dehydration temperature of 430 ºC under the reaction pressure of 20 kPa for 5 hours. Whereas the hydration experiments were carried out at water vapour pressures of 47 kPa (80 ºC) and of 58 kPa (85 ºC) for an initial bed temperatures of 110C and 120 ºC.

The inner bed temperature was kept at over 150 ºC for 3 h (180 min) under each hydration condition. However, the higher temperature (159 ºC) was achieved under the higher water vapour pressure (58 kPa) and the lowest initial bed temperature (110 ºC). Under the latter conditions, the average heat power output and the gross heat output were calculated for 100 min operation and were of 49 $W \cdot kg^{-1}$ and 296 $kJ \cdot kg^{-1}$, respectively.

Further research was carried out by Kim et al. [224] on the composite material of expanded graphite and magnesium hydroxide to enhance the thermal conductivity and reactivity of magnesium oxide/water chemical heat pump. In addition, calcium chloride was also introduced into the mixture of expanded graphite and $Mg(OH)_2$ to ensure smooth diffusion of vapour in materials and enhance fit ability between expanded graphite and $Mg(OH)_2$.

The mixing ratio of expanded graphite and $Mg(OH)_2$ was 1:1 and the mixing molar ratio of calcium chloride and $Mg(OH)_2$ was 0.11. The composite material was denoted as EMC and its reactivity was compared with a mixed material of $Mg(OH)_2$ and $CaCl_2$, which was denoted as MC.

The experiments were performed in a type of thermo-balance (thermo-gravimetric analysis) wherein the dehydration experiments were performed at 300 ºC and hydration experiments performed at initial temperature of 110 ºC under a vapour pressure of 57.8 kPa.

The authors found that $CaCl_2$ had no influence on the dehydration whilst the dehydration rate increased with the addition of expanded graphite due to its high thermal conductivity and porosity. On the other hand, during the initial hydration stage, the diffusivity of EMG was higher than that in MC. However, as the hydration progressed the $CaCl_2$ volume increased which reduced the vapour diffusivity and, thereby, the hydration rate in EMC was lower than that in MC during the subsequent period. Later, $CaCl_2$ in MC also

prevented vapour diffusion through the bulk MC particle whereas vapour diffusion was enhanced in EMC due to the porosity of expanded graphite and thus, the final hydration conversion in EMC was higher that that in MC.

Finally, the thermal performance of the heat pump was calculated numerically for the system using EMC. The average heat power output for 10 min operation under water vapour pressure of 58.7 kPa ranged from 320 W $\cdot kg_{EMC}^{-1}$ at 110 ºC to 76.3 $W \cdot kg_{EMC}^{-1}$ at 200 ºC. In addition, the authors also calculated the average heat power output per kilogram of $Mg(OH)_2$ at 110 ºC and 58 kPa which was 701.3 $W \cdot kg^{-1}$.

2.1.1.2 $Ca(OH)_2$

Chiba University

At Chiba University, Ogura et al [229-246] and by Fujimoto et al. [247,248] have extensively studied a chemical heat pump based on the reversible reaction of CaO with water for effective thermal energy utilization in domestic and industrial uses, such as electric power or drying. Most of the studies are reported in Japanese or are published but not easily accessible (the papers are not available). However, the reports in English are relevant enough to give an idea of the reaction performance. The reversible chemical reaction can be written as follows:

$$CaO(s) + H_2O(g) \Leftrightarrow Ca(OH)_2(s) \qquad \Delta Hr=104.2 kJ \cdot mol^{-1} \qquad (5)$$

Ogura et al. [243] performed experiments with the chemical heat pump using three modes of operation: a heat upgrading mode, a heat enhancement mode (heating and cooling) and a refrigeration mode. The difference between these modes depends on the operating conditions. In the heat upgrading mode, charging is carried out under low pressure and discharging under high pressure, whereas in the other two modes the opposite is true: charging is carried out under high pressure and discharging under low pressure. The experiments were performed in a system wherein the reactor consisted of particle beds (single tray or multitray) filled with CaO or $Ca(OH)_2$ particles. Depending on the working conditions, the amount of CaO used ranged from 200 g to 3.0 kg. The bulk density of the CaO particle bed was around 0.88 $g \cdot m^{-3}$ and that of the $Ca(OH)_2$ particle bed was around 0.82 $g \cdot cm^{-3}$.

In this study, most experiments were carried out with the heat upgrading mode. In the charging phase, dehydration was carried out at 410 ºC (9.57 kPa) and the condenser was kept at 15 ºC (1.68 kPa). In the discharging phase, the evaporator temperature was at 13 ºC (516 kPa) and the hydration equilibrium temperature was 600 ºC. The performance of the heat pump was studied for different decomposition temperatures from 410 ºC to 500 ºC, whilst the condenser temperature was kept at 15 ºC. The authors found that when the temperature was increased, the time to reach complete reaction was reduced from about 490 minutes at 410 ºC to about 60 min at 500 ºC. The effect of the heat transfer enhancement by inserting fins into the reactor was also studied in the hydration reaction. When the number of blades was 0, the time required for complete reaction was almost 120 min. When 20 blades were used, the time was reduced to about 25 min. The heat storage/releasing density was 1.86 $MJ \cdot kg^{-1}$ (1640 $MJ \cdot m^{-3}$).

In the heat transfer mode and the refrigeration mode, the dehydration of $Ca(OH)_2$ is carried out at 500 ºC and the condenser is kept at 94 ºC (81.5 kPa). However, the reverse process is carried out with the evaporator at 5 ºC and the hydration equilibrium temperature at 330 ºC. The authors calculated the COP for the three modes of operation. For the upgrading mode the COP was 1.4, for the heat enhancement mode it was 1.8 and for the refrigeration mode it was 0.4.

Further available research carried out by Ogura et al. focused on the feasibility of this chemical heat pump for drying applications [244,245]. The authors proposed a novel drying technology involving a chemical

heat pump dryer (CHPD). The proposed CHPD consists of two chemical heat pumps (CHP), both based on the same chemical reaction (5). The pumps produce hot air for the drying room by using the heat released from the reaction or from the condensation of water (see Figure 2.3).

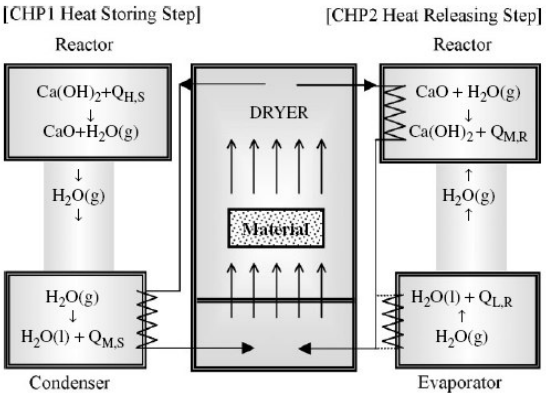

Figure 2.3: Schematic diagram of the $CaO/H_2O/Ca(OH)_2$ CHPD system operating in the heat-enhancement and refrigeration mode [244].

The two CHPs, 1 and 2, operate concurrently in the heat enhancement mode. CHP1 is in the heat storing step (charging), while CHP2 is in the heat releasing step (discharging). After every hour or so, the two heat pumps swap operating steps. In the charging step, the dehydration reaction is carried out using a heat source at a temperature above 470 ºC and the released water vapour is condensed at 80 ºC (47 kPa). However, in the discharging step, water is evaporated at 5 ºC (0.85 kPa) and the hydration reaction releases medium temperature heat at around 330 ºC. In addition, the heat consumed by the evaporator is used for cooling dehumidification.

In a first experimental study [244], Ogura et al. examined the controllability of the heat output characteristics of the CHPD on the reactor temperature, heat power and air temperature outputs for the heat storing step and releasing step. The reactor used for the experiments had an inside diameter of 360 mm and a height of 40 mm and consisted of a single shallow particle bed filled with CaO or $Ca(OH)_2$ particles to a height of about 20 mm. The amount of CaO loaded into the reactor was 600 g. The effect of the heat input temperature on the reaction conversion was studied for reactor temperatures (wall) ranging from 550 ºC to 700 ºC whilst the condenser temperature was kept at 80 ºC. The effect of the reactor temperature on the bed temperature and on the conversion is shown in Figure 2.4.

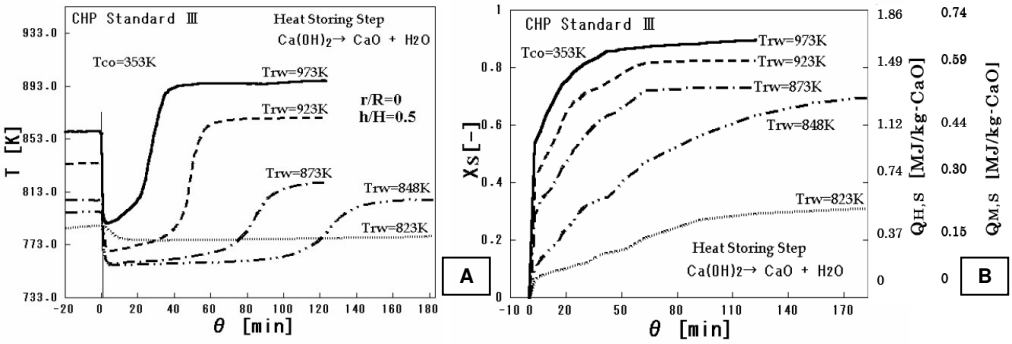

Figure 2.4: (A) effect of the heat storage temperature on temperature changes in the reactant bed. (B) Effect of the heat storage temperature on overall conversion changes, stored heat amount ($Q_{H,S}$) and released-medium temperature heat amount ($Q_{M,S}$) [244].

A temperature gap was observed between the reactor wall and the bed, which became larger with increasing decomposition temperature. For a decomposition temperature of 700 ºC (973 K), the temperature gap was about 80 ºC when the reaction was finished. The authors found that the reaction rate and the conversion rise as the temperature rises. The lowest conversion was about 30 % after more than 170 min for a decomposition temperature of 500 ºC (823 K), whereas the highest conversion was about 90% after 50 min for a decomposition temperature of 700 ºC. In any case, the authors pointed out that heat can be generated in the condenser at 80 ºC, even if the heat storage temperature is over 500 ºC.

In the heat releasing step, the evaporation temperature was varied from about 5 to 60 ºC. The authors selected these temperatures by considering the operating temperature level for hot dry air production and dehumidification with cooling. The effect of the evaporator temperature on the conversion rate, heat output and the outlet air temperature is shown in Figure 2.5.

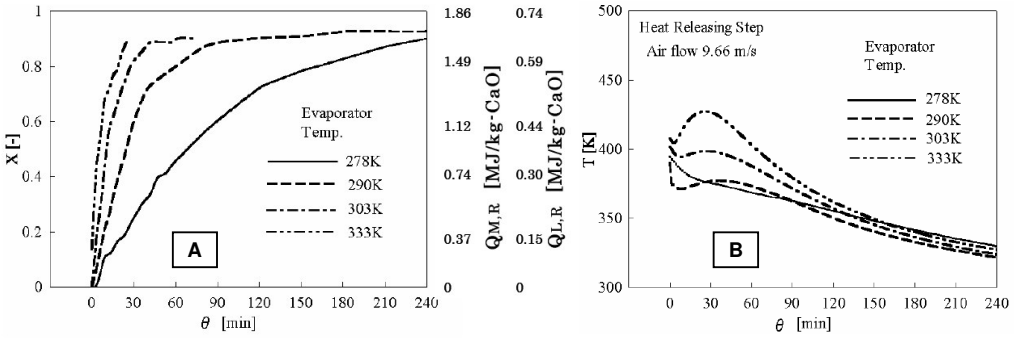

Figure 2.5: (A) Effect of evaporator temperature on overall conversion changes and released medium/low temperature heat amount $Q_{M,R}$, $Q_{L,R}$, (B) effect of evaporator temperature on air temperature changes at outlet heat exchanger [244].

The authors found that the reaction rate and the peak temperature (not shown) increase as the evaporator temperature rises, because of the increase in the pressure difference between evaporator and reactor. In any case, the peak temperature reached in the bed was always above 127 ºC. In addition, they found that the output air temperature was always kept above 77 ºC for 120 min

In a study by Ogura et al. [245], the sequential heat storing and heat releasing steps were studied experimentally. The aims of the experiments were to control the pressure in the reactor and to verify the feasibility of continuous repetition operations. The reactor used for the experiments had an inside diameter of 200 mm and a height of 40 mm and consisted of a single shallow particle bed filled with CaO or $Ca(OH)_2$ particles to a height of less than about 20 mm. The amount of CaO loaded in the reactor was 400 g. In the pressure control experiments, the condenser temperature was kept at 22 ºC and the heat source for the decomposition was at 600 ºC, while in the heat releasing step the temperature of the evaporator was kept at 40 ºC. Furthermore, some instant vacuuming was carried out during the initial heat storing/releasing steps and additional vacuuming was carried out after the second heat storing step to promote the reaction conversion. The final conversion after the first and second heat storing step was 63 % and 45 %, respectively. In contrast, it reached 63 % after the first and second heat releasing step. According to the authors, the high conversion in the second heat releasing step is due to the 5 min additional vacuuming after the second heat storing step.

In the continuous repetition experiments, the condenser temperature was kept at 12 ºC but the temperature of the heat source for the decomposition is not mentioned (it was probably also 600 ºC), while for the hydration reaction, the evaporator temperature was varied in a range between 5 ºC and 60 ºC. A temperature rise was confirmed in all the experiments. The maximum temperature was above 400 ºC for an evaporator temperature of 60 ºC. The authors found that the same temperature level was achieved after a few repetitions, which indicates the reproducibility of the CHP system. Finally, the authors also

found that the surface area increased after seven repetitions. It was suggested that this improved the reactivity of the material.

Ogura et al. [246] also studied the applicability of scallop material as an alternative source of $CaCO_3$ for the heat pump, due to the limited sources of limestone. The study was carried out by thermogravimetric analysis and in a chemical heat pump test rig. The authors found that the initial reactivity of the scallop CaO was very low, which was attributed to the low surface area (0.6 $m^2 \cdot kg^{-1}$) compared to the large surface area of the lime CaO (4.6 $m^2 \cdot kg^{-1}$). However, the authors found that after seven cycles the surface area of the scallop material increased to 4.2 $m^2 \cdot kg^{-1}$. The amount of heat released and the conversion of the scallop CaO increased to more than 80 % of that of the lime CaO, after seven repetitions.

Japan Coal Energy Centre

At the Japan Coal Energy Centre, Lin et al. [250,251] have studied the reversible chemical reaction between CaO and water to supply or transport heat. In the initial stage, Lin and Harada [250] used thermogravimetric analysis to study the hydration of CaO under steam pressure in the range of 0.67-3.8 MPa. At these pressures, CaO hydration proceeds at high temperatures of up to 750 ºC. As well as the effect of the steam pressure, the authors investigated the effect of temperature and particle size on the reaction rate.

The authors found that at a steam pressure of 2.0 MPa, the CaO hydration advanced fast until the temperature reached 973 ºC, at which point the hydration was very slow. After 10 min, only 10 % conversion was reached and the reaction was only completed after approximately 200 min. As the temperature decreased, the hydration rate increased. At temperatures of 923 ºC, 823 ºC and 773 ºC, the hydration was completed after 4.5 min, 3.5 min and 2.5 min, respectively. The authors pointed out that at a certain steam pressure, higher temperatures inhibited the hydration. In addition, they also found that at a constant temperature, the hydration rate also increased with increasing pressure. For instance, at 873 K and steam pressures of 2.3 MPa, 1.67 MPa and 1.33 MPa, complete conversion was observed at reaction times of 4.0, 4.5 and 6.0 min, respectively.

The highest temperatures reached during the hydration for different steam pressures are depicted in Table 2.2.

Table 2.2: Highest temperature reached during the hydration reaction of CaO under different steam pressures [250].

P (MPa)	T (ºC)	T (K)
3.8	750	1023
3.3	660	933
2.3	710	983
2	700	973
1.67	670	943
1.33	640	913

Furthermore, they also found that the hydration rate of CaO varied by the power of 2, with respect to the difference between the reactant steam pressure and the equilibrium steam pressure.

Finally, the effect of the particle size was found to hardly influence the CaO hydration rate.

A further study by Li et al [251] focused on the hydration and dehydration cycles of the $CaO/Ca(OH)_2$ system. The experiments were also carried out by thermogravimetric analysis and the experimental conditions are shown in Table 2.3.

Table 2.3: Experimental condition for the hydration of CaO and dehydration of $Ca(OH)_2$ [251].

Reaction	T (ºC)	T (K)	Total pressure (MPa)	Steam partial pressure (MPa)
CaO hydration	650	923	3.0	2.0
$Ca(OH)_2$ dehydration	550	823	0.1	0.06

The authors found that the CaO was completely converted to $Ca(OH)_2$ regardless of the number of cycles, as the particles remained porous after 20 cycles. However, the hydration rate decreased with the number of cycles. From the 1st cycle to the 20th, the time required for complete conversion increased from 8 min to 13.8 min. However, in the dehydration reaction, they found that the dehydration rate was not influenced by increasing the number of cycles and the time required for complete conversion remained between 3 and 4 min. The authors attributed the decrease in the hydration rate to a reduction of crystal growth and hence a decrease in surface area.

Finally, the eutectic melting of CaO and $Ca(OH)_2$ was not observed in this study. Curran et al. [270] reported that the melting temperature was as low as 777 ºC when the CaO/$Ca(OH)_2$ ratio was about 3/7 mol/mol. The authors suggested that the heat transfer rate may have been fast enough to protect the location temperature up to 777 ºC.

University of Ljubljana, ZAE Bayern and Tokyo Institute of technology (+ Technical University of Munich)

Cerkvenik et al. [254] studied the $Ca(OH)_2/H_2O/CaO$ system for refrigeration applications in a joint project between the university of Ljublijana (Slovenia), Zae Bayern (Germany) and the Tokyo Institute of Technology (Japan). The system had already been investigated in previous studies by Cerkvenik et al [255,256] and also proposed as a topping cycle of a gas-driven cascading sorption cooling device. However, these studies are difficult to access or not available, and are therefore only cited in these reports.

The CaO was combined with expanded graphite to increase the overall conductivity of the bed. The composite material was prepared by a suspension method and then pressed into the desired form. To increase the mass transfer of the reactive block, three vapour channels were made in the graphite matrix. In addition the effect of three vapour channels was compared with a study carried out by Depta [271] in which only one vapour channel was used. However, as this study is published in German, the information can only be extracted from the current paper [254] and presented in this section. The characteristics of the reactive blocks are shown in Table 2.4.

Table 2.4: Characteristics of the reactive bed for the system $CaO/H_2O/Ca(OH)_2$, with single and three vapour channels, [271] and [254].

Graphite matrix	Single vapour channel	Three vapour channel	Units
Length	150	139	mm
Diameter reactor bed	42.8	42.8	mm
Vapour channel diameter	10	10	mm
Volume	0.204	0.188	l
$Ca(OH)_2$ mass	20.593	18.673	g
Graphite mass	20.1012	18.401	g
Total mass	40.605	37.074	g
Total density	199	222	$kg \cdot m^{-3}$
Porosity of the matrix	0.912	0.901	-
Max. mass of reacted water	5	4.53	kg

The reactor is a tube with a length of 750 mm and an outer diameter of 48.3 mm. The 139 mm long reactive bed is inserted into the middle of the reactor. There is a pressed block of insulation material on both sides of the graphite matrix.

The dehydration experiments were carried out at 440 ºC and at three different operating pressures (0.75 kPa, 1.5 kPa and 3 kPa). It was found that the typical duration of the dehydration reaction, together with the heating phase, is about 1400 s. According to the authors, the increase in pressure at constant temperature would slow the reaction rate. However, due to the satisfactory difference between the current pressure and the equilibrium pressure, this effect was hardly seen. In contrast, the hydration experiments were carried out at 200 ºC. During the initial 500 s, the temperature rises above 200 ºC, but the heat rejection is fast enough to bring it back to 200 ºC. The measured increase is far from the equilibrium temperature. Therefore, it was concluded that the heat transfer is not limiting. In addition, the authors expected that heat transfer would have a stronger influence on the reaction if higher pressure was used. The total time used for the hydration varied from about 1250 s (3000 kPa) to 2000 s (750 kPa and 1500 kPa).

The results of the hydration at 200 ºC and under 1500 kPa were compared with the results obtained with the single vapour channel. The authors found that the mass transfer was enhanced with the three vapour channels. A conversion of 85 % was achieved after 2000 s. According to the authors, this corresponds to the 15 % of undecomposed $Ca(OH)_2$ determined by Hartman et al. [272]. However, the conversion with the single vapour channel was only 50% after 4000 s. In addition, the authors measured the reproducibility of the hydration reaction for 3 cycles and found the same conversion and reaction time for all cycles.

Finally, the authors calculated the specific cooling power (SCP) of the chemical heat pump. The results of the SCP are illustrated in Figure 2.6 for the three pressures and compared with the single vapour experiments.

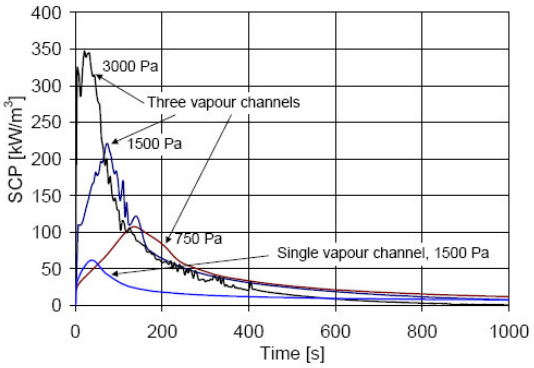

Figure 2.6: Comparison of specific cooling power for a hydration reaction at 200 ºC and different operating temperatures [254].

The average SCP obtained with three vapour channels is much larger than that obtained with the single channels. In addition, the hydration reaction time gets shorter as pressure increases, and thus the average SCP is higher. According to the authors, at a pressure of 750 kPa, which is normally used for refrigeration applications, an average SCP of 50 $kW \cdot m^{-3}$ could be achieved, if the cycle was limited to 1000 s. The average SCP that is given corresponds to a specific reactor volume of 20 $l \cdot kW^{-1}$.

Nottingham Trent University

Darkwa [253] experimentally evaluated the possibility of using the $CaO/H_2O/Ca(OH)_2$ heat pump to reduce energy consumption and pollutants from automobiles engines during cold starting, based on the analytical

concept developed in a previous study [252]. The study concerned the performance of the material after several cycles for the reaction of ½ moles of CaO with ½ moles of water. The test rig consisted mainly of an insulated cylindrical steel reaction chamber (130 mm in diameter and 400 mm in length) that housed a steel container (110 mm in diameter and 50 mm in length), which acted as the fixed bed. The mass of the fresh sample was 28 g of CaO and a total of 10 cycles were conducted with the same sample. The sample was hydrated at initial room temperature (17-21 ºC) under a water vapour pressure of 0.66 kPa. After hydration, the sample was dehydrated in a furnace for about 40 min and was allowed to cool completely overnight before being used again.

The summary of the test results is shown in Table 2.5.

Table 2.5: Summary of the test analysis [253].

Reaction time (min)	Maximum temperature attained (ºC)	Total net heat released (kJ)	Gross heat released (kJ)	Theoretical gross heat (kJ)
1.6	219	42.4	26.3	32

In the hydration experiments, the maximum temperatures measured in each cycle ranged between 207 ºC and 219 ºC (with an average maximum temperature of about 217 ºC). According to the authors, these results indicate that CaO is capable of being recycled provided it is well dehydrated and properly stored. Furthermore, according to the previous study [252], a minimum power input of 23.1 kW will be required to preheat a model 2-litre vehicle. The power output from the experiments was equivalent to 0.27 kW. Therefore, for a minimum power input of 23.1 kW, about 2.4 kg of CaO will be needed for typical thermal storage.

2.1.2 Carbonates

As mentioned in the Introduction, the carbonates studied so far are calcium carbonate, lead carbonate and barium carbonate.

2.1.2.1 $CaCO_3 + PbCO_3$

Kato et al. [225-228] studied a double reactor type of chemical heat pump based on the carbonation of calcium oxide (CaO) and lead (II) oxide (PbO) via carbon dioxide (CO_2). This chemical heat pump was developed to store heat above 800 ºC and upgrade it to higher temperatures. The reversible reaction systems are as follows:

$$CaO(s) + CO_2(g) \Leftrightarrow CaCO_3(s) \qquad \Delta H_r = -178.321\ kJ \cdot mol^{-1} \qquad (6)$$
$$PbO(s) + CO_2(g) \Leftrightarrow PbCO_3(s) \qquad \Delta H_r = -88.271\ kJ \cdot mol^{-1} \qquad (7)$$

Unlike the one-step reaction of CaO, the reaction of PbO proceeds via three equilibrium stages as follows:

$$2PbCO_3 \Leftrightarrow Pb \cdot PbCO_3 + CO_2 \qquad (8)$$
$$3(PbO \cdot PbCO_3) \Leftrightarrow 2(2PbO \cdot PbCO_3) + CO_2 \qquad (9)$$
$$2PbO \cdot PbCO_3 \Leftrightarrow 3PbO + CO_2 \qquad (10)$$

The authors determined that the last step (9) is the equilibrium of the heat pump operation, which is about 30 % of the reacted fraction [225,226].

At first, the authors proposed an operational pressure of 40.5 kPa (0.4 atm) for the heat storage mode (charging) and that of 101.3 kPa (1 atm) for the heat output mode (discharging). The kinetics of the

CaO/CO_2 and PbO/CO_2 reaction systems were studied by thermogravimetric analysis at different temperatures. The decarbonation of the lead carbonate ($PbCO_3$) only proceeds at temperatures higher than 420 ºC, because the equilibrium temperature of step (9) is higher than 420 ºC at 101.3 kPa. Decarbonation at 440 ºC and at 450 ºC was completed in about 60 min and 30 min. However, the reactivity of the PbO carbonation was maximal at 300 ºC and at 40.5 kPa. Although the reaction rate increased with the reaction temperature, it decreased once the equilibrium temperature had been reached.

In the CaO/CO_2 reaction system, the optimal decarbonation temperature of calcium carbonate ($CaCO_3$) was found to be 860 ºC at 40.5 kPa, as the reaction is completed within 30 min of the reaction time. However, the maximum temperature obtained during the carbonation was 880 ºC for a CO_2 pressure of 101.3 kPa.

The durability of the PbO/CO_2 and CaO/CO_2 systems was measured for 6 cycles. For the PbO/CO_2 system, reactivity initially decreased in the first four cycles, but was maintained in the next two cycles. For CaO/CO_2, a continuous decrease in reactivity was observed. The authors suggested the same solution as with the MgO/H_2O system: reduce the impurity content and the particle size [218,219].

The chemical heat pump is designed to store the heat output from a high temperature gas reactor. The heat from the carbonation of PbO would be used in a steam turbine and the heat from the carbonation of CaO would be used in a gas turbine, and thus electricity will be produced. However, the authors suggested that a higher pressure gradient between the reactors was required for optimal reaction conditions. In other words, a lower temperature input (charging) and a higher temperature output were needed. A lower temperature input was difficult to achieve, because of the low reactivity of PbO carbonation. For instance, if the decarbonation time of $CaCO_3$ was 1 hour, the amount of PbO required for the carbonation of PbO in the same time was 19.4 times higher than the amount of CaO. Even if 120 min were allowed for the carbonation of PbO, the amount of PbO required was 7.32 times higher than that of CaO.

Further experiments were carried out to study the influence of reaction pressure, but only with the CaO/CO_2 system [227,228]. In this case, the experiments were carried out in a packed bed reactor and thus the amount of reactant was increased to 600 g instead of the 18 mg used in the thermogravimetric analysis.

The effect of the pressure on the decarbonation reactivity was studied at 850 ºC and 900 ºC. Higher reactivity occurred under lower pressure. However, the reaction became saturated at approximately 70-80 % under 10.1 kPa (0.1 atm) or under 20.3 kPa (0.2 atm) at 900 ºC. The authors attributed the incomplete decarbonation to the temperature gradient inside the bed, due to the low thermal conductivity of the material. In contrast, the carbonation of CaO was performed at 101.3, 202.6 and 304 kPa with an initial bed temperature of 650 ºC. At 101.3 kPa, the temperature in the reactor was 895 ºC. However, complete carbonation of CaO was not possible. The authors suggested that the reaction process was limited by heat conduction in the bed. A maximum temperature of 979 ºC was measured at 304 kPa. In the next step of the experiments, the carbonation was carried out at an initial bed temperature of 900 ºC and at reaction pressures of 101.3 to 405.3 kPa. The heat output performance is summarized in Table 2.6.

Table 2.6: Experimental thermal performance of the heat pump at 60 minutes hydration operation [227].

P_c (kPa)	101.3	202.6	304	405.3
T_{max} (ºC)	896	944	975	998
W_{60} ($W \cdot kg^{-1}$)	173	202	225	238
q_{60} ($kJ \cdot kg^{-1}$)	623	727	810	860
V_{CaCO3} ($m^3 \cdot MW^{-1}$)	3.93	3.37	3.03	2.85

Pc, Tmax, W,q and V denotes the carbonation pressure, maximum temperature, gross heat output, heat output rate and volume for 1MW output respectively.

The maximum temperatures obtained at different pressures resemble those found in the previous experiments. The reactor requires a volume of 2.83 m^3 of CaO to generate a minimum heat output of 1 MW up to 998 ºC for 60 min at an operating pressure of 405.3 kPa.

2.1.2.2 $BaCO_3$

Kubota et al. [258] proposed a heat transformer based on the reversible carbonation of BaO as follows:

$$BaO(s) + CO_2(g) \Leftrightarrow BaCO_3 \qquad \Delta Hr = 269.5\ kJ \cdot mol^{-1}$$

The aim of the chemical heat pump was to store heat at 1000 ºC from a high-temperature gas reactor (HTGR) and to upgrade to 1527 ºC, and thus provide for the gasification melting process.

The carbonation and decarbonation of BaO and $BaCO_3$, respectively, were studied by thermogravimetric analysis. The experiments were carried out under various partial CO_2 pressures (0 - 101 kPa) in a temperature range from 700 to 1250 ºC for the carbonation and from 800 to 1250 ºC for the decarbonation. The authors found that the conversion and reaction rate for both reactions increase with the increase in temperature. Decarbonation is influenced by temperature and CO_2 pressure more than carbonation. However, both reactions were affected by the eutectic reaction between BaO and $BaCO_3$, in particular for carbonation with pressures around the equilibrium and for decarbonation under all the pressures below the equilibrium pressure and above 1030 ºC. According to the authors, in both reactions, when the conversion reached 40% to 60%, $BaCO_3$ and BaO began to form the eutectic mixture and to cover the surface of the sample in its liquid phase, thereby hindering the diffusion of CO_2 from the reaction region and decreasing the overall reaction rate. Finally, they estimated that the heat releasing step could be operated above the equilibrium pressure and at 1000 ºC or higher, but heat storage had to be carried out above 1000 ºC and below a quarter of the equilibrium pressure, on the assumption that carbonation and decarbonation had to reach conversions of over 60% within 30 and 60 min, respectively.

2.2 Solid-gas absorption

2.2.1 Hydrates

2.2.1.1 $MgSO_4$, $Al_2(SO_4)_3$, $CaCl_2$, $MgCl_2$

Long-term solar heat storage using salt hydrates have been studied at ECN (The Netherlands) to meet the heating demand for space heating and domestic hot water during the winter period. In a first theoretical study by Visscher et al. [83] magnesium sulphate heptahydrate ($MgSO_4 \cdot 7H_2O$) was identified as a promising material for seasonal heat storage, by means of the following reaction:

$$MgSO_4(s) + 7H_2O(g) \Leftrightarrow MgSO_4 \cdot 7H_2O(s) \qquad (11)$$

The theoretical energy density of $MgSO_4 \cdot 7H_2O$ was 2.8 $GJ \cdot m^{-3}$, which was 11 timer greater than that of water (0.25 GJ/m3 in the temperature range of 25 ºC to 85 ºC). In addition, the material is cheap, non-toxic and non-corrosive. Therefore, the hydration and dehydration behaviour and performance of the material was further studied by Essen et al. [84] using a thermogravimetric differential scanning calorimetry (TG-DSC), X-ray diffraction (XRD), particle distribution measurements and scanning electron microscope. In addition, the material was further investigated in a type of packed-bed reactor under practical conditions. However, the performance of the system is limited by two constraints. Firstly, the maximum hydration temperature was 150 ºC, which was the assumed maximum temperature that can be delivered by a medium temperature collector (vacuum tube) during the summer period. Secondly, the maximum water

vapour pressure during hydration was 1.3 kPa, as the evaporator/condenser was connected to a borehole heat exchanger at 10 ºC.

A TG-DSC analysis was performed in a nitrogen-water vapour atmosphere with a heating rate of 1 ºC·min^{-1} to study the dehydration behaviour of $MgSO_4 \cdot 7H_2O$. The authors found that dehydration occurs in a three-step process, corresponding to the following reactions:

$$MgSO_4 \cdot 6H_2O(s) + 7H_2O(g) \Leftrightarrow MgSO_4 \cdot 7H_2O(s) \quad (12)$$
$$MgSO_4 \cdot 0.1H_2O(s) + 5.9H_2O(g) \Leftrightarrow MgSO_4 \cdot 6H_2O(s) \quad (13)$$
$$MgSO_4(s) + 0.1H_2O(g) \Leftrightarrow MgSO_4 \cdot 0.1H_2O(s) \quad (14)$$

The first step occurs at low temperatures (25-55 ºC) and involves the loss of one water molecule. However, the fact that the first transition starts at 25 ºC suggests that when $MgSO_4 \cdot 7H_2O$ is stored in these conditions, the material (slowly) converts to $MgSO_4 \cdot 6H_2O$. Furthermore, it was found that $MgSO_4 \cdot 7H_2O$ melts at 52.5 ºC, which should be avoided as melting reduces the bed porosity of the material and thereby the vapour transport through the bed. The authors found that melting could be avoided at lower heating rates (≤1 ºC·min^{-1}), with small particles (> 200 μm) and/or small sample sizes (>5 mg).

The second dehydration step occurs between 60 ºC and 265 ºC, which corresponds to a loss of 5.9 water molecules. However, the authors pointed out that between 150 ºC and 265 ºC there is almost no energy stored in the material. This indicates that approximately 2.2 GJ·m^{-3} can be stored when $MgSO_4 \cdot 6H_2O$ is heated to 150 ºC.

Finally, the last step corresponds to the loss of 0.1 water molecules and also involves exothermic recrystallization at 300 ºC.

The hydration of $MgSO_4$ was studied at constant partial water vapour pressures of 1.3 kPa, 2.1 kPa and 2.3 kPa and at 25 ºC and 50 ºC. The last value of water pressure was estimated, as the exact value could not be determined due to technical difficulties. The hydration of $MgSO_4$ takes up only one water molecule in 16 h at 25 ºC and a partial water pressure of 1.3 kPa. At higher partial water pressures (2.1 and 2.3 kPa) and at 25 ºC, $MgSO_4$ takes up 6 water molecules. In addition, the reaction from $MgSO_4$ to $MgSO_4 \cdot 6H_2O$ occurs in a single step and the energy released by this reaction corresponds to the energy stored.

The influence of particle size and layer thickness on water uptake was also studied. The effect of particle size was studied for 20-38 m, 38-106 m, 106-200 m, and 200-300 m. However, it was found to have a limited effect on hydration. The effect of the layer thickness was studied for 0.1 mm, 0.4 mm and 1.1 mm. In this case, the layer thickness was found to strongly influence hydration: the thicker the layer, the slower the hydration proceeds.

The morphology of the material after hydration and dehydration was also studied. It was observed that a fraction of small particles were formed after dehydration. The authors indicated that this effect could lead to some problems, if, for instance, a fluidized bed is used as the small particles will flow away from the reactor. However, only a small shift to larger particles was observed after hydration. The variation in molar volume between $MgSO_4 \cdot H_2O$ and $MgSO_4 \cdot 6H_2O$ is a factor of 2.5, based on the solid density.

The authors concluded that $MgSO_4$ is not suitable for heat storage at atmospheric pressure as the hydration is unable to take up water at a partial water pressure of 1.3 kPa and at 50 ºC (approx. temperature for space heating). Therefore, further experiments were carried out under low pressure conditions (2.8 mbar) in a packed bed reactor. The hydration of $MgSO_4$ was carried out at an initial bed

temperature of 50 ºC and a water vapour pressure of 1.3 kPa. A maximum temperature increase of 4 ºC was measured in the bed. Apparently, the low pressure condition improves the vapour transport.

As a result of the first studies, salt hydrates of $Al_2(SO_4)_3 \cdot 18H_2O$, $CaCl_2.2H_2O$ and $MgCl_2 \cdot 7H_2O$ were also proposed for seasonal heat storage of solar energy by Essen et al. [85]. The dehydration of these salts was first assessed by thermogravimetric analysis. It was found that the salts can be dehydrated at 150 ºC. However, the hydration experiments were performed in the packed bed reactor under low pressure (2.8 mbar). The conditions of such hydrations were an initial bed temperature of 25 ºC with a water vapour pressure of 3.2 kPa and an initial bed temperature of 50 ºC with a water vapour pressure of 1.3 kPa. The results of the experiments are shown in Table 2.7.

Table 2.7: Temperature lift achieved during the hydration of the salts [85].

Conditions	Temperature lift (ºC)	
	Pv = 3.2 kPa; Tb= 25 ºC	Pv = 1.3 kPa; Tb= 50 ºC
$Al_2(SO_4)_3 \cdot 18H_2O$	6	1
$CaCl_2.2H_2O$	62	11
$MgCl_2 \cdot 7H_2O$	63	19

Pv and Tb denotes the water vapour pressure and the initial bed temperature respectively.

The chlorides showed a larger temperature lift than the sulphates. However, due to their hydroscopic nature they tend to form a gel-like material during hydration.

The $MgCl_2 \cdot 7H_2O$ was chosen as the best candidate for further research by Zondag et al. [77]. In this study, the authors found that HCl was formed during the dehydration of $MgCl_2 \cdot 7H_2O$ at temperatures above 135 ºC. The formation of this gas not only degrades the storage material, but is also strongly corrosive. Therefore, dehydration was limited to a temperature below 135 ºC. In addition, the over-hydration of $MgCl_2$ was avoided by impregnation into a carrier material.

The dehydration and hydration of $MgCl_2 \cdot 7H_2O$ were also carried out in a type of packed bed reactor, but in an open system (atmospheric). This choice was based on a previous techno-economical study at ECN, which had shown that this type of systems were more economical and reliable. The hydration experiments were performed using a moistened nitrogen flow of 20 slpm with a vapour pressure of 1.2 kPa and at an initial bed temperature of 25 ºC. A maximum temperature lift of 20 ºC was measured in the bed. In a further experiment, the reactor was up-scaled to increase the content of the material from 254 g to 3.5 g. The measured temperature lift was 15 ºC and a significant temperature rise was maintained in the bed after 24 hours. The calculated energy density of the material after 23 hours hydration was 0.14 $MJ \cdot kg^{-1}$.

2.2.1.2 Na_2S

Also at ECN, De Boer et al. [87] investigated structural, thermodynamic and phase properties in the Na_2S-H_2O system for application in a chemical heat pump. These properties were determined using X-ray diffraction, thermogravimetric differential scanning calorimetry and melting and vapour pressure measurements. The authors proved the existence of a new crystalline phase, $Na_2S \cdot 2H_2O$, among the known crystalline phases $Na_2S \cdot 9H_2O$, $Na_2S \cdot 5H_2O$ and Na_2S. Furthermore, the compound with composition $Na_2S \cdot 1/2H_2O$ is not a genuine phase, but a 1:3 mixture of Na_2S and $Na_2S \cdot 2H_2O$. The kinetics of the reaction $Na_2S \cdot 2H_2O$ to Na_2S in small domains of the dihydrate is so slow that under mild conditions this composition appears to be stable. The melting temperature of $Na_2S \cdot 9H_2O$ is 49 ºC and mixtures of $Na_2S \cdot 5H_2O$ with $Na_2S \cdot 2H_2O$ and of $Na_2S \cdot 2H_2O$ with Na_2S melt at 83 ºC. Thus, the theoretical operating window for the heat pump was established. The maximum operating temperature is 83 ºC and the useful equilibrium reactions are:

$$Na_2S \cdot 2H_2O\,(s) + 3H_2O(g) \Leftrightarrow Na_2S \cdot 5H_2O(s) \quad (15)$$

$$Na_2S \cdot 2H_2O(s) + 1½H_2O(g) \Leftrightarrow Na_2S \cdot 1/2H_2O(s) \quad (16)$$

Based on these reactions the theoretical heat storage is 3.84 MJ·kg^{-1} Na_2S (or 1.1 kWh·kg^{-1}) and the cold storage capacity is 2.54 MJ·kg^{-1} Na_2S (0.70 kWh·kg^{-1}).

The hydration and dehydration of the material was tested in a prototype reactor [88]. To increase the stability of the Na_2S, the material was impregnated on fibrous cellulose. The measured maximum thermal storage capacities of the prototype reactor are shown in Table 2.8.

Table 2.8: Thermal performance of the SWEAT module [88].

Heat storage capacity				
Heat in	13.3	MJ	3.7	kWh
Heat out	11.5	MJ		kWh
Efficiency		0.84		
Cold storage capacity	7.6	MJ	2.1	kWh
COP cooling		0.57		

2.2.1.3 $MnCl_2$

At the CNRS (France), Stitou et al. [164] studied the working pair $MnCl_2$-H_2O to store heat at 320-330 ºC (charging) and to produce heat at temperatures of around 145-160 ºC (discharging) from waste heat at 95 ºC (high pressure) or from an environment temperature of 40 ºC (low pressure), see Figure 2.7.

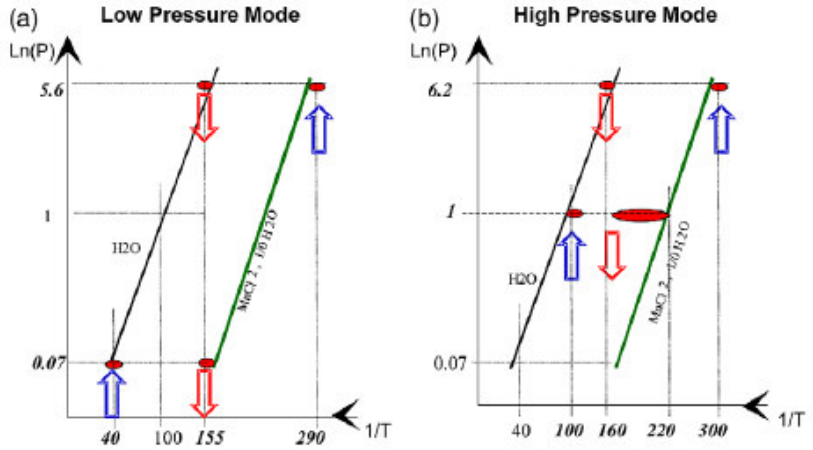

Figure 2.7: Water/hydrates cycles. Heat production at T=150 ºC: (a) Low-pressure mode, (b) high-pressure mode [164].

In addition, the system is also thought to be used as a topping cycle to drive a double-effect LiBr/H_2O absorption cycle and thus to increase the cooling performance.

The experiments were performed in a packed bed reactor, in which the bed is a solid porous composite consisting of a mixture of 20 % expanded graphite and 80 % $MnCl_2$. In this way, the conductivity of the porous bed increases up to 12 W·m^{-1}·K^{-1}, and the mass ratio leads to an acceptable porosity (about 80 %) for the mass transfer. The heat from the hydration process was extracted through a peripheral annular heat pipe evaporator, and the heat for the dehydration process was delivered by three inner electrical heaters. The results of the experiments are shown in Table 2.9.

Table 2.9: Thermal performance of the hydration and dehydration of $MnCl_2$ in high pressure mode and low pressure mode. The heat input and output are average values and the total mass of the reactive bed was 5.7 kg [164].

	High pressure mode			Low pressure mode		
	T (ºC)	Heat (W)	Time (min)	T (ºC)	Heat (W)	Time (min)
Dehydration						
Reactor	320-330	1290	52	310	1530	73
Condenser	120-140	530		100	410	
Hydration						
Reactor/Heat pipe	145-160	1790	35	125	820	105
Evaporator	95	560		50	240	

The lower power output and the longer hydration time in the low pressure mode were attributed to mass transfer limitations inside the porous reactive medium. In addition, the authors pointed out the problem of corrosion that may occur at low operating pressure, when the working conditions (pressure and temperature) are close to the solution limit. In addition, the formation of a hydrate solution is favoured by parasitic condensation in the reactor wall.

2.2.1.4 $SrBr_2$

At the CNRS (France), Lahmidi et al. [165] and Mauran et al. [166] investigated the $SrBr_2$ for solar heat storage in the built environment, by means of the following reaction:

$$SrBr_2 \cdot 1H_2O(s) + 5H_2O(g) \Leftrightarrow SrBr_2 \cdot 6H_2O(s) \quad (17)$$

The aim of the system is to provide heating and cooling through the floor of a house. During the summer, the cooling effect is provided by evaporation of water and the subsequent heat of the hydration of $SrBr_2 \cdot 1H_2O$ is released to the environment. Then, during the winter or mid-season, the heating effect is provided by the hydration of $SrBr_2 \cdot 1H_2O$. In addition, the heat source for the dehydration is provided by plane solar collectors. This type of solar collector is less costly than vacuum tube collectors, but it can only provide heat at a maximum temperature of 80 ºC.

In a first study [165], the experiments were carried out in a packed bed reactor wherein the reactive bed has a cylindrical shape with a diameter of 15 mm and a thickness of 12 mm. Heat is supplied or extracted to or from the bed through a heat exchanger that is placed below it. The water process is atomized with nozzles before the evaporation or condensation. The reactive bed is a consolidated composite material made of $SrBr_2 \cdot 6H_2O$ and expanded graphite (ENG). The optimum apparent density of the bed was also studied for effective high storage capacity and high power per unit volume. Basically, an increase in the apparent density of the reactive solid (the amount of $SrBr_2 \cdot 6H_2O$) improves the storage capacity, but entails mass transfer limitations (especially at low pressures). Three different consolidated matrices corresponding to storage capacities equal to 250, 300 and 400 $kWh \cdot m^{-3}$ were tested, see Table 2.10.

Table 2.10: Characteristics of the different reactive composites [165].

Sample	ρeng ($kg \cdot m^{-3}$)	ρ$SrBr_2$ ($kg \cdot m^{-3}$)	HSC ($kWh \cdot m^{-3}$)	CSC ($kWh \cdot m^{-3}$)	λo ($W \cdot m^{-1} \cdot K^{-1}$)	λ1 ($W \cdot m^{-1} \cdot K^{-1}$)	k0 x 10^{12} (m^2)	k1 x 10^{13} (m^2)
De250	40	660	250	150	0.89	0.4	1.73	5.74
De300	40	795	300	180	0.74	0.31	1.43	3.36
De400	40	1055	400	240	0.53	0.2	0.94	0.82

ρ denotes the apparent density and HSC and SCH the heating and cooling storage density, respectively.
λ and k denote the thermal conductivity and the permeability of the lowest hydrate (0) and the highest (hydrates), respectively.

The cooling effect was provided by evaporation of water at 12 ºC, and 1.5 kPa, whereas the heating effect was provided by the hydration of $SrBr_2 \cdot 1H_2O$ at 35 ºC with a water vapour pressure of 2.3 kPa (20 ºC). The results of the experiments are shown in Table 2.11.

Table 2.11: Mean experimental heating and cooling power between 0 and 90 % conversion (except De400) [165].

Sample	Cooling power ($kW \cdot m^{-3}$)	Heating power ($kW.m^{-3}$)
De250	49	36
De300	47	27
De400	-	14 (30 %)

The authors measured power outputs in the range of 40 $kW \cdot m^{-3}$ with reactive composites that have higher than 250 $kWh \cdot m^{-3}$ heat storage capacities. However, the composite De400, which has the highest density, has a considerable mass transfer limitation that leads to very low power.

For further research [166], the authors built a prototype reactor that is able to store, with a complete reaction, 60 kWh or 40 kWh for heating and cooling respectively. The total volume of the reactor is 1 m^3 and it is made up of a stack of modules. Each module consists of a heat exchanger, two reactive layers and two gas diffusers. The thickness of the reactive layer is 12 mm and the characteristics of the reactive layer are shown in Table 2.12

Table 2.12: Characteristic reactive composite in prototype Solux [166].

ρeng ($kg \cdot m^{-3}$)	$\rho SrBr_2$ ($kg \cdot m^{-3}$)	HSC ($kWh \cdot m^{-3}$)	λo ($W \cdot m^{-1} \cdot K^{-1}$)	λ_1 ($W \cdot m^{-1} \cdot K^{-1}$)	$k_0 \times 10^{12}$ (m^2)	$k_1 \times 10^{13}$ (m^2)
40	439	154	1.32	0.7	2.43	13.4

The experimental conditions were changed for the cooling mode (summer) and for the heating mode (mid-season). The cooling effect was provided by the evaporation of water at 18 ºC (~2.1 kPa) instead of 12 ºC and the heating effect was provided by the hydration reaction at 35 ºC with a water vapour pressure of 1.4 kPa (12 ºC) instead of 2.3 kPa (20 ºC). In addition, the dehydration temperature was lowered to ≤ 70 ºC.

In the cooling mode, the hydration was finished at 92 % conversion after 14 hours. Here too, the hydration temperature was kept at 35 ºC. The average cooling power delivered by the evaporator was -2.6 kW. The main limitation was found in the heat transfer between the reactive layer and the wall of the heat exchanger. The dehydration, on the other hand, was carried out at approximately 66 ºC and the temperature of the condenser was initially maintained at 35 ºC and lowered to 25 ºC after some time. The dehydration was almost complete (x varying from 0.92 to 0.12) after 48 hours.

In the heating mode, the dehydration of the salt was carried out at approximately 70 ºC instead of 66 ºC and the temperature of the condenser was lowered to 12 ºC. Dehydration was completed after 15 hours instead of the 48 hours required in the cooling mode experiments. However, hydration was stopped at 55 % conversion. The mean heating power delivered at 30 ºC in the reactor was only 2.2 kW. As in the cooling mode, the authors attributed the low power output to the heat transfer between the reactive layer and the wall of the heat exchanger.

2.2.2 Ammoniates

The solid-gas equilibriums of the chloride salts with ammonia are summarized in appendix A.

2.2.2.1 $BaCl_2$ + $MnCl_2$ + expanded graphite

CNRS

Lépinasse et al. [141-143] studied a double reactor type of chemical heat pump based on the reversible ammoniation of $BaCl_2$ and $MnCl_2$. The feasibility of the process involving the two solid-gas reactors was demonstrated by means of a 1-2 kW experimental test rig for refrigeration. The reactive bed consisted of anhydrous salts previously compacted in expanded graphite [107]. The reactors used in the test rig were of the catalytic type wherein each reactive medium was enclosed in several stainless steel pipes of 3 cm diameter and set in a casing with baffles through which the thermal fluid flows (in turbulent flow). The characteristics of the reactive medium and the reactor are shown in Table 2.13.

Table 2.13: Characteristics of the reactive medium and the reactor for the $BaCl_2/MnCl_2/NH_3$ system [142].

Characteristics	$BaCl_2$ 8/0 NH_3	$MnCl_2$ 6/2 NH_3	Units
Reactive medium			
Density	507	495	$kg.m^{-3}$
% mass graphite	35	35	
Mass of anhydrous salt	2.125	2.57	kg
Porosity	77	75	
Thermal conductivity	6-8	6-8	$W \cdot m^{-1} \cdot K^{-1}$
Reactor			
Number of tubes	19	19	
Tube length	500	620	mm
HEX surface area	0.95	1.2	m^2

The experiments were carried out using a closed protocol: before coupling, the reactors kept at 25 ºC ($BaCl_2$) and 50 ºC ($MnCl_2$) are near their real equilibrium pressure of 250 kPa and 12 kPa. The cooling power is provided during the decomposition of $BaCl_2 \cdot 8NH_3$, while the heating power is provided by the subsequent ammoniation of $MnCl_2 \cdot 2NH_3$. The measured heat transfer coefficients between the reactive bed and the heat transfer fluid were in the order of 190 ± 30 $W \cdot m^{-2} \cdot K^{-1}$ for both processes. Four different steps may be distinguished during the reactions:

- In the first phase (3 minutes and 20 % conversion), the pressure instantaneously equalizes at 70 kPa in the two reactors. Then, ammonia desorption from $BaCl_2 \cdot 8NH_3$ and subsequent absorption by $MnCl_2 \cdot 2NH_3$ occurs adiabatically at first, corresponding to the available heat in the reactive beds (sensible heat). This entails a decrease in the temperature of $BaCl_2$ to near the equilibrium temperature. At the same time, the temperature of the $MnCl_2$ increases to near its equilibrium temperature. Then, the heat is transferred or consumed by the thermal fluids. During this phase, the pressure changes as a function of the reaction rates in the two media.
- During the second phase (15 min and from 20 to 60 % conversion), the pressure is stabilized at a level which equalizes the rates of absorption and desorption. The temperatures of the two reactants are close to thermodynamic equilibrium and the exchange of heat is almost constant.
- Then, during the third phase (10 min), there is a slow decrease in the consumption and production of heat. The temperature in the $BaCl_2$ reactor starts to increase while the temperature in the $MnCl_2$ starts to decrease.
- Finally, the fourth phase corresponds to the end of the reactions (conversion > 80 %).

The cooling and heating power of the test rig were 1 kW (300 $W \cdot kg^{-1}$) and 1.3 kW (320 $W \cdot kg^{-1}$), respectively. These values are the average values, taken from the powers measured during the 25 minutes of the stationary phase (from 20 % to 80 % conversion).

Finally, the coefficient of performance was calculated for the whole cycle. It should be noted that the temperatures in the reverse cycle are 195 ºC for the decomposition of $MnCl_2 \cdot 8NH_3$ and 50 ºC for the ammoniation of $BaCl_2$. Table 2.14 summarizes the values of COP that were calculated.

Table 2.14: COP values for the system $BaCl_2/MnCl_2/NH_3$ [142].

	Ideal	With thermal masses of reactants	With thermal masses of reactants + reactors	With thermal masses of reactants + reactors + thermal fluids
COP	0.72	0.58	0.48	0.35

The results of the COP served to rapidly identify the potential improvements that could be made to the system. The authors suggested that the system requires better heat transfer between the reactive medium and the reactor wall.

Shangai Jiao Tong University

Li et al. [169-171] also studied a double-way sorption refrigeration system using consolidate $MnCl_2$-expanded graphite and $BaCl_2$-expanded graphite blocks as the reactive material. The double-way system consists in two reactors, one evaporator and one condenser. The working principle is divided in two phases (Figure 2.8). During the first phase, the high temperature salt ($MnCl_2$) is desorbed at a high temperature of 180 ºC and the ammonia at high pressure (P_h) is moved to the condenser. The ammonia rejects heat to the environment at 30 ºC and flows into the evaporator. At the same time, the low temperature salt ($BaCl_2$) is cooled by a heat sink (25 ºC) and absorbs the ammonia from the evaporator at medium pressure (P_e). The enthalpy of vaporization produces a cooling effect at 10 ºC by extracting heat from a chilled medium. In the second phase, the initial working modes of the two reactors are interchanged. When the high temperature reactor is connected to the low temperature reactor, a resorption process occurs at low pressure (P_L) between the HTS and the LTS. This process produces another cooling effect by absorbing heat from the chilled medium during desorption phase of the LTS.

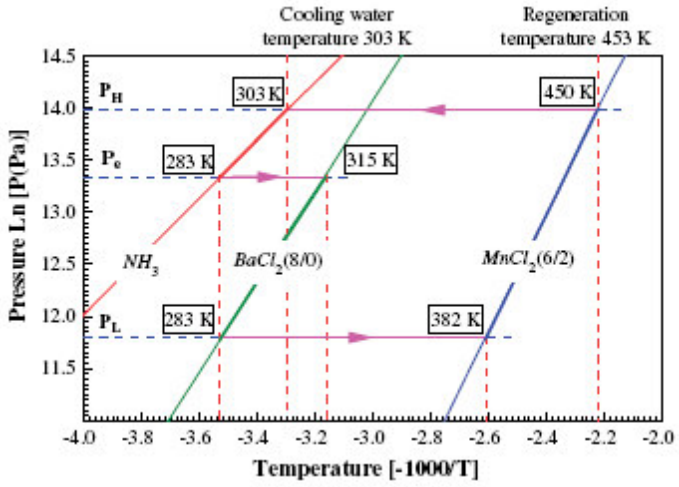

Figure 2.8: Theoretical Clapeyron diagram of the combined double-way sorption refrigeration cycle [169].

In a first study, the feasibility of the proposed system was experimentally evaluated. The characteristics of the reactor and the reactants are shown in Table 2.15.

Table 2.15: Characteristic of the reactor and the reactants for the $BaCl_2/MnCl_2/NH_3$ system [169].

Characteristics	$BaCl_2$ 8/0 NH_3	$MnCl_2$ 6/2 NH_3	Units
Reactive medium			
Density	250	300	$kg.m^{-3}$
% mass graphite	37	37	
Mass of salt	0.141	0.101	kg
Reactor			
Block inner diameter	25	25	mm
Block outer diameter	65	65	mm
Length	350	350	mm

The temperature evolution was followed for the $MnCl_2$ and $BaCl_2$ systems. In all cases, the authors measured the temperature gradients inside the reactive block, due to heat transfer limitations. However, the larger temperature differences were observed during the decomposition of $BaCl_2 \cdot 8NH_3$ to $BaCl_2$. The lowest temperature reached in the inner part (next to the gas channel) was -33 ºC, whereas the outer part (next to the cooling fluid) was around -15 ºC, due to heat and mass transfer limitations. The system's ideal COP was about 1.24 and the experimental COP was 0.64.

In another study [170], the experiments were carried out with reactive blocks that had an apparent density of 250 $kg \cdot m^{-3}$ and a graphite mass fraction equal to 0.5. In these experiments, the authors measured the conversion and the specific cooling power. The experimental conditions were the same as those of the first study. During the synthesis phase of $BaCl_2$, the maximum temperature difference measured inside the reactive block was about 9 ºC. At the end of the process (60 minutes), the conversion was higher than 0.8. The highest specific cooling capacity that was calculated was 1200 $W \cdot kg^{-1}$ and the average specific cooling capacity was 301 $W \cdot kg^{-1}$. However, during the decomposition of $MnCl_2 \cdot 6NH_3$, a larger temperature difference of 22 ºC was measured between the inner and the outer part during the process. In the reverse cycle, the authors pointed out that the conversion could not be measured due to some technical difficulties. Instead, the specific cooling capacity was measured. The process was finished at 105 minutes. The calculated experimental COP was 0.62, which is close to that found in the first experiment (0.64). The authors stressed that the heat transfer performance needed to be further improved.

In a further study, T.X. Li et al. [171] proposed a reheating process aimed to improve the system performance of the double-way sorption refrigeration system, see Figure 2.9. In addition, the heat required during the reheating process was supplied by cooling water at ambient temperature and thus no additional heat input from an external source is required during this operating period.

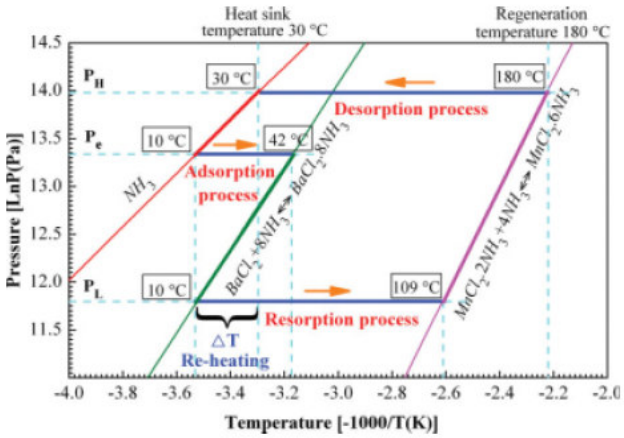

Figure 2.9: Working principle of the combined double-way sorption thermodynamic cycle with re-heating process [171].

The re-heating process was performed at the end of the re-sorption process just before the beginning of the adsorption process. The $BaCl_2$-reactor was re-heated by replacing the low-temperature heat transfer fluid (5-15 ºC) with a relatively higher temperature heat sink fluid (25-30 ºC)

As in the previous study, the experiments were carried out with reactive blocks having an apparent density of 250 $kg \cdot m^{-3}$ and a graphite mass fraction equal to 0.5. Table 2.16 shows the values of COP obtained with and without re-heating process at different operating temperatures for cooling water, evaporator and pseudo-evaporator (regeneration temperature of $BaCl_2 \cdot 8NH_3$).

Table 2.16: Performance of the double-way sorption cycle with and without re-heating process [148].

Cooling Water Temperature (ºC)	Evaporation Temperature (ºC)	Pseudo-evaporation Temperature (ºC)	Without Re-heating, COP	Improvement (%)
25	5	5	0.31	28
	10	10	0.57	12
30	10	10	0.32	48
	15	15	0.42	34

The authors found that the improvement in the COP varied from 12 % to 48 % according to the different experimental conditions. Furthermore, they found that the heat sink temperature had a strong influence on the performance improvement. For the evaporation and pseudo-evaporation temperature of 10 ºC the COP increased by 12 % at the heat sink temperature of 25 ºC whereas it was as high as 48 % at the heat sink temperature of 30 ºC. Finally, the authors pointed out that the COP obtained with the combined double-way cycle without reheating was 0.57, when the heat sink, evaporation, and pseudo-evaporation temperatures were 25 ºC, 10 ºC, and 10 ºC, respectively. However, at the same cycle conditions, the COP increased to 0.64 when the proposed reheating process was introduced in the combined double-way sorption cycle.

2.2.2.2 $BaCl_2$ + $NiCl_2$ + expanded graphite

Goetz et al. [144] studied a double reactor type of chemical heat pump based on the reversible ammoniation of $BaCl_2$ and $NiCl_2$. The aim of the study was to demonstrate the feasibility of this chemical heat pump for refrigeration at 0 ºC. However, it was also studied for air conditioning in buildings at 15 ºC and for personal air conditioning at 40 ºC. The cooling is provided during the decomposition of $BaCl_2 \cdot 8NH_3$. At the same time, the heat produced during the subsequent ammoniation of $NiCl_2 \cdot 2NH_3$ is dissipated into the environment.

The experiments were carried out in cylindrical packed bed reactors of 4 cm diameter. The reactive bed consisted of anhydrous salts previously compacted in expanded graphite. The use of graphite provides a medium with a high thermal conductivity of 5-8 $W \cdot m^{-1} \cdot K^{-1}$, while maintaining high mass transfer. Table 2.17 summarizes the characteristics of the reactive bed and the reactor.

Table 2.17: Characteristics of the reactive medium and the reactor for the $BaCl_2/NiCl_2/NH_3$ systems [144].

Characteristics	$BaCl_2$ 8/0 NH_3	$NiCl_2$ 6/2 NH_3	Units
Reactive medium			
Density	300	300	$kg.m^{-3}$
% mass graphite	35	35	
Mass of salt	0.066	0.044	kg
Reactor			
Tube length	300	380	mm
HEX surface area	0.04	0.05	m^2

The average measured values for the heat transfer coefficients between the reactive bed and the heat transfer fluid were 155 ± 20 $W \cdot m^{-2} \cdot K^{-1}$ for $BaCl_2$ and 300 ± 50 $W \cdot m^{-2} \cdot K^{-1}$ for $NiCl_2$ $W \cdot m^{-2} \cdot K^{-1}$. The results of these experiments are summarized in Table 2.18. The mean cooling power corresponds to 15 minutes operation.

Table 2.18: Results of the experiment with the $BaCl_2/NiCl_2/NH_3$ system [144].

	Cooling at 0 ºC	Cooling at 15 ºC	Cooling at 40 ºC	Units
T_{NiCl2}	40	40	40	ºC
T_{BaCl2}	0	15	40	ºC
P	10	20	30	kPa
Cooling Power	40	65	100	W

2.2.2.3 $PbCl_2$ + $MnCl_2$ + expanded graphite

The reversible ammoniation of $PbCl_2$ and $MnCl_2$ was also studied by Lépinnasse et al. [145]. The purpose of the study was to demonstrate the practical working of the resorption process by cooling down a box between 0 ºC and 5 ºC. The box was a cube with an internal volume of 0.088 m^3 (88 l). The walls were made up of 8 cm thick expanded polystyrene.

The experiments were carried out using two cylindrical reactors equipped with external blades to promote heat exchange with the air. The $PbCl_2$ reactor was placed inside the box and connected by a pipe to the $MnCl_2$ that was placed directly in the ambient environment. Each reactive bed was composed of the anhydrous salt and expanded graphite [107]. This allows the thermal conductivity of the reactant to increase to about 6 $W \cdot m^{-1} \cdot K^{-1}$. The heat exchange coefficient between the walls of the reactor and the reactants was higher than 500 $W \cdot m^{-2} \cdot K^{-1}$, [81]. Table 2.19 summarizes the characteristics of the reactor and the reactive medium.

Table 2.19: Characteristics of the reactor and reactive medium for the $PbCl_2/MnCl_2/NH_3$ system [145].

Characteristics	$PbCl_2$ 8/3.25 NH_3	$MnCl_2$ 6/2 NH_3	Units
Reactive medium			
Density	520	400	$kg.m^{-3}$
% mass graphite	35	35	
Mass of salt	0.401	0.217	kg
Reactor			
Diameter	60.4	60.4	mm
Tube length	485	400	mm
HEX surface area	0.41	0.41	m^2

The box was at ambient temperature (20 ºC) at the beginning of the experiments. In the first 10 minutes, the temperature of the reactor $PbCl_2$ dropped below -7 ºC, whereas the temperature of the reactor $MnCl_2$ increased up to 67 ºC. The cooling power produced by the decomposition of $PbCl_2 \cdot 8NH_3$ decreased the average temperature of the air inside the box to 5 ºC in 20 minutes. At that moment, the cooling power was 33 W. Then, the temperature of the $PbCl_2$ reactant decreased slowly to reach its minimum value of -15 ºC in 100 min. The temperature of the air inside the box was then equal to -3 ºC and the cooling power was 15 W. After 130 minutes, the reaction was over and there was no more cooling effect. However, the temperature of the air inside the box was maintained between -3 ºC and 5 ºC for 60 min, because of the thermal inertia of the reactor and the thermal insulation. Thus, the experimental setup maintained the

temperature of the air inside the box at below 5 ºC for almost 5 hours. The experimental cooling capacity obtained was equal to 47 kWh·m^{-3}.

To control the temperature inside the box, the authors suggested implementing a mechanical relief valve placed on the line between the two reactors. As the equilibrium temperature is controlled by the pressure inside the reactor, the control of the pressure corresponds to the control of the cooling power. The authors demonstrated the new feature control via simulations.

2.2.2.4 $MnCl_2$ + NH_4Cl + expanded graphite

Shangai Jiao Tong University – simultaneous cooling and freezing system

Bao et al. [173,174] investigated the $MnCl_2$ and NH_4Cl system with ammonia for simultaneously cooling a small refrigerator with a 33 L storage box at 0 ºC to 6 ºC and freezing at -16 ºC to -14.5 ºC. The system comprised two main parts, as shown in Figure 2.10 (A). Part 1 was the insulated storage box with eight NH_4Cl reactors (low temperature salt), whereas part 2 contained three $MnCl_2$ reactors. Furthermore, the box was divided into two zones to enhance the two refrigeration levels, see Figure 2.10 (C). The upper part was the zone of 0 ºC to 6 ºC (zone 1) and contained one group of NH_4Cl reactors placed vertically, while the bottom part was the zone of -16 ºC to -14.5 ºC (zone 2) and contained the other group of NH_4Cl reactors placed horizontally.

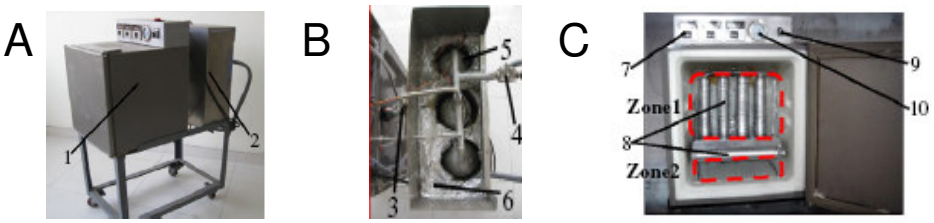

Figure 2.10: Resorption cold storage: (A) appearance of the device (B) $MnCl_2$ box (C) NH_4Cl box. (1) $MnCl_2$ box, (2) NH_4Cl box, (3) connection valve between the two parts, (4) valve for filling refrigeration, (5) $MnCl_2$ reactors, (6) insulation material, (7) temperature display, (8) NH_4Cl reactors, (9) electrical heater switch and (10) pressure gauge [174].

The reactive beds were made of expanded graphite and the inorganic salts. The characteristic of the reactive beds and the reactor are depicted in Table 2.20.

Table 2.20: Characteristics of the reactive bed and the reactor for the $MnCl_2$ and NH_4Cl system [174]

Characteristics	$MnCl_2$ 6/2 NH_3	NH_4Cl_2 3/0 NH_3	Units
Reactive medium			
Density	460	410	kg.m^{-3}
% mass graphite	80	80	
Mass of SALT	590	120	g
Reactor			
Diameter	106	45	mm
Height	300	300	mm
Porosity	0.55-0.75	0.4-0.7	

The authors obtained the cooling capacity of the system by measuring the mass amounts of ice produced under different ambient temperatures at 20 ºC, 25 ºC, 30 ºC and 35 ºC. The decomposition of the $MnCl_2$ salts was carried out with the reactor at 165 ºC to ensure a decomposition temperature of 155 ºC in every part of the reactive bed. The decomposition process was carried out for 2 hours. For the refrigeration

process, the reactors were cooled down to ambient temperature and then ice was used to further cool every component inside the NH_4Cl box to a temperature close to 0 ºC. Then, the ice was replaced by water and the decomposition started.

At the beginning of the process, the temperature at the wall of the NH_4Cl reactors dropped rapidly to reach -20 ºC to -18 ºC in 2 to 3 min. However, the temperature in the $MnCl_2$ reactor increased to 75 – 80 ºC. After 10 to 15 min, the decomposition rate slowed down and the temperature varied smoothly. The minimum temperature reached at the wall of the NH_4Cl reactors varied from -32 ºC to -26 ºC, as a function of the ambient temperature that ranged from 20 ºC to 35 ºC. Generally, the temperature of the NH_4Cl reactors started to rise again after 2 hours when the process was almost finished and the decomposition heat that was abstracted by the NH_4Cl reactors could not counteract the heat losses though the insulation.

The air in zone 2 reached a minimal temperature of -16 to -14 ºC and remained under -10 ºC for about 3 hours. Zone 1 could be cooled down to between -1 ºC and 6 ºC. Furthermore, the authors calculated the total cooling capacity of the system and found out that it was barely influenced by the ambient temperature. The calculated value was 475 kJ per kilogram of NH_4Cl. However, the consumption of cooling production due to the heat capacity of the metallic elements was about 110 $kJ \cdot kg_{NH4Cl}^{-1}$ and the heat losses were 33 % to 55 % of the total cooling production. Therefore, the effective cooling capacity was low and varied from 120 to 200 $kJ \cdot kg_{NH4Cl}^{-1}$. Finally, the average specific cooling power in 3 hours was calculated as 43 W per kg of NH_4Cl and the effective specific cooling power was 11 to 18 $W \cdot kg_{NH4Cl}^{-1}$.

Shangai Jiao Tong University – simultaneous heat and cold production system

Xu et al [175] also studied the $MnCl_2$ and NH_4Cl system but for simultaneously heat and cold production. The reactive salts were also impregnated in expanded graphite and consolidated in the form of cylindrical blocks. The characteristics of these reactive blocks are shown in Table 2.21.

Table 2.21: Characteristics of the consolidated blocks in the $MnCl_2$ and NH_4Cl system [175].

Characteristics	$MnCl_2$ 6/2 NH_3	NH_4Cl_2 3/0 NH_3	Units
Reactive medium			
Density	470	470	$kg \cdot m^{-3}$
Mass of salt	100.09	55.31	g
% expanded graphite	33.3	33.2	

The experiments were carried out under different temperatures and at different times. The conditions of such experiments are depicted in Table 2.22. In addition, each experiment was repeated at least three times.

Table 2.22: Experimental Condition in system NH_4Cl and $MnCl_2$ [175].

No. Experiment	NH_4Cl_2 3/0 NH_3		$MnCl_2$ 6/2 NH_3		Time (h)
	Synthesis	Decomposition	Synthesis	Decomposition	
1	0	75	30	140	6
2	0	75	35	145	6
3	0	80	35	140	6
4	-5	70	30	140	6
5	5	80	35	145	6
6	0	80	35	140	11
7	-5	70	30	140	10

The results of such experiments are shown in Table 2.23.

Table 2.23: Results of the experiments in the NH_4Cl/NH_3 and $MnCl_2/NH_3$ system [175].

No. Exp.	Heat production			Cold production			COP	COPA	SCP ($MJ \cdot kg^{-1} \cdot day^{-1}$)	SCP ($MJ \cdot kg^{-1} \cdot day^{-1}$)
	$MnCl_2$			NH_4Cl						
	Q (kJ)	Tmean (ºC)	Tmax (ºC)	Q (kJ)	Tmean (ºC)	Tmax (ºC)				
1	152.1	77.2	81	56.1	-1.6	-4.1	0.35	1.3	1.12	3.04
2	155.3	78.7	82.1	53	-1.2	-3.3	0.32	1.27	1.06	3.1
3	104.4	82.4	86.2	26.9	-1	-2.7	0.24	1.16	0.54	2.09
4	127.1	72.7	76.1	36.9	-6.4	-7.9	0.27	1.22	0.74	2.54
5	150.8	83	88.1	54.1	3.9	1.9	0.34	1.3	1.08	3.01
6	141.8	81.9	84.8	48.2	-0.6	-2.4	0.32	1.28	0.48	1.42
7	153.3	72.7	77.5	51.7	-6.5	-9	0.32	1.27	0.52	1.53

SCP and SHP denote the specific cooling power and the specific heat power, respectively.

The authors prolonged the reaction time in experiments 3 and 4 to 11 h and 10 h, respectively (experiments 6 and 7), to increase the conversion of the process. In experiment 3, the reaction conversion increased from 78 % to 89 %, and the cooling effect increased 80 %. In experiment 4 the reaction conversion increased from 67 % to 86 % and the cooling effect increased 40 %. The best results were obtained when cold was produced at 0ºC and heat was produced at 75 ºC. In this condition, the COPA reached 1.3, the specific cooling power was 1.2 $MJ \cdot kg^{-1} \cdot day^{-1}$, and the COP was 0.35.

2.2.2.5 NaBr + expanded graphite / NaBr + MnCl2 + expanded graphite

Oliveira et al [176] studied a sorption system using NaBr with NH_3 for air conditioning applications and a resorption system using NaBr and $MnCl_2$ with NH_3 for simultaneous heating and cooling. The salts were impregnated in expanded graphite and consolidated in the form of cylindrical blocs. The characteristic of these blocks are showed in Table 2.24.

Table 2.24: Characteristics of the consolidated blocks for the NaBr system and the $NaBr/NH_3$ + $MnCl_2/NH_3$ system [176].

Characteristics	Air-conditioning	Heat and cold production		Units
	NaBr (5.25/0) NH_3	NaBr (5.25/0) NH_3	$MnCl_2$ (6/2) NH_3	
Reactive medium				
Density	0.58	0.31	0.31	$g.cm^{-3}$
% mass graphite	50	35	35	
Mass of salt	56.7	34.58	55.51	g

In the air conditioning system, the authors found that the composite material produced 219 and 510 $kJ \cdot kg^{-1}$ of cooling, corresponding to an evaporator temperature of 5 ºC and 15 ºC respectively, when the reactor cooling was at 30 ºC and the decomposition was carried out at 65 ºC. The specific cooling capacity and the COP were calculated for the case of an evaporator temperature of 15 ºC and a 40-minute process. The specific cooling capacity was 129 ± 7 $W \cdot kg^{-1}$ and the COP was 0.46 ± 0.01. In addition, according to the authors, the higher absorption capacity when the evaporator was at 15 ºC was not only due to the

higher equilibrium temperature drop[4], but also because the reaction occurred in conditions that allowed the formation of ammonia solution inside the block.

In the resorption system, simultaneous cooling and heating production was studied with the NaBr-reactor (decomposition) at temperatures of -5 ºC and 10 ºC while the $MnCl_2$-reactor (synthesis) was kept at 50 ºC and 70 ºC respectively. The reverse process was carried out with the $MnCl_2$ reactor (decomposition) at 165 ºC and the NaBr-reactor (synthesis) at 30 ºC. The authors found a very low COP (0.02) when the NaBr-reactor was at -5ºC and the $MnCl_2$-reactor was at 50 ºC, which was attributed to the high sensible heat load of the reactors. However, when the NaBr-reactor was at -5 ºC and the $MnCl_2$-reactor at 50 ºC, the COP reached a value of 0.21 and the COPA was 1.11.

2.2.2.6 $CaCl_2$ + $MnCl_2$ + expanded graphite

A heat transformer system based on the $CaCl_2$ and $MnCl_2$ salts was investigated by Wang C. et al. [177,178]. The performance of the system was first investigated by considering multistep reactions between $CaCl_2$ and NH_3 as follows:

$$CaCl_2{\cdot}2NH_3(s) + 2NH_3(g) \Leftrightarrow CaCl_2{\cdot}4NH_3(s) \quad (18)$$
$$CaCl_2{\cdot}4NH_3(s) + 2NH_3(g) \Leftrightarrow CaCl_2{\cdot}8NH_3(s) \quad (19)$$

In the second study, the performance of the system with a gas valve control (closed protocol) was evaluated and compared to those without gas valve control (open protocol).

In both cases, the same experimental setup and composite materials were used. The experimental setup is depicted in Figure 2.11 and consists mainly of two $CaCl_2$ reactors and one $MnCl_2$ reactor. The valve V1was the control valve in the second study.

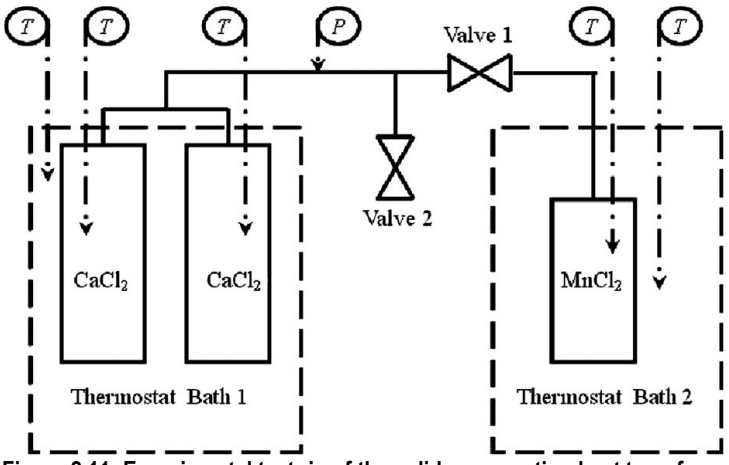

Figure 2.11: Experimental test rig of the solid-gas sorption heat transformer system [178].

The respective salts were impregnated in expanded graphite and consolidated in the form of cylindrical blocks. The manufacturing method is disclosed in [119]. The inner diameter of the reactive block was 20 mm and the outer diameter was 54 mm. The lengths of the reactive block with $CaCl_2$ and $MnCl_2$ were 160 and 120 mm, respectively. The other characteristics of the reactive blocks are presented in Table 2.25.

[4] The equilibrium temperature drop refers to the difference between the temperature of the salt and the equilibrium temperature.

Table 2.25: Characteristics of the reactive blocks for the $CaCl_2$ + $MnCl_2$ system [177].

Apparent density of the block ($kg.m^{-3}$)		Mass fraction of expanded graphite		Porosity of the reactive block				
				$CaCl_2 \cdot yNH_3$			$MnCl_2 \cdot yNH_3$	
$CaCl_2$	$MnCl_2$	$CaCl_2$	$MnCl_2$	2	4	8	2	6
200	200	0.5	0.4	0.68	0.6	0.46	0.72	0.52

In the first study, the occurrence of multistep reactions between $CaCl_2$ and NH_3 was studied experimentally and theoretically [177]. The synthesis and decomposition of $CaCl_2$ was studied for the initial states of $CaCl_2 \cdot 2NH_3$ and $CaCl_2 \cdot 4NH_3$. Depending on this initial state, the decomposition temperature of $MnCl_2$ and $CaCl_2$ varied from 90 to 120 ºC. The initial synthesis temperature varied from 25 to 30 ºC for the $CaCl_2$ reactor and from 90 to 120 ºC for the $MnCl_2$ reactor.

The authors concluded that the two reactions might occur simultaneously in the solid-gas reactor. For the initial state of $CaCl_2 \cdot NH_3$, the reaction of $CaCl_2 \cdot 4NH_3$ to $CaCl_2 \cdot 8NH_3$ only occurred when the decomposition temperature of $MnCl_2 \cdot 6NH_3$ was higher than 150 ºC. Furthermore, they concluded that for the initial state of $CaCl_2 \cdot 2NH_3$, the occurrence of the reaction $CaCl_2 \cdot (4/8)NH_3$ led to a larger temperature lift, a higher specific power and a larger system COP. However, for the initial state of $CaCl_2 \cdot 4NH_3$, the occurrence of the reaction $CaCl_2 \cdot (2/4)NH_3$ would lead to a lower specific power. Thus, the system for the initial state of $CaCl_2 \cdot 4NH_3$ was better than that for the initial state of $CaCl_2 \cdot 2NH_3$. In addition, the authors experimentally measured the heat transfer coefficient between the heat transfer fluid and the reactor and obtained a value of 150 $W \cdot m^{-2} \cdot ºC^{-1}$.

In the second study [178], the influence of a gas valve control on the performance of the heat transformer was studied. The experimental temperatures in the high pressure cycle were 120 ºC for the decomposition of $CaCl_2 \cdot 8NH_3$ and 150 ºC for the synthesis of $MnCl_2 \cdot 2NH_3$. In the low pressure cycle, the temperatures were 120 ºC for the decomposition of $MnCl_2 \cdot 6NH_3$ and 40 ºC for the synthesis of $CaCl_2 \cdot 2NH_3$. Two modes of operation were carried out in the experiments: the open protocol and the closed protocol. The difference was the control of V1 (see Figure 2.11) when the experimental test rig was transferred from the low pressure process to the high pressure process. In the open protocol, V1 was kept open; while in the closed protocol, V1 was closed at the beginning of the process. When the reactors with $CaCl_2$ were transferred to the thermostat bath at 120 ºC, the reactive salt of $CaCl_2$ was decomposed and the gas pressure in the reactors started to increase. The valve V1 was opened when the pressure reached 2.1 MPa.

In the low pressure cycle, the measured temperature lift ranged from 5 to 30 ºC in the open and closed protocols. The authors concluded that the system performance was improved with the closed protocol when the temperature difference was 30 ºC, see Table 2.26.

Table 2.26: System and performance indicators of the experimental set-up (ΔT = 30 ºC) [178].

Protocol	Heat transfer temperature difference (ºC)	SHP ($W \cdot kg^{-1}$ of $MnCl_2$-block)	COP	COP_{exp}
Open	10	235	0.17	0.22
Closed	14	248	0.2	0.25

The specific heating power (SHP) was increased by 6%, the COP was improved by 18% and the experimental COP was improved by 14%. Furthermore, the authors found that the multistep ($CaCl_2/NH_3$) reaction was not responsible for the improvement in system performance. They further concluded from the experiments that the improvement was due to the difference in gas pressure in the open and closed protocols.

2.2.2.7 $SrCl_2$ + $CoCl_2$ / $SrBr_2$ + $NiCl_2$ / $MnCl_2$ + $NiCl_2$ / + expanded graphite

Llobet et al. [146] proposed a double-effect sorption process system for cooling applications with heat recovery by direct contact with the reactors. Unfortunately, the study is published in French and therefore a clear and detailed summary cannot be given in this report. The double-effect system consists of two concentric reactors, as shown in Figure 2.12 one evaporator and one condenser.

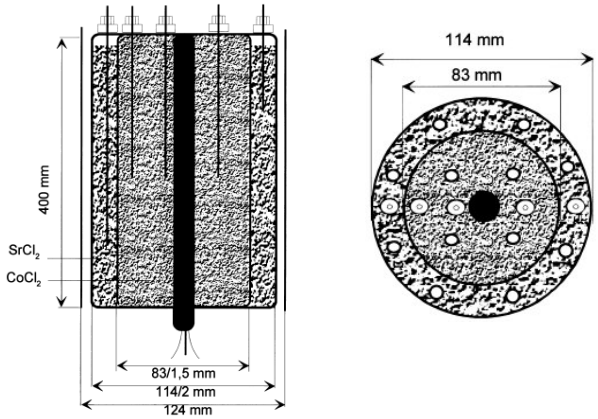

Figure 2.12: Scheme of the reactor used for the experiments [146].

The selected working pairs for the process are $SrCl_2$(8/1)NH3 and $CoCl_2$(6/2)NH_3. $SrCl_2$ is the low-temperature salt and $CoCl_2$ is the high-temperature salt. The thermodynamic cycle of the double effect by contact process is shown in Figure 2.13.

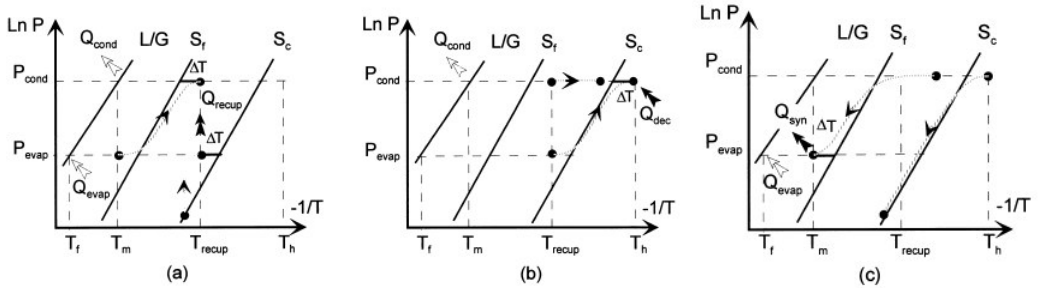

Figure 2.13: Thermodynamic cycle of the double effect by direct contact process; (a) heat recovery step: synthesis of Sc ($CoCl_2$) and decomposition of Sf ($SrCl_2$); (b) Sc decomposition step; (c) Sf synthesis step [146].

The cycle works in three steps:

- The first step is the heat recovery step that is carried out during the synthesis of $CoCl_2 \cdot 2NH_3$ and decomposition of $SrCl_2 \cdot 8NH_3$.
- The second step is the decomposition of $CoCl_2 \cdot 8NH_3$.
- The third step is the synthesis of $SrCl_2 \cdot NH_3$.

The authors claimed that the double effect by direct contact allows us to consider high energetic performances, a simple working mode and a compact installation. The results of the experiments and the reactant characteristics are shown in Table 2.27. In addition, the authors compared the results of the current system with the experimental results obtained by Nevau et al. [147] and Wagner in two different types of double-effect system. Nevau et al. [147] studied a double-effect system using $MnCl_2$ and $NiCl_2$

salts and Wagner [148] investigated a double effect system controlled by heat pipes using $SrBr_2$ and $NiCl_2$ salts. However, both studies are also reported in French and are hard to obtain or are not available. Therefore, only information from the current paper can be given for these two systems.

Table 2.27: A comparison of the experimental laboratory results of the three double-effect systems. The thermodynamic working conditions for the hot salt are the same for both the single- and double effect process [146].

	Nevau et al. [147]	Wagner [148]	Llobet et al. [146]
Mass			
Low temperature salt (ºC)	26.5 ($MnCl_2$)	2.35 ($SrBr_2$)	0.170 ($SrCl_2$)
High temperature salt (ºC)	27 ($NiCl_2$)	0.89 ($NiCl_2$)	0.270 ($CoCl_2$)
Temperature for cold production, T_f (ºC)	-5	-4	-4
Temperature regeneration (ºC)	280/10	340/8	240/7.7
$\Delta T/\Delta T_{recup}$ (ºC)	30/40	90/50	45/45
Q_{evap} (W)	1530	434	64
Specific cooling power of the salt ($W \cdot kg^{-1}$)	29	134	145
Specific heating power of the salt ($W \cdot kg^{-1}$)	-	760	1320
Experimental COP	0.21	0.38	0.25
Experimental COP simple effect	0.1	0.2	0.127

2.2.2.8 $MgCl_2$ + LiCl + metal foam

A heat transformer based on the reversible ammoniation of $MgCl_2$ and LiCl has been extensively studied at ECN by Haije et al. [124] and van der Paal et al. [192,193]. The target of the system is to upgrade the waste heat from a temperature level between 100 to 150 ºC to a temperature level between 180 to 220 ºC and thus produce medium pressure steam.

During the discharging mode (high pressure) the waste heat is used for the decomposition of $LiCl_2 \cdot 3NH_3$. The ammonia produced is then absorbed by $MgCl_2 \cdot 2NH_3$ and heat is released at a higher temperature. However, during the charging mode (low pressure), the waste heat is used to decompose $MgCl_2 \cdot 6H_2O$. The ammonia is then absorbed by $LiCl_2.NH_3$ and heat is released to the environment at ambient temperature.

In a first study [124], the feasibility of the system was studied in an experimental test rig on the scale of 1 kW heating power output at 200 ºC. The reactor was based on the concept of a tube-fin heat exchanger that includes a novel concept: heat transfer flows through hollow fins. The hollow heat exchanger fin consists of two parallel stainless steel plates that are vacuum brazed together. The space in between is filled with a metal wire mesh that serves to break up the laminar flow within the fins for better heat transfer, and increases the strength of the whole body. On the outside of both plates, the metal foam is connected using the same technique. The porosity of the foam was 92 %, the average pore diameter 0.51 to 0.05 mm, and the filament thickness 0.10 to 0.02 mm. The foam was impregnated with the salts that reduced the porosity of the whole body to 77.2 %. Each reactor was loaded with 1.8 kg of salt ($MgCl_2$ or LiCl). The experimental conditions are presented on Table 2.28.

Table 2.28: Experimental conditions used in the LiCl/$MgCl_2$ system with ammonia [124].

Temperature (ºC)			
Charging		Discharging	
LiCl	$MgCl_2$	LiCl	$MgCl_2$
20	165	150	165
20	175	150	175
20	190	150	190
20	200	155	200

The authors found that the cycling behaviour was stable for at least 50 cycles for both reactors. The peak power output at 200 ºC was about 0.8 kW and the mean power was 0.4 kW (40 min). In addition, the COP was calculated to be 0.11, which is 40 % lower than the theoretical value. The authors attributed the low COP mainly to the thermal mass of the reactor. Finally, the calculated effective thermal conductivity of the composite material was 1.5 $W.m^{-1}.K^{-1}$.

In a further study [192], the poor performance of the previous system was attributed to the degradation of the salts, salts escaping from the matrix, and the poor heat and mass transfer to and from the salts. To overcome these problems, a new method was developed for impregnating the salts into the metal foam. The design of the reactor was based on a shell and tube type of heat exchanger in which each fin supports a sheet of metal foam that contains salt. The $MgCl_2$ reactor was charged with 2.49 kg and the LiCl reactor was charged with 1.21 kg. The temperature of the LiCl reactor was varied between 20 ºC and 80 ºC for the $MgCl_2$ reactor at 130 ºC and between 20 ºC and 130 ºC for $MgCl_2$ at 180 ºC and 200 ºC.

The authors found that only 40 % of the $MgCl_2 \cdot 2NH_3$ absorbed ammonia to form $MgCl_2 \cdot 6NH_3$. This was attributed to the short cycle time (1 h). The system was stable for at least the 100 cycles performed with an average heat in/output of about 300 W and a peak power in/output of about 600 W. In addition, the authors suggested that the regeneration of $MgCl_2 \cdot 6H_2O$ was limited by the heat transfer. The thermal conductivity of the reactive bed was estimated to be around 0.5 $W \cdot m^{-1} \cdot K^{-1}$, which is much lower than the previous results. Finally, the calculated COP was close to 0. The low value was also attributed to the large thermal mass of the reactor.

In a recent study [193], the absorption of ammonia by $LiCl \cdot NH_3$ at 50 ºC with an ammonia pressure of 540 kPa was studied at 50 ºC. The authors found that only 36 % of the theoretically available amount of ammonia was absorbed in the 10 cycles performed. Furthermore, the authors observed the formation of the liquid phase at this pressure. This phase change was also found in a previous study [273].

2.2.2.9 $CaCl_2$ + expanded graphite

Oliveira et al. [113,114] and by Li et al. [179] studied a consolidated composite material made of expanded graphite powder and impregnated with $CaCl_2$ for refrigeration systems.

In the first study by Oliveira et al. [113], the block of composite material was formed after compression under a pressure of 10 MPa to enhance its heat transfer properties. According to a previous study by K. Wank et al. [115], the consolidated composite can have a thermal conductivity that is 30 times higher than the unconsolidated composite (powder). The apparent density of the expanded graphite was 0.2 $g \cdot cm^{-3}$ and that of the block was 0.56 $\pm$ 0.01 $g \cdot cm^{-3}$. A photograph of the block after compression is shown in Figure 2.14. The reactor employed four blocks.

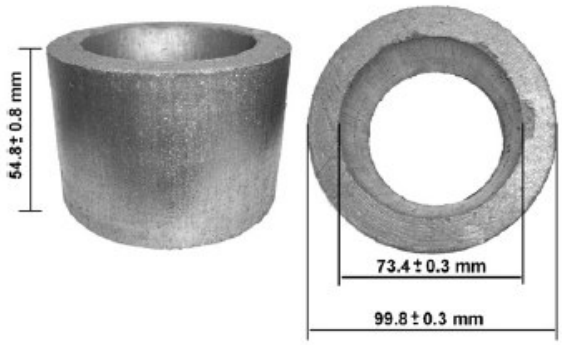

Figure 2.14: Consolidated composite blocks [114].

Two experiments were carried out in a test rig with temperature constraints in the reactor of 98 ºC for the decomposition and 30 ºC for the synthesis. However, the initial temperature in the evaporator was 0 ºC in a first experiment and -15 ºC in a second experiment. In addition, the synthesis constraint in the first experiment and the decomposition constraint were not kept constant during the experiments.

The results showed that conversion was complete (98 %) for both decomposition and synthesis, and that the agglomeration phenomenon was avoided. However, the authors observed that the blocks expanded. The inner radius changed from 73 mm to 60 mm, the apparent density of the block from 0.56 $g \cdot cm^{-3}$ to about 0.34 $g \cdot cm^{-3}$ and the porosity increased up to 0.53. The pressure drop was measured for the first experiment and was almost negligible. The maximum pressure drop was 5.2 kPa, and the measured average value was 1.7 kPa. However, the authors stressed that the heat transfer could be improved, as the temperature difference inside the block could reach 15 ºC.

In the first experiment, the highest specific cooling capacity was 415 $W \cdot kg^{-1}$ obtained at 35 minutes. At this moment, the reactor coolant temperature was 42 ºC, the evaporation temperature dropped to -5 ºC and the overall conversion was 0.74. When the conversion was completed (100 min), the average specific cooling power was 306 $W \cdot kg^{-1}$. In the second experiment, the highest specific cooling power was 255 $W \cdot kg^{-1}$ at a synthesis time of 40 minutes. At this moment, the overall conversion was 0.48 and the evaporation temperature dropped to -22 ºC. The average specific cooling power measured for the whole process was 194 $W \cdot kg^{-1}$ (140 min). The calculated COP ranged from 0.36 to 0.46 when the overall conversion was equal to or higher than 0.5.

In another study by Oliveira et al. [114], the composite blocks were manufactured with an apparent density of expanded graphite equal to 0.29 $g \cdot cm^{-3}$. The reactor was charged with two composite blocks, each one weighed 113 g. The synthesis experiments were carried out at an initial bed temperature of 90 ºC. The reactor coolant temperature was varied from 20 to 30 ºC and the evaporator temperature from -11 to -22 ºC. The dehydration experiments were carried out at 150 ºC. The authors obtained a specific cooling power and cooling power density above 1000 $W \cdot kg_{salt}^{-1}$ and 290 $kW \cdot m^{-3}$, respectively, in the range of evaporation temperature normally used for iced production (-10 ºC to -20 ºC). These results were obtained when the temperature of the coolant utilized to remove the heat of the reaction from the reactive bed was between 20 ºC and 30 ºC. Furthermore, the authors experimentally identified a heat transfer coefficient of the bed of 787 $W \cdot m^{-2} \cdot ºC^{-1}$ when the salt was in the form of $CaCl_2 \cdot 2NH_3$. The calculated COP was 0.35 when the consumed mass of NH_3 was 0.8 $kg \cdot kg_{salt}^{-1}$ (87 % conversion, $CaCl_2 \cdot 2NH_3$ to $CaCl_2 \cdot 6NH_3$).

Li et al. [179] tested also a $CaCl_2$/expanded graphite adsorption refrigerator. The refrigerator test-rig included two adsorbers, a cooler, a vapour generator, a pump, two condensers, two evaporators, a three-way vapour valve, a three-way water valve and an ammonia valve as illustrated in Figure 2.15.

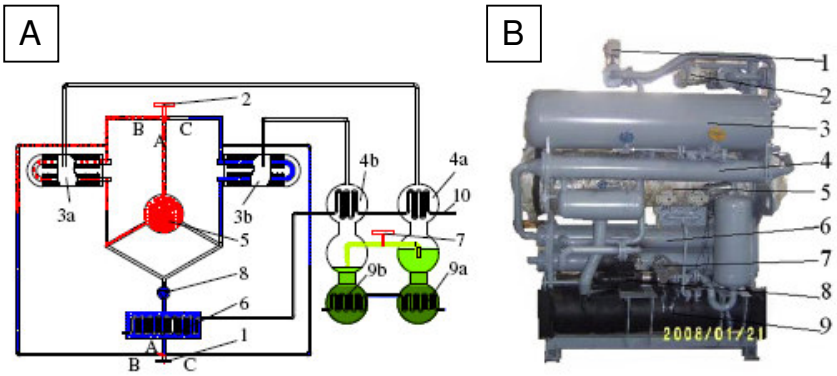

Figure 2.15: Structure of refrigerator. (A) Schematic diagram. (B) Photo of refrigerator. (1) water valve, (2) vapour valve, (3) adsorbers, (4) condensers, (5) vaporgenerator, (6) cooler, (7) ammonia valve, (8) pump, (9) evaporators and (10) cooling water [179].

The structure of each adsorber is shown in Figure 2.16, A. There were 40 tubes in each adsorber, which were composed of 37 adsorption unit tubes (Figure 2.16, B) and 3 plain tubes. The length of the fin tube was 1500 mm, the fin thickness was 0.3 mm, the external diameter of the fin was 58 mm, the internal diameter of the fin was 28 mm and the fin pitch was 2.5 mm.

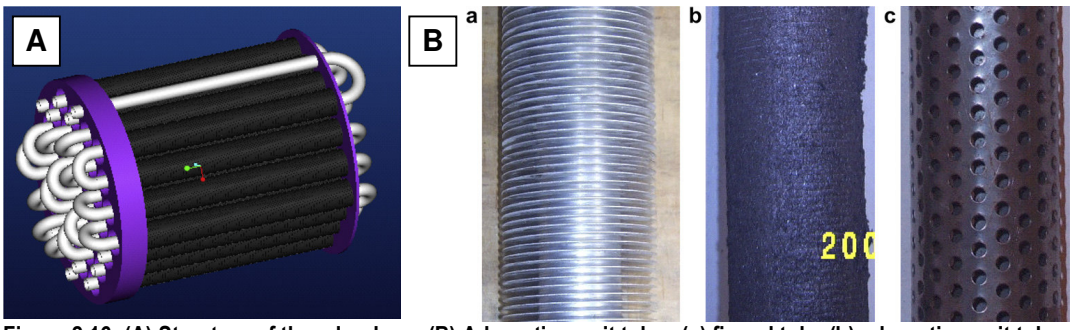

Figure 2.16: (A) Structure of the adsorbers. (B) Adsorption unit tubes (a) finned tube (b) adsorption unit tube after filled compound adsorbent solution (c) adsorption unit tube after manufacturing [179].

The mass ratio of the calcium chloride and expanded graphite was about 4:1. The mass of the compound adsorbent in each adsorption tube was 0.94 kg, which contained about 0.75 kg calcium chloride. Thus, the total amount of calcium chloride contained in each adsorber was about 27 kg.

The effect of the cycle time on the performance of the refrigerator was studied for cycle times ranging from 16 min to 28 min, at evaporation temperature of -15 ºC, cooling water temperature of 25 ºC, mass recovery time of 45 s. The results of these experiments are shown in Table 2.29.

Table 2.29: Thermal performance variation of $CaCl_2$-expanded graphite/NH_3 refrigerator with cycle time [179].

Cycle time (min)	Highest heating temperature (ºC)	Refrigerating power (kW)	SCP ($W \cdot kg^{-1}$)	COP
16	121.7	10.1	374.1	0.24
19	126.7	10.7	396.4	0.26
22	130.4	10.8	400.0	0.26
25	140.3	11.4	422.2	0.27
28	152.7	11	407.4	0.26

In addition, the previous results were completed with the obtained previously by Xia et al. [180] in the same refrigerator but under lower heating source temperature and depicted in Table 2.30.

Table 2.30: Thermal performance variation of $CaCl_2$-expanded graphite/NH_3 refrigerator with cycle time [179,180].

Cycle time (min)	Highest heating temperature (ºC)	Refrigerating power (kW)	SCP ($W \cdot kg^{-1}$)	COP
15	101.4	7.8	281.2	0.296
20	103.2	8.3	299.5	0.316
25	110.6	8.4	302.7	0.319
30	114.5	7.7	292.8	0.294
35	117.3	7.6	289.0	0.288

In both cases, the optimum cycle time was found to be 25 min. The average SCP and the COP were 422.2 $W \cdot kg^{-1}$ and 0.27, respectively, in the experiments carried out by Li et al. [179], and were 302.7 $W \cdot kg^{-1}$ and 0.319 respectively, in the experiments carried out by Xia et al. [180].

Further, the effect of mass recovery time on the refrigerator performance was studied also at evaporation temperature of -15 ºC, cooling water temperature of 25 ºC and cycle time of 25 min. Table 2.31, shows the results of such experiments.

Table 2.31: Thermal performance variation of $CaCl_2$-expanded graphite/NH_3 refrigerator with mass recovery time [179].

Mass recovery time (s)	Highest heating temperature (ºC)	Refrigerating power (kW)	SCP ($W \cdot kg^{-1}$)	COP
30	138	10.8	374.1	0.24
35	137.6	11.1	396.4	0.26
40	141.4	11.1	400	0.26
45	140.3	11.4	422.2	0.27
50	136.4	11.2	407.4	0.26

The authors found that the optimal mass recovery time was 45 s.

Finally, the effect of evaporation temperature and cooling water temperature on the refrigeration power variation were studied for evaporation temperatures ranging from -25 to -10 ºC and for cooling water temperatures ranging from 20 to 35 ºC as illustrated in Figure 2.17, A and B.

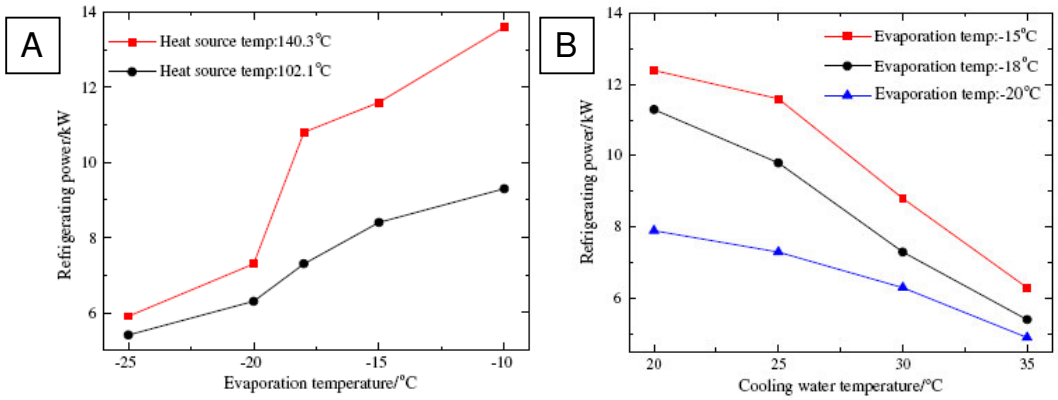

Figure 2.17: (A) Refrigeration power variations with the evaporation temperature. (B) Refrigeration power variations with the cooling water temperature [179].

The authors found that an increase of 1 ºC on the evaporation temperature could cause approximate 8.7 % and 4.8 % improvement of the refrigeration power at higher heat source temperature of 140 ºC and lower heat source temperature of 120 ºC, with the same cooling water temperature, mass recovery time and heating/cooling time. On the other hand, a decrease of 1 ºC in the cooling water temperature, the refrigerating power of the refrigerator could increased 6.5 %, 6.3 % and 4.0 % at evaporation temperatures of -15 ºC, -18 ºC and -20 ºC, respectively.

2.2.2.10 $MnCl_2$ + expanded graphite

T.X. Li et al [118] studied the performance of a consolidated composite material made of expanded graphite and $MnCl_2$ for the deep-freezing process (-35 ºC). The apparent density of the consolidated composite block was 300 $kg \cdot m^{-3}$, with a mass fraction of graphite inside the block of 0.37. The decomposition of $MnCl_2 \cdot 6NH_3$ was carried out at 180 ºC, whilst the condenser was kept at 30 ºC. These conditions were maintained for all the experiments. The synthesis of $MnCl_2 \cdot 2NH_3$ was carried out at different evaporator temperatures, ranging from 0 to -35 ºC. The reactor coolant temperature was kept at 25 ºC and the initial reactor temperature was 180 ºC.

The authors measured large temperature gradients inside the block, due to heat transfer limitations. A maximum temperature of 50 ºC was measured between the outer part and the inner part of the bed when there was no reaction inside the bed. After 30 minutes, the synthesis conversion and the average specific cooling power varied from approximately 53 % to 100 % and from 200 $W \cdot kg^{-1}$ to 700 $W \cdot kg^{-1}$, respectively, when the evaporation temperature ranged from -35 to 0 ºC. Furthermore, the calculated COP for the deep-freezing process was 0.34 at an evaporation temperature of -30 ºC.

2.2.2.11 LiCl + expanded graphite

Kiplagat et al. [181] proposed consolidated composite materials made of expanded graphite powder impregnated with LiCl salt for use in solar powered adsorption ice makers. The salt was impregnated into the expanded graphite according to the methodology given by [113]. The experiments were carried out with a composite material comprising 42.11 g of expanded graphite and 41.11 g of LiCl. The results showed that more than 75% of $LiCl \cdot 3NH_3$ was converted to $LiCl \cdot 4NH_3$ after 30 minutes at an evaporation temperature of -10 ºC and -5 ºC and an absorption temperature between 25 ºC and 30 ºC. However, low conversions of less than 30 % were obtained at an evaporation temperature of 5 ºC and 10 ºC when the LiCl-reactor was at 35 ºC and 30 ºC, respectively. The authors found that conversions ranging from 95 to 96 % can be achieved when the process time is increased to 10 hours.

For the decomposition process, more than 80% conversion was achieved in 30 minutes of operation when the temperature ranged between 75 ºC and 80 ºC, and the condensation temperature between 25 ºC and 35 ºC. However, only an 11 % conversion was obtained at a decomposition temperature of 70 ºC and a condenser temperature of 25 ºC. When the reaction time was increased to 6 hours, the conversion rose to 90% under the same conditions.

The average specific cooling power varied from 91 W to 117 W per kg of the block. The highest value was obtained at an evaporation temperature of -5 ºC and at a reactor temperature of 25 ºC. The calculated COP was nearly constant at 0.47.

The proportion of expanded graphite in the composite material was also studied for a fixed amount of LiCl of 42.11 g. The authors found that the proportion of expanded graphite influenced the cooling power per unit mass of salt. The highest specific cooling power was obtained with the composite that had the highest amount of expanded graphite (42.11 g). However, they found that there was no influence on the cooling power per unit mass of block.

2.2.2.12 $SrCl_2$ + expanded graphite

Chen et al. [182] studied a consolidated material made of $SrCl_2$ impregnated with 35 % expanded graphite for use in solar powered adsorption ice-makers. Unfortunately, the research was reported in Chinese and only the information from the English abstract can be given.

The calculated average specific cooling power and COP of solar ice-making chemical heat pump was 738 $W \cdot kg^{-1}$ and 0.435, respectively.

2.2.2.13 $NiCl_2$ + expanded graphite

Cerknenik et al. [194] investigated a device based on the $NiCl_2(6/2)NH_3$ system with two reactors working in counter-phase. The device was tested as part of a cascading triple-effect sorption device, to increase the COP of the cooling system (see Figure 2.18). The cascade cooling device is based on coupling a

double-effect LiBr-H_2O cooling device as the bottom part of the cascade with the $NiCl_2(6/2)NH_3$ cooling device as the top part of the cascade. The $NiCl_2(6/2)NH_3$ cooling device can be used at higher temperatures (above 200 ºC) at which efficient absorption devices cannot be used.

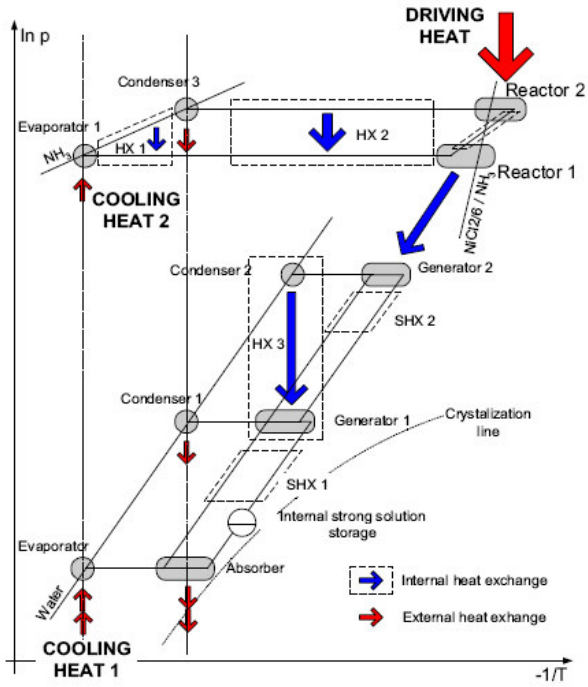

Figure 2.18: Cascading sorption cycle in Pressure-Temperature diagram [194].

Driving heat to the cascade is brought into the system in the $NiCl_2(6/2)NH_3$ device by heating the reactor R2 to perform the decomposition process. At the same time, the synthesis process is carried out in reactor R1 and the released heat is used to drive the absorption LiBr/H_2O cooling device. The heat transfer between the devices is performed by a loop-type heat pipe.

The main part of the $NiCl_2(6/2)NH_3$ device was the reactors, each of which consisted of 27 vertical reaction tubes. The heat pipe evaporator was located in the middle of each tube. The rest was filled with the consolidated composite material of expanded graphite impregnated with the reactive salt. The reactors were heated by external heating of the reactors tubes.

The authors studied the cyclic performance of the device. The two reactors were constantly switching between decomposition and synthesis phase. The decomposition temperature was 300 ºC and the synthesis temperature was 200 ºC. The condensation ammonia pressure was about 1000 kPa (10 bar) and the evaporation ammonia pressure was about 450 kPa (4.5 bar). The operation of the device was cut into half-cycles, in which the reactors performed one reaction phase. The average calculated values for the heat flows and the COP are presented in Table 2.32 for the 26 half-cycles that were measured.

Table 2.32: Calculated values from the measurements on the $NiCl_2(6/2)NH3$ device [194].

Phase	Qevaporation (kJ)	Qcondenation (kJ)	Qsynthesis (kJ)	Qdecomposition (kJ)	Qloss (kJ)	COP
R1 DEC	5609	5764	29981	24759	4488	0.19
R1 SYN	4488	5857	30974	19570	4403	0.15
Mean	5048	5810	30477	22165	4446	0.17

R1 DEC: R1 in decomposition phase, R2 in synthesis phase.
R1 SYN: R1 in synthesis phase, R2 in decomposition phase.

The authors found that reactor R1 produced less cooling energy than reactor R2, which was attributed to the loss of ammonia mass in the device. The average calculated COP was about 0.17, which was lower than the expected COP value of 0.25. According to the authors, a COP value over 0.2 can be reached with minimization of heat loss to the environment and reduction of the inert mass of the reactors.

2.2.2.14 $BaCl_2$ + expanded graphite

Le Pierrès et al. [149-152] studied two cascade chemical heat pumps using $BaCl_2$ as the reactive salt. The purpose of this study was to cool down a box of 0.53 m^3 (560 L) to about -25 ºC using only low grade heat produced by two simple flat plate solar collectors.

The experimental prototype is shown in Figure 2.19 and the working principle is explained with the experimental results.

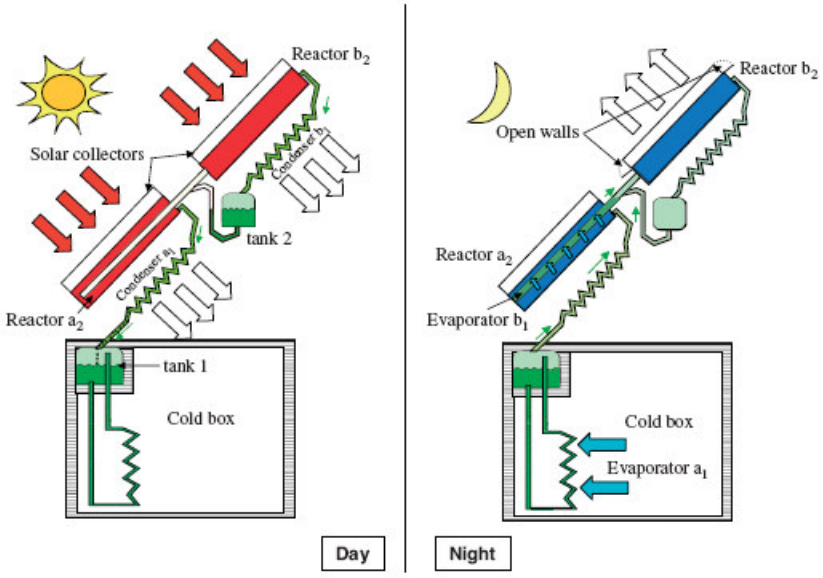

Figure 2.19: Simplified scheme of the prototype during the regeneration and cold production phases [149].

The reactive beds also consist of anhydrous salt inserted into consolidated reactive blocks of expanded graphite. The main characteristics of the prototype are shown in Table 2.33.

Table 2.33: Characteristics of the prototype based on $BaCl_2$ + expanded graphite [151]

Characteristics	A	b	Units
Reactive medium			
Moles of salt	41	82	moles
Mass of salt	5.6	11.3	kg
Mass composite	12.7	25.4	kg
% EG	55.7	55.7	
Prototype			
Area solar collector	2	3.8	m^2
Area evaporators	5	1	m^2
Area condensers	9	22	m^2

The experiments were carried out in Perpignan (South of France) from 24 May to 28 July 2005 and from 9 September to 10 October 2005. The performance of the prototype was described for the experiments

carried out on 3 and 4 of July 2005 [151]. The first day was warm and sunny and the second day was cloudy and milder.

The evolution begun at sunrise (t=0). The two reactors, a2 and b2, were heated up and once the temperature reached about 50 ºC the decomposition of $BaCl_2 \cdot 8NH_3$ started. The desorbed ammonia was condensed in the condensers, a1 and b1, at ambient temperature. Then, a plateau was observed in the temperature evolution, as the heat absorbed by the solar collectors was mainly used by the endothermic decomposition process. The decomposition rate at reactor a1 decreased when the content of NH_3 in $BaCl_2$ was about 20 % and the temperature of the reactor a1 rose again to over 130 ºC. The plateau temperature was longer for reactor b2, due to the lower efficiency of this collector. The decomposition of the salt was finished at 8 h.

During the daytime (0-15 h), evaporator b1 is empty and its temperature follows the temperature of reactor a2 exactly. In addition, evaporator a1, inside the cold box, was heated slowly from -23 to 5 ºC.

After 8 h, the solar radiation started to decrease and after 11 hours the reactors started to cool down progressively. Consequently, the pressure also decreased. When the pressure in evaporator b1 became lower than the pressure in tank 2, ammonia, which was stored in tank 2 at ambient temperature, flowed to b1 through the check-valves (not shown in Figure 2.19). Thus, the temperature in evaporator b1 decreases strongly at 14 h and the synthesis reaction begins in reactor a2, as the reaction heat can be transferred from a2 to b1.

The night phase began at sunset (15 h) with the opening of the side walls of the secondary solar collector in order to enhance b2 cooling. Thus, there was an abrupt decrease in fin temperature at 15 h, toward the ambient temperature. The salt in b2 began to react with gaseous ammonia and the reaction heat was rejected to the environment. Pressure then decreased in system b and the evaporation rate of ammonia in b2 was enhanced. This evaporation absorbs heat from reactor a1 through the evaporator walls. Consequently, the temperature of reactor a1 decreased below the ambient temperature to about 10 ºC (24 h). The synthesis reaction in a1 proceeded from 14 h to 27 h and a maximum conversion of about 65 % was achieved in reactor a2. Evaporator a1 was cooled down to about -22 ºC.

The evolution during the second day was similar to the first day. However, the performance of the system decreased, since the weather conditions were worse than on the first day. The decomposition process stopped after 6 hours (31 h), as the temperatures of the reactors remained between 50 ºC to 60 ºC during the whole day. The content of NH_3 in $BaCl_2$ was about 30 %. During the night, the cold box was cooled down to -10 ºC (38 h). The temperatures of reactor a2 remained at ambient temperature.

The authors found that the process's ability to produce deep-freezing temperatures depends strongly on the solar irradiation. During the 93 days of measurements, the lowest temperature achieved by evaporator a1 was -31 ºC. Temperatures lower than -20 ºC were achieved mainly when the solar irradiation was higher than 18 $MJ \cdot m^{-2} day^{-1}$ and during 72 % of the night. The cold box temperatures were always between 3 ºC and 6 ºC higher than those of the evaporator a1. In addition, the authors found that the heat losses of the cold box were 65 W, instead of the 40 W calculated in the design phase.

Finally, the authors plan to improve the cold box insulation by the use of a PCM. This would ensure a low temperature during the whole day.

Shanghai Jiaotong University

Chen et al. [183] studied a consolidated composite material made of $BaCl_2$ impregnated with expanded graphite for use in a solar-powered sorption air-conditioning system. Unfortunately, the research was reported in Chinese and only the information from the English abstract can be given.

The values of COP and average specific cooling power reached 0.5 and 192 $W \cdot kg^{-1}$, respectively, at evaporation temperature of 15 ºC, at heating water temperature of 80 ºC and cooling water temperature of 30 ºC.

2.2.2.15 $BaCl_2$

A solar-assisted thermo-chemical refrigerator using the barium chloride-ammonia system was studied experimentally by Rivera et al. [98]. The decomposition of $BaCl_2 \cdot 8NH_3$ was carried out in a temperature range from 70 to 95 ºC (heating fluid) and the condenser temperature was kept at 23 ºC. The authors found that the decomposition temperature was about 53 ºC in the middle of the reactor for a heat transfer fluid (water) temperature of 70 ºC and 95 ºC. During the synthesis, the evaporation pressure remained almost constant at about 250 kPa and the authors observed that the evaporation temperature varied from -8 to 0 ºC for approximately 1.5 hours.

2.2.2.16 $CoCl_2$ + activated carbon

Aidoun and Ternan [125,195-197] experimentally investigated a chemical heat pump based on a $CoCl_2$-activated carbon system with NH_3 for heating and cooling in the food processing industry. The experiments were carried out in a cylindrical packed bed reactor with an inner diameter of 44.5 mm and a length of 1.372 m. The reactor was loaded with 1.7 kg of the composite material, which was manufactured by impregnation of $CoCl_2$ on carbon fibres in a mass ratio of 70:30.

The first study [125] was focused on the decomposition of $CoCl_2 \cdot 6NH_3$. The reactor was weighed continuously during the decomposition reaction, thereby providing an instantaneous measurement of the reaction rate that was independent of the heat transfer measurements. The typical operating conditions were a reactor pressure of 1000 kPa (decomposition); 250 kPa (synthesis) and a cooling water temperature between 5 ºC and 30 ºC. Once enough ammonia gas had been formed in the reactor to exceed the desired 1000 kPa pressure, the connecting valve between the reactor and the condenser was opened and the decomposition started (23 min). The heat input to the reactor was 2000 W.

The power densities measured during the decomposition reaction had values of 280 $kW \cdot m^{-3}$, which were sustained for 30 minutes. However, the authors observed that the total weight change of the reactor during the decomposition decreased after a few months of operation. This was attributed to the salt degradation. In previous studies carried out at CanmetENERGY [95,195], it was found that there was a threshold temperature beyond which degradation occurred. Under some conditions, the compound $CoCl_2 \cdot 2NH_3$ was found to be unstable at approximately 300 ºC. The instability was explained in terms of a combination of the following three reactions:

$$2NH_3 \Leftrightarrow N_2 + 3H_2 \quad (20)$$
$$CoCl_2 + H_2 \Leftrightarrow Co + 2HCl \quad (21)$$
$$HCl + NH_3 \Leftrightarrow NH_4Cl \quad (22)$$

Although the equilibrium reaction (20) is not favourable until the temperature exceeds 500 ºC, a small amount of hydrogen can be formed. The hydrogen can then react with $CoCl_2$ according to (21) to produce the weight loss that was observed. The maximum temperature measured in the reactor was below 250 ºC. However, the authors suggested that some temperature peaks at locations adjacent to the heating element may have caused this degradation.

The second study [196] was focused on the hydration of $CoCl_2 \cdot 2NH_3$. The initial reactor pressure was 101 kPa. The ammonia vapour generated in the evaporator was first fed into the reactor via a pressure control valve set to maintain the reactor at a constant pressure of approximately 450 kPa. The prevailing

evaporator pressure was in the range of 700-795 kPa. The reactor cooling maintained the temperature of the reactor below the equilibrium temperature of the salt (150 ºC, 450 kPa), thereby thermodynamically favouring the synthesis reaction. The maximum temperature reached in the reactor was in the range of 80 ºC to 100 ºC.

The authors measured the power density of 235 $kW \cdot m^{-3}$ and the apparent overall heat transfer coefficient varied from 35 to 350 $W \cdot m^{-2} \cdot K^{-1}$ during the synthesis. Furthermore, the instantaneous reaction rate that was measured by weighing the reactor throughout the course of the synthesis was found to be virtually the same as the rate that heat was transferred to the cooling water stream. Therefore, the authors suggested that the rate controlling step could be the diffusion of ammonia rather than the heat transfer, as demonstrated experimentally.

In a further study on the same test-rig [197], the authors determined the thermal inertia of the reactor as the difference between the instantaneous heat generated by the synthesis and the heat transferred to the reactor cooling. The authors found that the steady state approach to determining the overall heat transfer coefficient did not apply to the unsteady-state process. Therefore, the unsteady-state data were expressed in terms of an instantaneous overall heat transfer coefficient that varied with cycle time by a factor of seven from the minimum to the maximum (~ 50 to 350 $W \cdot m^{-2} \cdot K^{-1}$). Furthermore, the maximum heat flux occurred when the overall heat transfer coefficient had its smallest value. The authors suggested that the instantaneous values of the overall heat transfer coefficient measured in this study could be applied to the performance analysis of larger reactors.

2.2.2.17 $BaCl_2$ + vermiculite

Veselovskaya et al. [204,205] studied a composite made of $BaCl_2$ and vermiculite for a sorption chiller under typical air conditioning conditions. The authors chose vermiculite as the porous matrix because of its macroporous structure, which was expected to prevent agglomeration of the salt and improve the mass transfer. The composite material was prepared at the Borestov Institute of Catalysis and presented in [127,129]. The salt content in the composite is 45 wt. % and the total mass of the composite loaded inside the reactor was 570 g. The grain size was 1-2 mm. The reactor is a nickel brazed stainless steel design with 29 layers of composite material each 4 mm thick. Each layer was separated by stainless steel plates which were constructed from chemically etched shims with 0.5 mm square water flow channels on a 1mm pitch.

Generally, the experiment were conducted at an evaporation temperature of 10 ºC, corresponding to an ammonia pressure of 584 kPa while the reactor cooling was kept at 30 ºC. The decomposition was carried out at 90 ºC and the condenser was kept at 30 ºC, corresponding to an ammonia saturation pressure of 1.12 MPa. However, to study the influence of the driving temperature (the equilibrium temperature drop) on the system performance, the authors carried out experiments in which they varied one of the previous parameters. One experiment was carried out at an evaporation temperature of 15 ºC, another at a condenser temperature of 18 ºC and another at a decomposition temperature of 80 ºC. In addition, they also studied the influence of the sorption time on the specific cooling power (SCP) and the COP. Since the rate of sorption tends to decrease in the course of time, the SCP falls with the increase of the sorption time. Nevertheless an increase in sorption time results in an increase in the conversion and consequently in an increase of the COP. However, the values of COP obtained from the experiments were almost constant for sorption times between 6 min and 12 min, varying from 0.53 to 0.55. In addition, these values were very close to the ideal COP of 0.6. However, the authors found that the SCP depended strongly on the driving temperature and the cycle duration. For decomposition temperatures of 80 ºC and 90 ºC, the specific cooling power ranged from 300 to 680 $W \cdot kg^{-1}$.

2.2.2.18 $CaCl_2$ / $BaCl_2$ + $NiCl_2$ / + $MnCl_2$ +carbon fiber "Busofit"

At the Luikov Heat & Mass Transfer Institute (Belarus), research has been focused on ammonia sorption by composite materials made of $CaCl_2$, $NiCl_2$ and $MnCl_2$ impregnated in "Busofit" carbon fibres. These composite materials were suggested due to their stability, low cost and suitable temperature range. In addition, the composite, compared to salt systems alone, accelerates the sorption rate, improves the total absorption capacity, makes the hysteresis narrower, partially compensates for the expansion of the salt and eliminates the contact of corrosive substances with the wall, Aristov et al. [35]. During the regeneration phase, a solution of the salt is formed due to ammonia capillary condensation. However, this was found to promote or stimulate the distribution of the salt micro-crystals through the whole volume of the bed (liquid motion through the reactive bed due to capillary forces).

The experiments were carried out in cylindrical reactors using an inner heat pipe as the heat exchanger. Metal fins were fixed on the heat transfer surface to increase the heat transfer between the reactive bed and the heat pipe envelope. Further details on the experimental test rigs can be found in [131,199-201].

In a first study Vasiliev et al. [131,199,200] performed experiments in a single-stage system and in a double-stage system. The experiment in a single-stage system was carried out with $CaCl_2$ impregnated in Busofit. The amount of $CaCl_2$ was 0.32 kg and that of Busofit was 0.75 kg. The experiments were carried with desorption temperature of 120 ºC, condenser temperature of 50 ºC and evaporation temperature of -18 ºC. The cycle time of the refrigeration was 25-30 min and the calculated COP was 0.43. On the other hand the experiments in a double-stage system were carried out with $BaCl_2$ + Busofit and $NiCl_2$ + Busofit. The $BaCl_2$-reactor was charged with 120 g of the composite material (50 % Busofit) and the $NiCl_2$-reactor was charged with 135 g of the composite material (48 % Busofit). During the decomposition of $NiCl_2$-Busofit and consequent synthesis of the $BaCl_2$-Busofit the maximum temperatures of the sorbent beds were 240 ºC in the $NiCl_2$-reactor and 50 ºC in the $BaCl_2$-reactor. The total time was about 40 min (30 minutes of heating + 10 minutes of adiabatic conditions). On the other hand, during the reverse cycle, the temperature of the $BaCl_2$-reactor (decomposition) decreased from 28 ºC to 0 ºC in 3 min and then was constant during 7 min whereas the temperature of the $NiCl_2$-reactor (synthesis) decreased from 240 ºC to 130 ºC in 3 min with the water vapour generation (with a temperature drop inside the sorbent bed of 40 ºC), subsequently the temperature field remained nearly constant for about 7 min. The refrigeration COP of the system during the experiment was 0.44, while the heat pump COP was near 1.44.

Vasiliev et al [202] performed a further experiment with the composites of $BaCl_2$ + Busofit and of $NiCl_2$ + Busofit in a double-stage system. The $BaCl_2$-reactor was charged with 610 g of the composite material (56 % Busofit) and the $NiCl_2$-reactor was charged with 430 g of the composite material (58 % Busofit). The temperature profile measured during the cycle was similar to that of the previous experiment [131], however, in that case, the calculated heat pump COP was about 1.2 instead of 1.44.

Further experiments were carried out with a three cascade system comprising a high temperature sorbent ($NiCl_2$-Busofit/NH_3), a medium-temperature sorbent ($MnCl_2$-Busofit/NH_3), a low-temperature sorbent ($BaCl_2$-Busofit/NH_3) and an evaporator/condenser (NH_3). The experiments were carried also by Vasiliev et al. [202] but the information is also extracted from the review of Aristov and Vasiliev [203]. Two prototypes with different working principles were used in the experiments. In the first prototype, the Busofit composites based on $NiCl_2$, $MnCl_2$ and $BaCl_2$ were decomposed at 230 ºC, 180 ºC and 90 ºC respectively by the waste gases of internal engines (230 ºC and 180 ºC) or by hot liquid from the cooling system engine (90 ºC). The desorbed ammonia was condensed in the condenser. In the reverse cycle, the sorption process was carried out simultaneously for the three reactors and the evaporator decreased to -3 ºC (refrigeration). The calculated COP was 0.41.

The second prototype was a more complex system comprising 4 steps. In the first steps, the Busofit composite based $MnCl_2$ and $NiCl_2$ were decomposed at temperature between 400 and 450 ºC and the

ammonia was part condensed in the condenser and part sorbed by $BaCl_2$-Busofit. In the second step the $MnCl_2$ and $NiCl_2$ reactors were separated from the condenser using a valve and started to cool down. Then $BaCl_2$-Busofit was decomposed at 95 ºC using the hot liquid from the cooling system engine (95 ºC) and the ammonia flowed to the condenser. In the third step, the $MnCl_2$ and $NiCl_2$ reactors reached ambient temperature. The $BaCl_2$-reactor was separated from the condenser by a valve and the process of cooling of the $BaCl_2$-reactor (the process of refrigeration) with desorption of ammonia began, since the stronger sorbents in the $MnCl_2$ and $NiCl_2$ reactor take up ammonia. Finally in the fourth step, the valves were opened and the sorption of ammonia began for the three absorbents. The refrigeration process with the evaporation of ammonia began.

The cold produced in the evaporator cooled water down to 10 ºC (200 W). The heat power input in the $MnCl_2$ and $NiCl_2$ reactors was 400 W per absorber. The value of COP for refrigeration calculated in the second prototype was 0.62.

2.2.2.19 $CaCl_2$ + activated carbon

The $CaCl_2$-activated carbon system with NH_3 has been extensively studied at the Shanghai Jiao Tong University (China) by Wang L.W. et al. [120,184,185], Lu et al. [186,187] and Li et al. [188,189] for ice production in fishing boats. The first studies [120,184] were focused on finding the optimum method for preparing the composite material and comparing its performance to other sorbent materials. Solidified $CaCl_2$-activated carbon was found to perform best. The mass ratio between the mass of $CaCl_2$ and the activated carbon was 4:1, and cement was used to bind the two substances together.

The next studies [185] were focused on the performance of the material under practical conditions. The authors designed a heat pipe sorption ice maker test rig to perform the experiments. The test rig consisted basically of two sorption reactors, a condenser, an evaporator, a cooler and a heating boiler, among other components. Further details of the test rig are given in [185]. In addition, the system incorporated heat and/or mass recovery, depending on the study, to improve the coefficient of performance (COP) and the specific cooling power (SCP), respectively. The working principle of heat and mass recovery can be found elsewhere [274,275] among the previous papers [184-186,188,189]. However, heat recovery consists of reusing some part of the sensible heat and the heat from the synthesis, while mass recovery consists of conveying ammonia from the high pressure reactive bed to the low pressure reactive bed for some period of time.

L. W. Wang et al. [185] studied the performance of the system using 1.88 kg of $CaCl_2$ with the incorporation of a mass recovery system. The system was designed to have a cooling power of 1.5 kW at an evaporation temperature of -15 ºC. The main results are shown in Table 2.34.

Table 2.34: Performance at different evaporating temperature ($CaCl_2$-active carbon) [185].

Evaporating temperature (ºC)	Average heating power (kW)	Average cooling power (kW)	COP	SCP ($W \cdot kg^{-1}$)
-35	3.3	0.89	0.27	473.4
-25	3.28	1.18	0.36	627.7
-15	3.34	1.37	0.41	731

The authors obtained an average heat transfer coefficient for heating and cooling of 155.8 $W \cdot m^{-2} \cdot ºC^{-1}$.

Experiments combining heat and mass recovery were carried out by Lu et al. [186,187]. Here, the mass fraction of $CaCl_2$, activated carbon and cement were in the proportion of 16:4:1. The authors investigated the performance of adsorption ice-maker powered by waste heat from exhausting gases of fishing boats and powered by solar energy. In the former case, they found that the average specific cooling power for

the cycle without heat or mass recovery process, with mass recovery only, and with heat and mass recovery were 514.3 W·kg^{-1}, 795.5 W·kg^{-1} and 1026.2 W·kg^{-1}, respectively, at the condition of 40 min of cycle time and about -20 ºC of evaporating temperature, about 114 ºC of desorption temperature and about 30 ºC of condensing temperature. In addition, the authors studied the influence of the seawater temperature as the sink temperature on the system performance for temperatures ranging from 15 ºC to 30 ºC. They found that the average SCP and the COP increased as the temperature of the seawater decreased as depicted in Table 2.35. The selected working conditions were 70 min of cycle time, 40 s of mass recovery and 2 min of heat recovery.

Table 2.35: Sorption ice-maker performance powered by waste heat from exhausting gases of fishing boats [187].

Cooling water temperature (ºC)	Desorption Temp. (ºC)	Evaporation Temp (ºC)	Average SCP (W·kg^{-1})	COP
16	110.1	-19.1	865.8	0.43
20	114.7	-21.3	770.4	0.39
25	114.0	-18.1	676.8	0.34
30	113.7	-19.4	528.0	0.26

The authors stressed that even at the highest temperature of cooling water (30 ºC), the average SCP and COP were still as high as 528 W·kg^{-1} and 0.26, respectively.

In the latter case, the performance of the solar ice-maker was simulated using different heating power. The experimental conditions were 40 s of mass recovery, 24 min of cycle time, approximately 30 ºC of cooling water temperature, and approximately -15 ºC of evaporating temperature. The results of these experiments are shown in Table 2.36.

Table 2.36: Sorption ice-maker performance powered by solar energy [187].

Heating power (kW)	Desorption Temp. (ºC)	Evaporating Temp. (ºC)	Cooling water temp. (ºC)	Average SCP (W/·kg^{-1})	COP
1.69	76.5	-15.1	33.5	112.2	0.12
2.05	79.2	-13.8	33.7	113.8	0.1
2.42	82.4	-15.2	31.2	161.2	0.12

The authors found that the average SCP increased with heating power and the highest value was 161.2 W·kg^{-1} with a COP of 0.12 when powered with 80 ºC hot water.

The performance of the sorption ice-maker was further studied by Lu et al. [186] stressed on the optimum conditions for heat and mass recovery. They found that 40 s of mass recovery and 2 min of heat recovery were the optimum conditions for the highest performance of the system. At a decomposition temperature of 126 ºC, a cooling water temperature of 12 ºC and ice produced at -7.5 ºC, the ice production was 26.1 kg·h^{-1}, the SCP was 494.5 W·kg^{-1} and the COP was 0.3 for 36 min of cycle time. Further, the influence of the sea water temperature on the system performance was studied for temperatures ranging from 12 ºC to 27 ºC. The experimental conditions were also 126 ºC of decomposition temperature, -7.5 ºC of ice production, 40 s mass recovery and 2 min of heat recovery. Table 2.37 shows the results of these experiments.

Table 2.37: Sorption ice-maker performance with different sea water temperatures [186].

Cooling water temperature (ºC)	Mass of ice (kg·h^{-1})	Average SCP (W·kg^{-1})	COP
27	14.8	324.6	0.2
22	17.6	369.1	0.2
17	22.2	443.0	0.3
12	26.1	494.5	0.3

As in the previous study [186], the authors found that that the average SCP and the COP increased as the temperature of the seawater decreased. At the highest cooling water temperature, the average SCP and the COP were 324.6 $W \cdot kg^{-1}$ and 0.2, respectively.

Finally, the authors also calculated the average heat transfer coefficient of the absorbers for heating and cooling, which were 204.9 $W \cdot m^{-2} \cdot ºC^{-1}$ and 208.8 $W \cdot m^{-2} \cdot ºC^{-1}$, respectively.

The performance of the system was also studied by T.X. Li et al. [188] using heat and mass recovery. However, in this case, the mass recovery process was carried out before the heat recovery process. The desorption reactor was heated and the sorption reactor was cooled during the mass recovery phase (MHR2). Here, the mass of the reactive bed was 7.8 kg, which included 5.9 kg of $CaCl_2$. The results obtained from the experiments were compared to the conventional mass and heat recovery system (MHR1) without a heating and cooling process for the reactive beds during the mass recovery phase and the basic cycle (with no heat and mass recovery), see Table 2.38.

Table 2.38: Comparison of the performances of different sorption cycles at an evaporating temperature of -18.9 ºC and a cooling water temperature of 10 ºC ($CaCl_2$-activated carbon) [188].

Mass recovery time (s)	Cycle type	Heating power (kW)	Ice production ($kg \cdot h^{-1}$)	SCP ($W \cdot kg^{-1}$)	COP
0	Basic	12.13	16.58	329.1	0.16
20	MHR1	10.55	18.71	367.5	0.21
	MHR2	10.61	22.59	442.8	0.25
40	MHR1	10.55	20.82	409.1	0.23
	MHR2	10.66	24.81	486.5	0.27

The authors found that the system performed better with heat and mass recovery and that the optimal mass recovery time was 40 s. In addition, they found that the performance of the cycle with the novel heat and mass recovery process was much better than that of the basic cycle with the conventional heat and mass recovery process. The COP and the SCP in the novel process were more than 17 % better than in the conventional process.

The performance of the mass and heat recovery sorption cycle was further studied by Li et al. [189]. In addition, the performance of the sorption cycle was also studied using a two-stage heat recovery process. This two-stage heat recovery process corresponds to the two switching times between the decomposition and synthesis in a cycle. The results of the experiments are shown in Table 2.39.

Table 2.39: Performance comparison of different sorption refrigeration cycles at an evaporating temperature of -19.7 ºC and a cooling water temperature of 30 ºC. ($CaCl_2$-activated carbon) [189].

Sorption cycled time	T_{decom} (ºC)	Heating power (kW)	Ice production ($kg \cdot h^{-1}$)	Cooling capacity (kW)	COP	SCP ($W \cdot kg^{-1}$)
Conventional basic cycle	145	11.04	11.73	1.61	0.15	271.6
Mass and heat recovery cycle	145	10.46	17.93	2.57	0.25	435.2
Conventional two-stage cycle	103	10.24	7.44	1.09	0.11	185.5
Two-stage heat recovery cycle	103	10.01	9.08	1.35	0.14	228.4

As in the previous experiment, the authors found that the cycle with heat and mass recovery performed better than that without. In comparison with the conventional cycle, the COP and the specific cooling power were increased by 60 % and 66 %, respectively. Furthermore, the two-stage heat recovery cycle also performed better than the two-stage conventional cycle. The COP and SCP in the former cycle were more than 23 % better than in the conventional cycle. The authors also pointed out that although the two-

stage heat recovery cycle performs worse than the one-stage cycle, it can be driven by low generation temperature heat.

2.2.2.20 $CaCl_2$

Fadhel et al. [97] investigated the performance of a solar-assisted chemical heat pump drier under the meteorological conditions of Malaysia. The working pair used for the chemical heat pump was $CaCl_2$ with NH_3.

In this system, the air was heated by the condensation of ammonia during the decomposition of $CaCl_2 \cdot 8NH_3$ and was entered into the drying chamber. Part of the moist air stream produced after the drying process was diverted through the evaporator, where it was cooled. Dehumidification took place as the heat was given by the evaporation of ammonia and consequent synthesis of $CaCl_2 \cdot 2NH_3$. The heat released from the synthesis of $CaCl_2 \cdot 2NH_3$ was released to the environment. The air was then passed through the condenser again, where it was reheated by the ammonia condensation and then passed to the drying chamber.

The performance of the system was evaluated over 9 h (drying time, 8 am – 17:00 pm) on a typical clear December day in Malaysia, see Figure 2.20. The operating conditions were a decomposition temperature of ≥ 100 ºC, a condensing temperature of 40 ºC (1.5 MPa) and an evaporating temperature of 5 ºC (0.5 MPa).

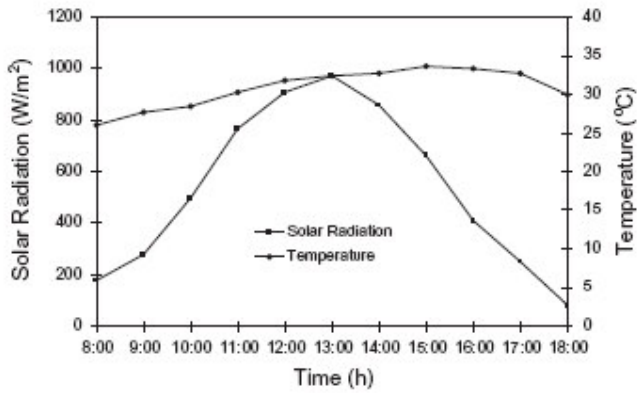

Figure 2.20: Average hourly radiation and ambient temperature on a typically clear December day in Malaysia [97].

The reactor (0.9 m x 0.18 m) was of the shell-and-tube type and included finned tubes. The $CaCl_2$ was located between the fins of a heat exchanger inside the reactor and the total amount loaded into the reactor was of 3 kg. In addition, the solar collector consisted of 30 evacuated tubes and the total area was of 0.726 m^2 (2.210 m x 2.040 m x 0.161 m)

The maximum values obtained from the experiments for the evacuated tubes' collector efficiency, the solar fraction and the coefficient of performance for heating were 74 %, 0.713 and 2, respectively. The total energy required to maintain a drying temperature of 55 ºC (air speed 1 $m \cdot s^{-1}$) was about 60 kWh over nine hours of drying time. The system contributed to 51 kWh, which amounts to approximately 85 % of the overall energy requirements and 15 % of those provided by the auxiliary heater which is mounted after the condenser.

2.2.3 Methanolates

Chemical heat pumps using calcium chloride ($CaCl_2$) with methanol (CH_3OH) were experimentally studied by Song et al. [104] at the Xi'an Jiaotong University (China) and, by Sun et al. [100,101] in a cooperation project between the Yantai University and the Beijing University of Chemical Technology (China). Unfortunately, further description cannot be given since these studies are reported in Chinese.

2.2.4 Methyl-ammoniates

Balat and Spinner [80], studied a chemical heat pump based on the system $CaCl_2$-expaded graphite with methylamine (CH_3NH_2) as follows:

$$CaCl_2 \cdot 2CH_3NH_2(s) + 2CH_3NH_2(g) \Leftrightarrow CaCl_2 \cdot 4CH_3NH_2(s) \quad (23)$$
$$CaCl_2 \cdot 4CH_3NH_2(s) + 2CH_3NH_2(g) \Leftrightarrow CaCl_2 \cdot 6CH_3NH_2(s) \quad (24)$$

The authors measured the conversion rate of the process with different proportions of expanded graphite (15 %, 20 %, 25 % and 35 %) and with increasing salt packing density under the same experimental conditions. The temperature of the evaporator-condenser was kept at 10 ºC for both synthesis and decomposition, corresponding to a pressure constraint of 200 kPa. The decomposition process of the $CaCl_2$-expanded graphite was carried out at 60 ºC while the synthesis process was carried out at 26 ºC. These conditions led to an equilibrium gap of 10.8 ºC in synthesis and 16.5 ºC in decomposition.

The reactor was a cylindrical packed bed reactor with a volume of $3 \cdot 10^{-4}$ m^3, wherein the central axis is occupied by a heat exchanger with an available surface area for heat exchange of $5 \cdot 10^{-2}$ m^2.

The authors found that the optimum proportion of expanded graphite was above 25 %. However, beyond this value, there was a maximum packing density which separated the two zones. Beyond the peak, the power decreased with the packing density and before the peak the power increased with the packing density. These peaks were found at packing densities of 1647 $mol \cdot m^{-3}$ and 1088 $mol \cdot m^{-3}$ for 25 % and 35 % expanded graphite, respectively. The average power per unit mass reached (salt) in the synthesis was equal to 516 $W \cdot kg^{-1}$ (126 $kW \cdot m^{-3}$) for 25 % expanded graphite and 654 $W \cdot kg^{-1}$(122 $kW \cdot m^{-3}$) for 35 % expanded graphite. These values were obtained until 70 % conversion was reached, but they were lower for the complete conversion. In addition, the authors investigated the effects of the equilibrium gap on the conversion rate and the power output of the salt for a composite material with a packing density of 1389 $mol \cdot m^{-3}$ and 25 % expanded graphite. They found that the conversion rate and the power rose when the equilibrium gap increased. For an equilibrium gap of 10.8 ºC in synthesis, the average power was 310 $W \cdot kg^{-1}$ and for 17.8 ºC it was 682 $W \cdot kg^{-1}$, whereas in decomposition, for 16.5 ºC the power was 797 $W \cdot kg^{-1}$ and for 26ºC it was 1727 $W \cdot kg^{-1}$.

2.3 Solid-gas chemisorption – Metal hydrides

2.3.1 $Zr_{0.9}Ti_{0.1}Cr_{0.9}Fe_{1.1}$ + $Zr_{0.9}$ $Ti_{0.1}Cr_{0.6}Fe_{1.4}$

A prototype heat pump using Zr-based Laves phase alloys pairs was constructed and experimentally investigated by Lee et al. [56] for air-cooling applications. The purpose of such metal hydride heat pump is to recover waste heat exhausted from automobile and industrial plants.

$Zr_{0.9}Ti_{0.1}Cr_{0.9}Fe_{1.1}$ was selected as the high-temperature hydride whereas $Zr_{0.9}$ $Ti_{0.1}Cr_{0.6}Fe_{1.4}$ as the low-temperature hydride, see Figure 2.21.

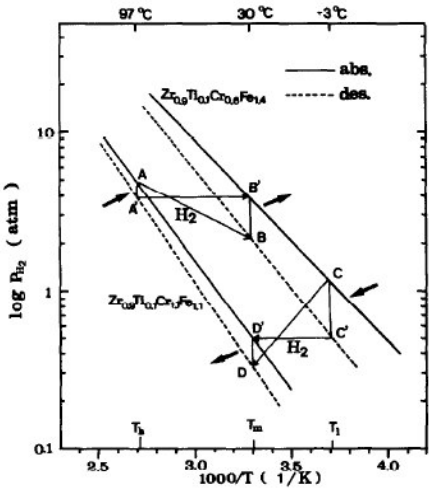

Figure 2.21: Schematic diagram of a hydrogen heat pump, base don the equilibrium pressure versus 1/T relationships for high temperature hydride (MH-1), $Zr_{0.9}Ti_{0.1}Cr_{0.9}Fe_{1.1}$ and the low temperature hydride (MH-2), $Zr_{0.9}Ti_{0.1}Cr_{0.6}Fe_{1.4}$ [56].

The reactors were of tubular-type and each comprised 14 Cu tubes of 19.1 mm in diameter and 210 mm in length. Aluminium fins were installed at the outer part of the tube to improve the heat transfer characteristics between the air and the reactor surface. At inner part of the reactor, 120 mesh brass screens were used as metallic structure to enhance the heat transfer rate in the hydride bed. In addition, two sheets of screen were inserted perpendicularly to the axial direction at intervals of 2 mm. The mass ratio of the metallic screen to the hydride was about 0.13 which gives an effective thermal conductivity of the bed of about 6 $W \cdot m^{-1} \cdot K^{-1}$. The arteries for the hydrogen flow were 5 cm in diameter and located at the centre of the reactor. Finally, the amount of metal hydrides loaded in the high-temperature and the low-temperature hydride were 2005 g and 2513 g, respectively.

The authors investigated the dependence of the cooling power output on operating parameters such as the hydrogen charged amount, cycle time, air flow rate, heat source temperature. Table 2.40 shows the optimum operating conditions and the cooling power output obtained.

Table 2.40: Optimum operating condition and cooling power output of the $Zr_{0.9}Ti_{0.1}Cr_{0.9}Fe_{1.1}$/$Zr_{0.9}$ $Ti_{0.1}Cr_{0.6}Fe_{1.4}$ pair. [56].

Initial amount of H_2 charged	12.8-13.2	mol
Total cycle time	11-12	min
Heating time	4	min
Cooling time	7-8	min
Air flow rate	> 3.8	$m^3 \cdot min^{-1}$
Heat source temperature	220	ºC
Cooling power output	150	$W \cdot kg^{-1}$

The air temperature of about 30 ºC was cooled down to 18 ºC during the cooling period and heated to about 48 ºC during the heating period, using the 220 ºC heat source. The hydrogen pressure reached a maximum of 1823.8 kPa during the heating period and reached a minim value of 101.3 kPa. The maximum cooling power output was 150 $W \cdot kg^{-1}$.

2.3.2 $LaNi_{4.6}Mn_{0.3}Al_{0.1}$ + $La_{0.6}Y_{0.4}Ni_{4.8}Mn_{0.2}$

Imoto et al [57] developed an F-class refrigerator system driven by solar heat using a pair of hydrogen absorbing allows, $LaNi_{4.6}Mn_{0.3}Al_{0.1}$ and $La_{0.6}Y_{0.4}Ni_{4.8}Mn_{0.2}$. The system was developed to generate cold at a

temperature below -20 ºC and to have a thermal power of about 1800 W with a total alloy quantity of 90 kg.

The refrigeration was produced by desorbing hydrogen from allow $La_{0.6}Y_{0.4}Ni_{4.8}Mn_{0.2}$ (M_2) at -20 ºC and using methyl alcohol as the heat transfer fluid while alloy $LaNi_{4.6}Mn_{0.3}Al_{0.1}$ (M_1) absorbs hydrogen at 20 ºC using pressurized water as the cooling medium. In the reverse cycle (regeneration), virtual solar heat of temperature 140 ºC was applied to $LaNi_{4.6}Mn_{0.3}Al_{0.1}$.Consequently, hydrogen is desorbed from allow $LaNi_{4.6}Mn_{0.3}Al_{0.1}$ and absorbed by $La_{0.6}Y_{0.4}Ni_{4.8}Mn_{0.2}$ which is cooled by water at 20 ºC.

The experimental test rig is detailed in a previous study by Moroto et al. [276], but the reactors employed were of cylindrical type with internal aluminium fins. The switching time between refrigeration and regeneration process was set for 1140 s.

The authors found that, during the initial 100 s the temperature of the refrigeration medium outlet dropped to -20 ºC and remained at this temperature level until the switching time, while the temperature of $La_{0.6}Y_{0.4}Ni_{4.8}Mn_{0.2}$ bed was kept in the range from -22 ºC to -25 ºC. The amount of effective hydrogen transfer measured was about 0.8 mass %. The thermal power and COP calculated from the heat media inlet/outlet temperature difference were 1860 W and 0.42, respectively. Furthermore, they also investigated the effect of the cycle time on the thermal power and the COP. A shorter cycle time yields a larger thermal power but a lower COP. According to the authors, maintenance of a cycle time between 900 to 2000 s provides a COP larger than 0.4 and a thermal power between 1200 W (2000 s) to 2000 W (900 s).

2.3.3 ZrMnFe + $MmNi_{4.5}Al_{0.5}$

Ram Gopal and Srinivasa Murthy [58] carried out experimental studies on a metal hydride cooling system working with ZrMnFe/$MmNi_{4.5}Al_{0.5}$ pair. The metal hydride cooling system consisted of two identical reactors in shape and size which were of tube and coil-type, see Figure 2.22.

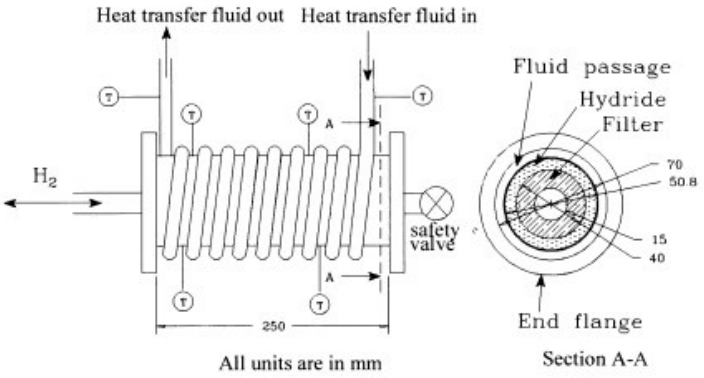

Figure 2.22: Detail of the hydride reactor for the metal hydride cooling system working with ZrMnFe/$MmNi_{4.5}Al_{0.5}$ pair [58].

The high-temperature (HT) reactor was filled with 700 g of ZrMnFe, while the low-temperature (LT) reactor was filled with 800 g of $MmNi_{4.5}Al_{0.5}$.The average bed density of the high-temperature reactor was about 4.5 $g \cdot cm^{-3}$ and that of the low-temperature reactor was about 5.14 $g \cdot cm^{-3}$.

The effects of half-cycle time, heat-source temperature, heat-sink temperature and refrigeration temperature on the system performance were studied for the following range presented in Table 2.41.

Table 2.41: Operating parameters of the metal hydride cooling system working with ZrMnFe/$MmNi_{4.5}Al_{0.5}$ pair [58].

Half-cycle time	3-12	min
Heat source temperature	110-130	ºC
Heat-sink temperature	25-30	ºC
Refrigeration temperature	5-15	ºC

During the experiments, the authors observed that the hydrogen storage capacity of ZrMnFe was only 60 % of its maximum capacity as reported by Dantzer and Meunier [277], which was about 2 $g \cdot mol^{-1}$ of alloy. The authors suggested that this may be due to impurities and/or the higher dynamic hysteresis and plateau slope for the high-temperature alloys. On the other hand, the hydrogen storage capacity of $MmNi_{4.5}Al_{0.5}$ was found to be about 90 % of its maximum capacity. Because of this, the absorption capacity of the LT bed was higher than the desorption capacity of the HT bed during the H_2 transfer from HT reactor to LT reactor. Similarly, the desorption capacity of the LT reactor bed was higher than the absorption capacity of the HT bed during the H_2 transfer from the LT reactor to HT reactor. According to the authors, this influences the bed pressures behaviour in such a way that the H_2 pressure is always pulled towards the faster reactor which here happened to be the LT reactor.

Depending upon the operating conditions, the specific cooling rate was found to lie between 30-45 $W \cdot kg^{-1}$ and the COP varied between 0.2 - 0.35. In general, the authors found a decrease of the specific cooling power with the half-cycle time as the rate of H_2 transfer decreased with the half-cycle time. However, the COP increased with the half-cycle time as the amount of H_2 transferred and hence the total amount of energy increases with the half-cycle time. The increase of the heat source temperature increased the COP until reached a maximum, after which the COP decreased. Further, the increase of the refrigeration temperature increased the COP however, reduced the availability of the cooling output.

2.3.4 $MmNi_{4.15}Fe_{0.85}$ + $LaNi_{4.6}Al_{0.4}$

A metal hydride heat pump for cold water production at temperatures below 4 ºC was presented by Chernikov et al. [60]. The experimental test-rig consisted of 4 tubular modules, each containing the high-temperature and the low-temperature metal hydrides which are separated by a collector filter for hydrogen transfer. In addition, corrugated aluminium foil was used to increase the thermal conductivity of the metal hydride to 8 $W \cdot m^{-1} \cdot K^{-1}$. Each module was filled with 1.5 kg of $LaNi_{4.6}Al_{0.4}$ powder (high-temperature) and 1.5 kg of $MmNi_{4.15}Fe_{0.85}$ powder (low-temperature).

The regeneration process was carried out by heating the high-temperature part to 200 ºC. Consequently, hydrogen was desorbed from $LaNi_{4.6}Al_{0.4}$ and absorbed by $MmNi_{4.15}Fe_{0.85}$ which was cooled with water. In addition, after the regeneration process is finished, the cooling of the high-temperature reactor was used to obtain water heated to 50 ºC which can then be used for technical or households needs in accordance to the authors. On the other hand, refrigeration process was achieved by desorbing hydrogen from $MmNi_{4.15}Fe_{0.85}$ while heat was removed from the absorption of hydrogen by $LaNi_{4.6}Al_{0.4}$. The performance of the system is presented in Table 2.42. The volume of the cooled water was 18 l and the initial reference temperature was of 20.1 ºC.

Table 2.42: Performance of the metal hydride heat pump system based on $MmNi_{4.15}Fe_{0.85}$ and $LaNi_{4.6}Al_{0.4}$ [60].

Number of cycles	8	-
Operating time installation	160	min
Output temperature of cooled water	1.5	ºC
Average cold productivity	154	W
Quantity of produced cold	$1.48 \cdot 10^6$	J
Quantity of supplied energy	$12.6 \cdot 10^6$	J

Thus the calculated specific cooling capacity of the system is about 103 $W \cdot kg^{-1}$.

2.3.5 $LaNi_{4.7}Al_{0.3}$+ $MmNi_{4.15}Fe_{0.85}$

Kang et al. [59] investigated a metal hydride cooling system using $LaNi_{4.7}Al_{0.3}$ as the high-temperature hydride and $MmNi_{4.15}Fe_{0.85}$ as the low-temperature hydride. The material and reactor specifications for the experimental test-rig are shown in Table 2.43.

Table 2.43: Material and reactor specifications for the experimental metal hydride heat pump using the pair $LaNi_{4.7}Al_{0.3}$ and $MmNi_{4.15}Fe_{0.85}$ [59].

	$LaNi_{4.7}Al_{0.3}$	$MmNi_{4.15}Fe_{0.85}$	
Tube type	Finned tube	Finned tube	
Reactor size	100x200	100x250	
Al Fin area	0.587	0.71	m^2
Cu tube area	0.033	0.04	m^2
Reactor weight	13	19.5	kg
Hydride weight	4.5	5.7	kg

The metal hydride heat pump operated at cooling temperature of 20 ºC, at heat sink temperature of 30 ºC and heat source temperature of 150 ºC. The time for regeneration and refrigeration processes was selected to be 10 min each.

The authors found that the optimum value of the charged hydrogen amount for the maximum hydrogen transfer was in the range of 3.5-4.0 mol $H_2 \cdot kg^{-1}_{alloy}$. The measured COP for the system was about 0.2.

2.3.6 $LmNi_{4.85}Sn_{0.15}$ + $LmNi_{4.49}Co_{0.1}Mn_{0.205}Al_{0.205}$ + $LmNi_{4.08}Co_{0.2}Mn_{0.62}Al_{0.1}$

Willers and Groll [64] designed and tested a two-stage metal hydride heat transformer. The thermodynamic and working principle of the two stage metal-hydride is illustrated in Figure 2.23.

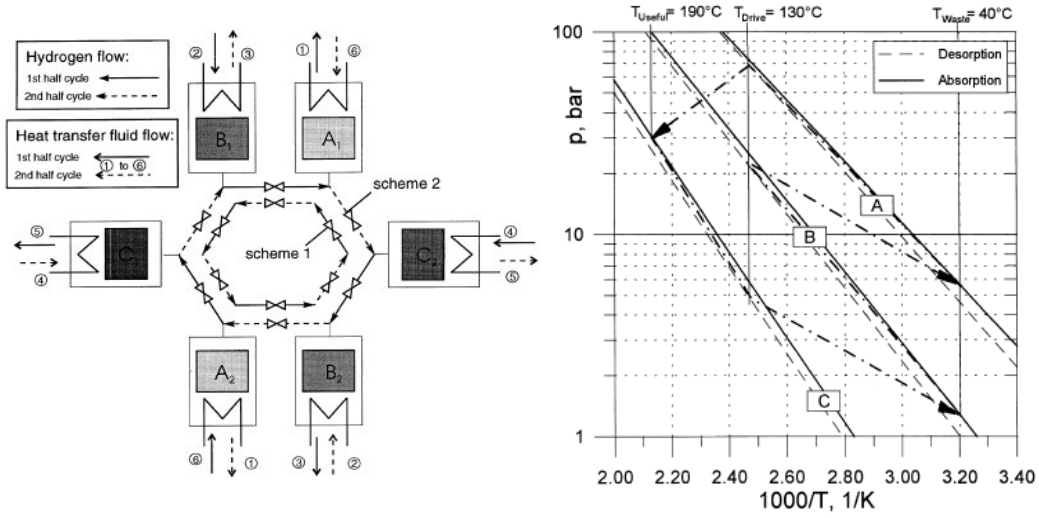

Figure 2.23: Working and thermodynamic principle of the two-stage metal hydride heat transformer [64].

The heat transformer consisted of six reactors filled with metal hydrides $LmNi_{4.85}Sn_{0.15}$ (A1/2), $LmNi_{4.49}Co_{0.1}Mn_{0.205}Al_{0.205}$ (B1/2) and $LmNi_{4.08}Co_{0.2}Mn_{0.62}Al_{0.1}$ (C1/2), interconnected in a special "star-scheme". The useful heat was generated at 190 ºC by the hydrogen absorption in hydride C, which absorbed hydrogen released from hydride A at the driving temperature 130 ºC. Hydride C was regenerated at 130 ºC and the released hydrogen was absorbed in hydride B. Finally, hydrogen flowed from B to A by desorption of B at 130 ºC. Driving heat at temperature level 130 ºC must be supplied three times, while useful heat $Q_{useful,C}$ is generated only once. After the first half cycle, the gas valves were closed an internal heat recovery could take place between A1 and A2, B1 and B2, and C1 and C2. The theoretical COP was about 1/3, if thermal masses are neglected.

Each hydride reactor consisted of two units containing a tube bundle of seven cylindrical reactors beds filled with the respective metal hydride and arranged in a hexagonal structure (Figure 2.24, A). Each reactor contained about 35 kg of metal hydride. To increase the thermal conductivity of the bed, a helical copper band, which is helically soldered into the reactor, was used as heat conduction matrix (Figure 2.24, B).

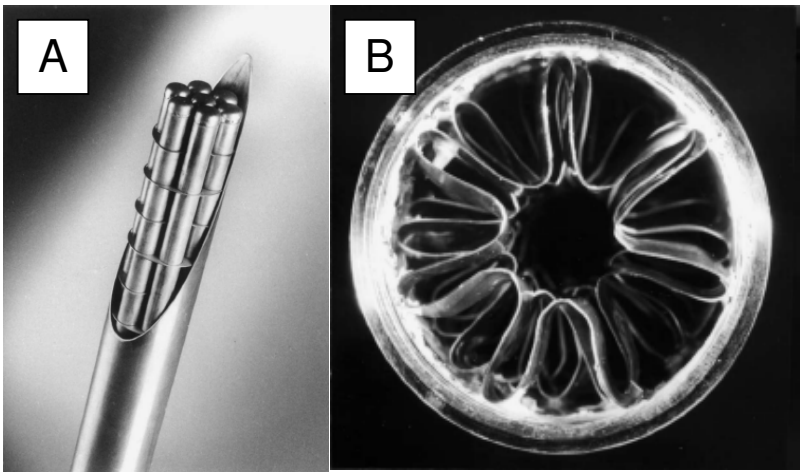

Figure 2.24: (A) opened reactor unit; (B) reaction bed with a copper band as heat conduction matrix [64].

The characteristics of the reactor are shown in Table 2.44.

Table 2.44: Reaction bed data [64].

Length	1360	mm
Outer diameter	29	mm
Wall thickness	1.5	mm
Filter diameter	6	mm
Metal hydride mass	2.5	kg
Effective thermal conductivity	7	$W \cdot m^{-1} \cdot K^{-1}$
Overall weight	4.45	kg
Reaction beds per reactor	7	

The authors obtained temperatures above 190 ºC and the power output was about 7 kW which corresponded to a cycle time of about 20 min, i.e. 10 min for each cycle time.

2.3.7 $LmNi_{4.91}Sn_{0.15}$ + $LaNi_{4.1}Al_{0.52}Mn_{0.38}$ + $Ti_{0.99}Zr_{0.01}V_{0.43}Fe_{0.09}Cr_{0.05}Mn_{1.5}$

Klein et al. [62] investigated experimentally a two-stage metal hydride system with $LmNi_{4.91}Sn_{0.15}$, $LaNi_{4.1}Al_{0.52}Mn_{0.38}$ and $Ti_{0.99}Zr_{0.01}V_{0.43}Fe_{0.09}Cr_{0.05}Mn_{1.5}$ in a cascading system as a topping cycle together

with a double-effect lithium bromide/water system as the bottoming cycle. The current system was already investigated theoretically and designed in a previous study by Klein and Groll [61]. The system comprised 6 reactors, each of which consisted of 4 reaction beds. The reaction bed design is shown on Figure 2.25 and was the same for the 24 reaction beds.

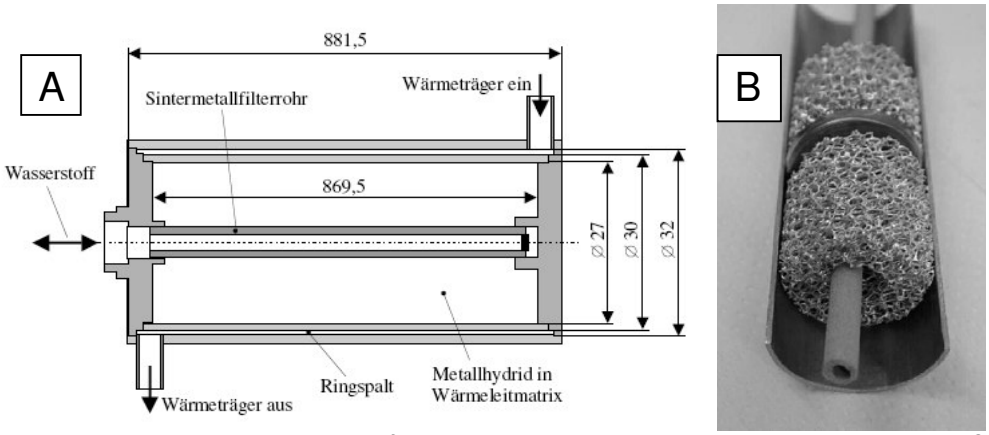

Figure 2.25: (A) Reaction bed design for the two-stage metal hydride system with $LmNi_{4.91}Sn_{0.15}$, $LaNi_{4.1}Al_{0.52}Mn_{0.38}$ and $Ti_{0.99}Zr_{0.01}V_{0.43}Fe_{0.09}Cr_{0.05}Mn_{1.5}$; (B) Cross-section of a reaction bed [61].

The reaction bed consisted of 3 concentrically tubes. The inner tube was a sinter metal tube for the hydrogen flow with a pore size of 1 μm, inner diameter of 3 mm and outer diameter of 6 mm. The middle tube contained the hydride powder and was 27 mm in diameter with a thickness of 1.5 mm. The outer tube had an annular gap of 1mm for the heat transfer fluid flow. Further the hydride powder is contained in Aluminium-foam cyclinders to improve heat and mass transfer. The aluminium cylinders had a porosity of 92 % with 2.5 mm pore size and an average thermal conductivity of 8 $W \cdot m^{-1} \cdot K^{-1}$.

The amount of metal hydride in each reaction bed was 1.96 kg, 1.85 kg and 1.8 kg for the $LaNi_{4.1}Al_{0.52}Mn_{0.38}$, $LmNi_{4.91}Sn_{0.15}$ and $Ti_{0.99}Zr_{0.01}V_{0.43}Fe_{0.09}Cr_{0.05}Mn_{1.5}$, respectively. Thus the total amount of metal hydride in the system was about 44.8 kg. However, further information on the experiments carried out by Klein et al. [62] could only be given from the English abstract, since unfortunately the thesis was reported in German. The average cooling power of the system was about 970 W while the heating power for driving the bottoming cycle of the cascade was 1.63 kW. The cooling temperatures were in the range from 2 to 16 ºC, a heat sink temperature of 23 ºC, a temperature of the heat transferred to the bottoming cycle of 100 ºC and a heat source temperature of 330 ºC. The coefficient of performance for cooling was of 0.51 and for heat amplification of 0.86.

2.3.8 $LaNi_{4.61}Mn_{0.26}Al_{0.13}$ + $La_{0.6}Y_{0.4}Ni_{4.8}Mn_{0.2}$

Qin et al. [68] and, Ni and Liu [67] carried out an experimental research on refrigeration characteristics of a metal hydride heat pump using exhaust gas from an automobile as heat source. The hydride pair selected for the heat pump was $LaNi_{4.61}Mn_{0.26}Al_{0.13}$ for the high-temperature (HT) reactor and $La_{0.6}Y_{0.4}Ni_{4.8}Mn_{0.2}$ for the low-temperature (LT) reactor.

Shanghai Jiatong University, Chinese Academy of Sciences and Zhejiang Yinlun Machinery Co. Ltd.

In the study carried out by Qin et al. [68], the experimental metal hydride refrigeration system was composed of two pair of cylindrical reactors (regeneration/refrigeration). Each reactor (Figure 2.26) was 500 mm in length and 75 mm in outer diameter. A hollow sintered filter of 50 mm in diameter with 2 μm nominal pore size was fixed inside the cylinder. Further, a copper tube of 10 mm in diameter was inserted

through the filter with 40 mm fin diameter and 20 mm fin intervals. Each regeneration and refrigeration reactor was filled with 2.75 kg of the respective metal hydride alloy, with filling density around 3.38 g·cm-3.

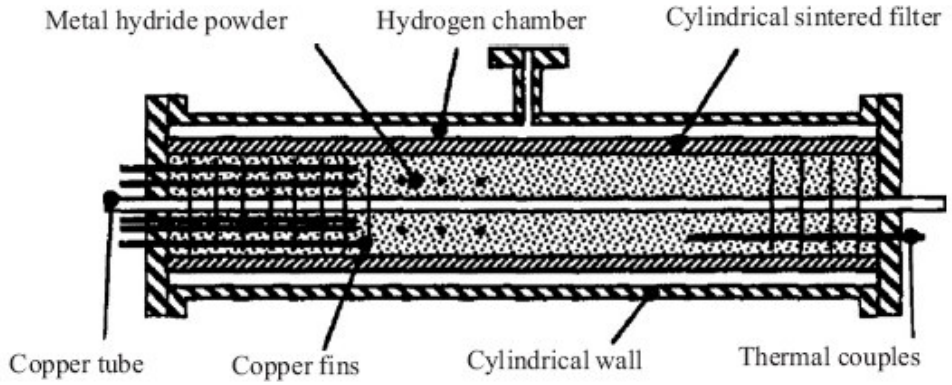

Figure 2.26: Reactor structure of the $LaNi_{4.61}Mn_{0.26}Al_{0.13}/La_{0.6}Y_{0.4}Ni_{4.8}Mn_{0.2}$ refrigeration system [68].

The measured thermal conductivity of the bed was in the ranger between 1.1 to 1.6 $W \cdot m^{-1} \cdot K^{-1}$.

The performance of the system was studied at heat source temperature of 150 ºC, at heat sink temperature of 30 ºC and at refrigeration temperature of 0 ºC. According to the repeated tests, the operation time was as 800 s for pre-heating, 850 s for regeneration, 650 s for pre-cooling and 1300 s for refrigeration. The maximum cooling power was 639 W, which was achieved at the beginning of the refrigeration period, while the average cooling power of this period was 238 W. The average cooling power of the whole cycle was 84.6 W and the cooling power per alloy was 7.7 $W \cdot kg^{-1}$ (15.4 W per kg of desorbing alloy).

The influence of the heat source temperature on the system performance and the refrigeration temperature was studied for 115 ºC, 130 ºC and 150 ºC. The authors found that cooling power and system COP increased while the minimum refrigeration temperature decreased with increasing of the heat source temperature as shown in Table 2.45.

Table 2.45: Influence of the heat source temperature on the system performance and the minimum refrigeration temperature (MRT) [68].

Average heat source temperature (ºc)	Total heating input (kJ)	Total refrigeration output (kJ)	Average cooling power in refrigeration period (W)	COP	MRT (ºC)
115	662	82	61	0.12	6.7
130	1010	214	165	0.21	0.5
150	1187	309	238	0.26	0.5

Trane Air Conditioning and Shanghai Maritime University

In the work from Ni and Li [67], the experimental test-rig of metal hydride heat pump comprised a total of 4 cylindrical reaction beds. Each reactor was composed of 4 concentric tubes wherein the innermost cooper tube acts as the heat-transfer liquid passage. The next annular space is equipped with copper fins and filled with a metal hydride alloy. The reaction bed with outermost diameter of 50 mm was about 500 mm in length and contained 2.75 kg of metal hydride alloy. All the reactors are identical in shape and size. The experiments were conducted under three operating temperature as shown in Table 2.46.

Table 2.46: Operating temperatures of metal hydride heat pump using $LaNi_{4.61}Mn_{0.26}Al_{0.13}$ + $La_{0.6}Y_{0.4}Ni_{4.8}Mn_{0.2}$ [67].

Experiment	1	2	3
Heat source temperature	115	130	150
Heat sink temperature			
Desorption	30	32	30
Absorption	32	35	32
Cooling temperature	20	20	20

The variables tested are shown in Table 2.47 and included the refrigeration cycle time, the available lowest refrigeration temperature, the values of COP and the cooling power output.

Table 2.47: Experimental results of the metal hydride heat pump using $LaNi_{4.61}Mn_{0.26}Al_{0.13}$ + $La_{0.6}Y_{0.4}Ni_{4.8}Mn_{0.2}$. [67].

Experiment	Refrigeration cycle time (min)	Lowest refrigeration temperature	Average cooling power output (W)	COP
1	31	6.5	186.77	0.22
2	48	2.5	203.94	0.27
3	64	1.9	244.23	0.3

The authors found that as the heat source temperature increased, the refrigeration cycle time, the COP and the average cooling power, increased, while the lowest refrigeration temperature decreased.

2.3.9 $LmNi_{4.91}Sn_{0.15}$ + $Ti_{0.99}Zr_{0.01}V_{0.43}Fe_{0.09}Cr_{0.05}Mn_{1.5}$

A thermally driven metal hydride heat pump for automotive cooling was presented by Linder et al. [63]. $LmNi_{4.91}Sn_{0.15}$ was chosen for the high temperature side while $Ti_{0.99}Zr_{0.01}V_{0.43}Fe_{0.09}Cr_{0.05}Mn_{1.5}$ for the low temperature side (cooling effect). The experiments were carried out using a capillary tube bundle reaction bed with the purpose of increasing the heat and mass transfer within the reaction bed. The realized bundle consisted of 372 stainless steal tubes with an inner diameter of 1.4 mm and a thickness of 0.2 mm. The total length of the bed was of 135 mm and the outer diameter of the reactor was of 76 mm. Both reactors were apparently identical and each of them was charged with about 900 kg of the respectively metal alloy.

The performance of the system was studied at desorption temperatures of 130 ºC for $LmNi_{4.91}Sn_{0.15}$ (regeneration) and of 20 ºC for $Ti_{0.99}Zr_{0.01}V_{0.43}Fe_{0.09}Cr_{0.05}Mn_{1.5}$ (cooling) while the heat of absorption was removed by cooling water at simulated ambient temperature of 28 ºC. The optimum half-cycle time was found to be between 100 s and 120 s and the calculated specific cooling power was about 780 W per kilogram desorbing metal hydride. In addition, the system performance was studied for different ambient temperatures ranging from 20 ºC to 35 ºC and cooling temperatures ranging from 10 ºC to 20 ºC, whereas the regeneration temperature was kept at 130 ºC. The authors found that the cooling power was reduced by increasing the ambient temperature or by lowering the cooling temperature which was attributed to the thermal masses of the system and to the reduction of exchangeable hydrogen for higher temperatures differences between ambient and cooling temperature.

2.3.10 Several hydrides – thermal wave

A multi-hydride thermal wave device for simultaneous heating and cooling was investigated by Willers et al [65]. The process flow diagram and the thermodynamic cycle of the device are illustrated on a van't Hoff plot in Figure 2.27.

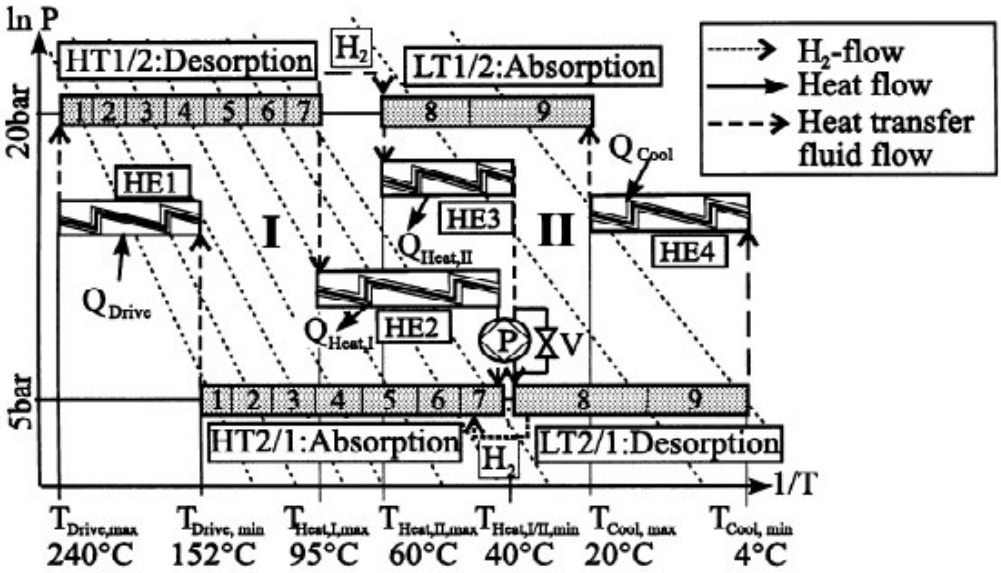

Figure 2.27: Van't Hoff Plot of the process, design pressure and temperature are indicated [65].

Seven different metal hydrides have been implemented on the high temperature side and two on the low temperature side as shown in Table 2.48.

Table 2.48: Properties of the metal hydrides used in the multi-hydride thermal wave device [65].

Hydride	No	Equilibrium temperature (ºC)			
		at 2000 kPa		at 500 kPa	
		Abs	Des	Abs	Des
$LaNi_{4.3}Al_{0.4}Mn_{0.3}$	1	212	222	152	161
$LaNi_{4.4}Al_{0.34}Mn_{0.26}$	2	196	205	139	147
$LaNi_{4.5}Al_{0.29}Mn_{0.21}$	3	172	181	125	134
$LaNi_{4.7}Sn_{0.3}$	4	154	163	107	115
$LaNi_{4.75}Al_{0.25}$	5	126	136	81	90
$LaNi_{4.85}Al_{0.15}$	6	113	122	66	75
$LaNi_5$	7	95	105	47	55
$La_{0.555}Co_{0.03}Pr_{0.12}Nd_{0.295}Ni_5$	8	60	66	18	25
$Ti_{0.98}$	9	35	44	-3	4

Each reaction bed had a diameter of 3 mm and a length of 880 mm with an annular channel for the heat transfer fluid of 5 mm around it. The reactors HT1/2 contained 7 metal hydrides (1 to 7) and the reactors LT1/2 contained two metal hydrides (8 and 9). Aluminium foam cylinders (a length of 20 mm, a porosity of 92 %, a pore size of 1 mm and a thermal conductivity of 8 $W \cdot m^{-1} \cdot K^{-1}$) were used to increase the heat and mass transfer of the hydride bed. The pores and gaps between the cylinders were filled with metal hydrides. However, due to the low thermal conductivity of the hydride in the gaps, the overall axial conductivity was reduced to 1 $W \cdot m^{-1} \cdot K^{-1}$ while the overall radial conductivity was about 8 $W \cdot m^{-1} \cdot K^{-1}$. According to the authors this particular design allows the propagation of a sharp thermal and reaction front along the length of each hydride section of a reaction bed.

The experiments were carried out with a heat source temperature (driving temperature) of 235 ºC, a heat-sink temperature of 33 ºC and a maximum cooling temperature of 18 ºC. The actual hydrogen inventory was 60 % of the maximum hydrogen capacity. The overall time was 1500 s. The authors obtained a

cooling power in the range of 230 W (outlet temperature 10 ºC) to 500 W (outlet temperature 0 ºC) with an average of 360 W. The COP during the cold generation period (550 s) was about 0.6 for cooling and 0.33 for the complete cycle.

3 Summary

The research on thermal energy storage systems based on solid-gas sorption process and chemicals reaction was increased rapidly over the last two decades. This fact was especially noticeable for the last teen years with a large number of publications on the experimental performance of these types of systems. The coefficient of performance (COP) and the specific cooling or/and heating power of these systems was also increased largely, in fact due to the improvements on the heat and mass transfer of the reactive bed and on the cycle performance. The combination of inorganic salts with a porous host matrix, such as expanded graphite, activated carbon, activated carbon fibers, metallic foam or expanded vermiculite, increased the porosity and the thermal conductivity of the reactive bed, and reduced the swelling and agglomeration of the inorganic salt during the sorption process or the chemical reaction. Therefore, the heat and mass transfer performance of the original bulk salt was improved by its combination with a porous host matrix. Further, the cycle performance was improved by the implementation of heat and/or mass recovery cycle. The research on this topic was studied specially in sorption cooling applications for continuous operation. Heat recovery cycle is used in systems with more than one reactive bed, a condenser and an evaporator. After switching between sorption and desorption, the part of the sensible heat from the hot-reactor can be recovered by the cold reactor [36,274] and thus increase the cycle COP. Mass recovery cycle, is usually applied after switching between sorption and desorption and before the heat recovery, the mass channels between the high pressure reactor and the low pressure reactor are connected each other. The high pressure reactor is further desorbed and the low pressure reactor further absorbs. If the heat and mass recovery times are proper, the COP and the power of the system will increase [36,274]. Table 3.1,Table 3.2, Table 3.3, Table 3.4 and Table 3.5 give the experimental thermal performances obtained by the different prototypes built over the last two decades. These results are a merely indication of the efficiency and power of such systems and should not be compared as they are obtained under different working conditions.

Ammoniates

So far, the most studied working pairs are ammonia with composite materials made of a metal salt of chloride or bromide and a host matrix. Expanded graphite, activated carbon, or carbon fibers is commonly used as the host matrix, but also metallic foam or expanded vermiculite is used as well. Most of the systems studied are for refrigeration applications like air conditioning, icemakers, deep-freezing among other applications. However, there are also some studies focused on the simultaneous heat and cold production and some just focused on the heat production (heat transformer).

The specific cooling power of the refrigeration prototypes are generally in the range between 100 to 750 $W \cdot kg^{-1}$ and with a COP in the range between 0.2-0.6. The sorption ice-makers prototypes for fishing boats showed very promising results with the composite material made of $CaCl_2$ and activated carbon. Wang et al. [185] obtained a specific cooling of about 731 $W \cdot kg^{-1}$ and a COP of 0.41 for 50 min cycle time at evaporating temperature of -15 ºC, a heat sink temperature (sea water temperature) of 30 ºC and a heat source temperature as low as about 100 ºC. Lu et al. [187] obtained similar results as Wang et al. [185] with a specific cooling power of 528 $W \cdot kg^{-1}$ and a COP of 0.26 for a cycle time of 70 min at evaporating temperature of -19 ºC, a heat sink temperature as high as 30 ºC (sea water temperature) and a heat source temperature of about 114 ºC. However, the SCP and COP can be as high as 865.8 W·kg-1 and 0.41, respectively, when the heat sink temperature is 16 ºC. Further, the composite made of $CaCl_2$ and expanded graphite showed also promising results. Oliveira et al. [114] obtained a SCP higher than 1000 $W \cdot kg^{-1}$salt when the heat sink temperature was at 20 ºC, the evaporating temperature was higher than -18 ºC and the heat source temperature was 135 ºC. The prototype could reach a maximum SCP of 1502 $W \cdot kg^{-1}$ when the evaporation temperature was -12 ºC

.

Table 3.1: Resume of the thermal performance of the chemical heat pumps based on sorption process between inorganic salts and ammonia for the last 20 years.

Reagents	Additive	Type	Mass (kg)	Th / Tm / Tc	SCP ($W \cdot kg^{-1}$)	SHP ($W \cdot kg^{-1}$)	Time (min)		COP (COPA)	Authors	Year	Application
							Half-cycle	cycle				
$MnCl_2$ / $NiCl_2$	EG	DE	26.5 / 27 [a]	280 / 10 / -5	29	-	-	-	0.21	Nevau et al. [147]	1992	Refrigeration
$BaCl_2$ / $MnCl_2$	EG (35 %)	SE	3.27 / 3.96	195 / 50 / 25	300[b]	320	25	-	0.35	Lépinasse et al. [142]	1993	Refrigeration
$BaCl_2$ / $NiCl_2$	EG (35 %)	SE	0.10 / 0.13	- / - 40 / 0	396[b]	-	15	-	-	Goetz et al. [144]	1996	Refrigeration
$SrBr_2$ / $NiCl_2$	EG	DE	2.35 / 0.89 [a]	340 / 8 / -4	134	760	-	-	0.38	Wagner [148]	1996	Refrigeration
$SrCl_2$ / $CoCl_2$	EG (49 % / 41%)	DE	0.17 / 0.27 [a]	240 / 7.5 / -4	145	1320	-	-	0.25	Llobet and Goetz [146]	2000	Refrigeration
$BaCl_2$	-	SE	1	95-70 / 23 / 0-(-8)	-	-	90	-	-	Rivera et al. [98]	2007	Refrigeration
$BaCl_2$ / $MnCl_2$	EG (37 %)	DE	0.23 / 0.27	180 / 30 / 10				140	0.64	Li et al. [169]	2009	Refrigeration
$BaCl_2$ / $MnCl_2$	EG (50 %)	DE	-	180 / 30 25 / 10	301	-	60	-	0.62	Li et al. [170]	2009	Refrigeration
$BaCl_2$ / $MnCl_2$	EG (50 %)	DE	-	180 / 30 25 / 10	-	-		150	0.64	Li et al. [171]	2010	Refrigeration
$CaCl_2$	AC (25 %)	DE-MR	2x1.88[a]	100 / 25 / -15	731	-		50	0.41	Wang et al. [185]	2006	icemaker
$CaCl_2$	AC (25 %)	DE-HMR	2x1.88[a]	113.7 / 30 / -19.4	528	-	-	70	0.26	Lu et al. [187]	2006	icemaker
$CaCl_2$	AC (25 %)	DE-HMR	2x1.88[a]	82.4 / 30 / -15.2	161			24	0.12	Lu et al. [187]	2006	icemaker
$CaCl_2$	AC (25 %)	DE–HMR	2x1.88[a]	126 / 27 / -7.5	325	-		36	0.2	Lu et al. [186]	2007	icemaker
$CaCl_2$	AC (25 %)	DE-HMR	7.4	160 / 10 / -18.9	486	-		20	0.27	Li et al. [188]	2007	icemaker
$CaCl_2$	AC (25 %)	DE-HMR	7.4	145 / 30 / -19.5	435	-		~36	0.25	Li et al. [189]	2008	icemaker
$CaCl_2$	AC (25 %)	DE-HMR	7.4	103 / 30 / -19.5	228	-		~27.5	0.14	Li et al. [189]	2008	icemaker
$CaCl_2$	EG (50 %)	SE	0.23	135 / 35 20 / -11	1500	-	-	-	0.35	Oliveira et al. [114]	2007	icemaker
$CaCl_2$	EG (35 %)	SE	-	97 / 30 / -18.3	255		40	-		Oliveira et al. [113]	2007	icemaker
$CaCl_2$	EG (25 %)	DE-MR	2x33.75	110.6 / 25 / -15	303	-	-	25	0.32	Xia et al. [180]	2008	Refrigeration (icemaker)
LiCl	EG (50 %)	SE	0.083	80 / 25 / -5	117[b]		30		0.47	Kiplagat et al. [181]	2009	icemaker
$SrCl_2$	EG (35 %)	SE	-	-	738	-	-	-	0.435	Chen et al. [182]	2010	icemaker
$CaCl_2$	EG (25 %)	DE-MR	2x33.75	140 / 25 / -15	422	-		25	0.27	S.L. Li et al. [179]	2010	Refrigeration (icemaker)
$PbCl_2$ / $MnCl_2$	EG (35 %)	SE	0.62 / 0.33	150 / 20 / 20	(47)[C]	-	120	-	-	Lépinasse et al. [145]	2001	Cooling a 88 L box
$BaCl_2$	EG (56 %)	SS	38.1	-	-	-	-	1440	0.031	Le Pierres et al. [151]	2007	560 l cold box (-30 ºC)
NH_4Cl / $MnCl_2$	EG (20 %)	SE	0.32 / 0.74	165 / AT / AT	43 / 11-18	-	180	-	-	Bao et al. [174]	2011	Cooling and freezing a 33 L box

Reagents	Additive	Type	Mass (kg)	Th / Tm / Tc	SCP ($W \cdot kg^{-1}$)	SHP ($W \cdot kg^{-1}$)	Time (min)		COP (COPA)	Author	Year	Application
							Half-cycle	cycle				
$MnCl_2$	EG (37 %)	SE	-	180 / 25 / -30	350	-	30		0.34	T.X. Li et al. [118]	2009	Deep-freezing
NaBr	EG (50 %)	SE	0.11	65 / 30 / 15	129[b]	-	40	-	0.46	Oliveira et al. [176]	2008	Air conditioning
NaBr / $MnCl_2$	EG (35 %)	SE	0.05 / 0.08	165 / 30 70 / 10	-	-	45		0.21 (1.11)	Oliveira et al. [176]	2008	Air conditioning
$BaCl_2$	EG	SE	-	80 / 30 / 15	192	-	-	-	0.5	Chen et al. [183]	2009	Air conditioning
$BaCl_2$	Vermiculite	SE	0.57	90 / 30 / 10	370 - 500	-		~ 9 - 15	0.54	Veselovskaya et al. [204]	2010	Air conditioning
NH_4Cl / $MnCl_2$	EG (33 %)	SE	0.08 / 0.15	140 / 30 75 / 0	(1.12)[d]	(3.04)	360	720	0.35 (1.3)	Xu et al. [175]	2011	Heat & cold
$CoCl_2$	AC (30 %)	SE	1.7	-	(235)[e]	-	-	-	-	Aidoun and Ternan [196]	2002	Heat & cold
$CaCl_2$	Busofit (70 %)	SE	1.07	120 / 50 / -18	-	-	-	25-30	0.43	Vasiliev et al. [131]	2001	Refrigeration
$BaCl_2$ + $NiCl_2$	Busofit (50 % / 48 %)	DE	0.55	240 / 50 - / 18	-	-	-	60	0.44	Vasiliev et al. [202]		Chilled water & steam
$BaCl_2$ + $MnCl_2$ + $NiCl_2$	Busofit	ME	-	230 -180-90 / - / -	-	-	-	-	0.41	Vasiliev et al. [202] Aristov and Vasiliev [203]	2003	Chilled water & steam
$BaCl_2$ + $MnCl_2$ + $NiCl_2$	Busofit	ME	-	450 - 400 - 96 / - / -	-	-	-	-	0.62	Vasiliev et al. [202] Aristov and Vasiliev [203]	2003	Chilled water & steam
$CaCl_2$ / $MnCl_2$	EG (50 % / 40 %)	SE	-	150 / 120 / 40	-	248	50		0.25	C. Wang et al. [178]	2010	Heat transformer
LiCl / $MgCl_2$	Metal foam	SE	1.8 / 1.8 [a]	200 / 155 200 / 20	-	222	40	-	0.11	Haije et al. [124]	2007	Heat transformer
LiCl / $MgCl_2$	Metal foam	SE	1.2 / 2.49 [a]	130 / 80 130 / 20	-	120	60	-	-	van der Pal et al. [192]	2009	Heat transformer
$CaCl_2$		SE	3	-	-	-	-	-	1.2 - 2	Fadhel et al. [97]	2010	Drying
$NiCl_2$	EG	DE	-	300 / - 200 / -	-	-	-	-	0.17	Cerkvenik et al. [194]	2009	Topping cycle

Th is the heat source temperature (ºC), Tm is the heat sink or condensing temperature (ºC) and Tc is the cooling or evaporating temperature (ºC).
SCP is the average specific cooling power (W per kg of desorbing composite material) and SHP is the average specific heating power (W per kg of absorbing composite material)
SE is a single-stage cycle (basic cycle), DE is a double stage cycle, ME is a multi-stage cycle, HMR is heat and mass recover.
[a] Mass of the anhydrous salt, [b] W per kg of desorbing salt, [c] kWh per m^3, [d] $MJ \cdot kg^{-1} \cdot day^{-1}$ (kg of absorbing composite), [e] kW per m^3 (peak power)

Table 3.2: Resume of the thermal performance of the chemical heat pumps based on sorption process between inorganic salts and water for the last 20 years.

Material	Additive	Mass salt (kg)	Th / Tm / Tc	SCP[c] ($W \cdot kg^{-1}$)	SHP ($W \cdot kg^{-1}$)	Time (min)		COP (COPA)	Author	Year	Application
						Half-cycle	cycle				
$MgSO_4$	-	0.04	150/10 50/10	-	-	-	-	-	van Essen et al. [84]	2009	Seasonal heat storage
$Al_2(SO_4)$	-	0.04	150/10 50/10	-	-	-	-	-	van Essen et al. [85]	2009	Seasonal heat storage
$CaCl_2$	-	0.04	150/10 50/10	-	-	-	-	-	van Essen et al. [85]	2009	Seasonal heat storage
$MgCl_2$	Cellulose	3.6(2)	135/10 25/10	-	-	-	-	-	Zondag et al. [77]	2010	Seasonal heat storage
Na_2S	Cellulose	3	86-77/25-15 -/20-5	500[a]	-	-	-	0.57	De Boer et al. [88]	2004	Heating & Cooling
$SrBr_2$	EG (6 %)	0.14	70/35/12		26[b]	~376	-	-	Lahmidi et al. [165]	2006	Heating (winter) & cooling (summer)
$SrBr_2$	EG (6 %)	0.14	70/35/12	49[b]		~188	-	-	Lahmidi et al. [165]	2006	Heating (winter) & cooling (summer)
$SrBr_2$	EG (8 %)	171.3	70/12 35/12	-	13	-	-	-	Mauran et al. [166]	2008	Heating (winter) & cooling (summer)
$SrBr_2$	EG (8 %)	171.3	70/35/18	15	-	840	-	-	Mauran et al. [166]	2008	Heating (winter) & cooling (summer)
$MnCl_2$	EG (20 %)	4.56	330-320/120-145 145-160/95	-	-	-	87	(1.25)	Stitou et al. [164]	2004	Heat transformer

Th is the heat source temperature (ºC), Tm is the heat sink or condensing temperature (ºC) and Tc is the cooling or evaporating temperature (ºC).
SCP is the average specific cooling power (W per kg of desorbing composite material) and SHP is the average specific heating power (W per kg of absorbing composite material)
[a] highest specific cooling power (W per kg of Na_2S).
[b] kW per m^3

Table 3.3: Resume of the thermal performance of the chemical heat pumps based on sorption process between inorganic salts and methyl-ammoniates for the last 20 years.

Material	Additive	Mass salt (kg)	Th / Tm / Tc	SCP ($W \cdot kg^{-1}$)	SHP ($W \cdot kg^{-1}$)	Time (min)		COP (COPA)	Author	Year	Application
						Half-cycle	cycle				
$CaCl_2$	EG (35%)	-	60/10 25/10	654	-		-	-	Balat and Spinner [80]	1993	Refrigeration

Th is the heat source temperature (ºC), Tm is the heat sink or condensing temperature (ºC) and Tc is the cooling or evaporating temperature (ºC).
SCP is the average specific cooling power (W per kg of desorbing composite material) and SHP is the average specific heating power (W per kg of absorbing composite material)

Table 3.4: Resume of the thermal performance of the chemical heat pumps based on solid-gas chemical reactions for the last 20 years.

Reagents	Additive	Mass (kg)	Th / Tm / Tc	SCP ($W \cdot kg^{-1}$)	SHP ($W \cdot kg^{-1}$)	Time		COP (COPA)	Author	Year	Application
						Half-cycle	Cycle				
$Mg(OH)_2/MgO$	-	0.052	400/30 145/121	-	119	60	-	-	Kato et al. [216]		Heat amplifier
$Ca(OH)_2/CaO$	-	-	410/15 600/153	-	-	-	-	-	Ogura et al. [243]		Heat transformer
$Ca(OH)_2/CaO$	-	0.6	470/80 330/5	-	-	-	-	-	Ogura et al. [244]		Dryer
$Ca(OH)_2/CaO$	EG (50%)	0.0187	440/3 200/3	225	-	17	-	-	Cerkvenik et al. [254]	2002	Refrigeration
$Ca(OH)_2/CaO$[a]	-	-	550/- 650/-	-	-	-	-	-	Lin et al. [251]	2009	Heat transformer
$CaCO_3/CaO + PbCO_3/PbO$	-	1/-	900/300 900/460	-	225[b]	60	-	-	Kato et al. [227]	2001	Steam Turbine
$BaCO_3/BaO$[a]	-	-	1580/1000/595	-	-	-	-	-	Kubota et al. [258]	2001	Heat storage

Th is the heat source temperature (ºC), Tm is the heat sink or condensing temperature (ºC) and Tc is the cooling or evaporating temperature (ºC).
SCP is the average specific cooling power (W per kg of material) and SHP is the average specific heating power (W per kg of material)
[a] Proposed system and kinetic study, [b] calculated from experiments

Table 3.5: Resume of the thermal performance of the metal hydride heat pumps for the last 20 years.

Metal hydrides	Mass (kg)	Th / Tm / Tc	COP (COA)	SCP ($W \cdot kg^{-1}$)		SHP ($W \cdot kg^{-1}$) Whole cycle	Time (min)		Authors	Year
				Cooling cycle	Whole cycle		Half-cycle	cycle		
$Zr_{0.9}Ti_{0.1}Cr_{0.6}Fe_{1.4}$ / $Zr_{0.9}Ti_{0.1}Cr_{0.9}Fe_{1.1}$	2.5 / 2	200 / 30 / 18	-	-	151	-	-	12	Lee et al. [56]	1996
$LaNi_{4.6}Mn_{0.3}Al_{0.1}$ / $La_{0.6}Y_{0.4}Ni_{4.8}Mn_{0.2}$	90	140 / 20 / -15	0.42	-	41	-	-	19	Imoto et al. [57]	1995
$MmNi_{4.5}Al_{0.5}$ / ZrMnFe	0.8 / 0.7	130-110 / 25-30 / 5-15	0.2-0.35		30-45	-	3-12	-	Gopal and Murthy [58]	1999
Thermal wave	-	235 / 33 / 18	0.33	20[1]	10[1]	-	-	25	Willers et al. [65]	1999
$LaNi_{4.7}Al_{0.3}$ / $MmNi_{4.15}Fe_{0.85}$	4.5 / 5.7	140 / 30 / 20	0.2	-	-	-	10	20	Kang et al. [59]	1996
$LmNi_{4.85}Sn_{0.15}$ / $LmNi_{4.49}Co_{0.1}Mn_{0.205}Al_{0.205}$ / $LmNi_{4.08}Co_{0.2}Mn_{0.62}Al_{0.1}$	70 / 70 / 70	190 / 130 / 40	-	-	-	30[b]	10	20	Willer and Groll [64]	1999
$MmNi_{4.15}Fe_{0.85}$ / $LaNi_{4.6}Al_{0.4}$	6 / 6	130 / 25 / 1.5[a]	0.11	-	25.6	-	20	-	Chernikov et al. [60]	2002
$LaNi_{4.1}Al_{0.52}Mn_{0.38}$ / $LmNi_{4.91}Sn_{0.15}$ / $Ti_{0.99}Zr_{0.01}V_{0.43}Fe_{0.09}Cr_{0.05}Mn_{1.5}$	15.7 / 14.8 / 14.4	330 / 100 23 / 16-2	0.51 (0.86)	-	42[a]	-	-	56[a]	Klein et al. [62]	2007
$La_{0.6}Y_{0.4}Ni_{4.8}Mn_{0.2}$ / $LaNi_{4.61}Mn_{0.26}Al_{0.13}$	5.5 / 5.5	150 / 30 / 0	0.26	-	15.4	-	-	60	Qin et al. [68]	2007
$La_{0.6}Y_{0.4}Ni_{4.8}Mn_{0.2}$ / $LaNi_{4.61}Mn_{0.26}Al_{0.13}$	5.5 / 5.5	130 / 30 32 / 20	0.3	-	44.4	-	-	64	Ni and Liu [67]	2007
$Ti_{0.99}Zr_{0.01}V_{0.43}Fe_{0.09}Cr_{0.05}Mn_{1.5}$ / $LmNi_{4.91}Sn_{0.15}$	0.9 / 0.9	130 / 28 / 20	-	780	-	-	2.15	-	Linder et al. [63]	2010

Th is the heat source temperature (ºC), Tm is the heat sink temperature (ºC) and Tc is the cooling temperature (ºC).
SCP is the average specific cooling power (W per kg of desorbing material)
[a] According to Muthukumar et al. [47], [b] W per kg of hydride.

Solar powered sorption systems were tested also under practical conditions. Le Pierrès et al. [151] carried out experiments with the solar-powered sorption system to cool down a 560 l box to below -20 ºC. The process involved two cascaded thermochemical system using the composite material of $BaCl_2$-expanded graphite and two flat plate solar collectors. The charging of the system was carried out during the day-time while the discharging was carried during the night-time. The system was tested during the summer and autumn 2005 in Perpignan, France. The authors found that the capability of the process to produce deep-freezing temperature depended strongly on the solar irradiations. Temperatures lower than -20 ºC were obtained mainly when the solar radiation was higher than 18 $MJ \cdot m^{-2} \cdot day^{-1}$. Fadhel et al. [97] also carried out experiments with a solar powered sorption drier using $BaCl_2$ as the reagent. The system was evaluated for nine hours drying time in a typical clear day in Malaysia. According to the authors, the total energy required to maintain a drying temperature of 55 ºC was about 60 kWh over nine hours drying time and the sorption system contributed to 51 kWh.

Heat production with inorganic salts and ammonia were studied the less. However, the specific heating powers obtained were in the range between 100 to 300 $W \cdot kg^{-1}$. Generally, the prototypes were designed for steam production at the temperature level ranging from 100 to 200 ºC. Wang et al. [178] tested a heat transformer using the composites of $CaCl_2$ and $MnCl_2$ with expanded graphite for the production of heat at 150 ºC from heat source of 120 ºC. They obtained a specific heating power of about 248 W per kg of composite reactive block with $MnCl_2$ and an experimental COP of 0.25. Haije et al. [124] performed experiments with a heat transformer using the composites materials made of LiCl and $MgCl_2$ with metallic foam. The average specific heating power was about 222 W per kg of $MgCl_2$. Vasiliev et al. [202] performed experiments with different multi-cascade prototypes using the salts of $NiCl_2$, $MnCl_2$ and $BaCl_2$ impregnated in an activated carbon named "Busofit". The target of the system was to produce simultaneous heat generation (steam temperature at about 120–130 ºC) and cold generation (chilled water at about 3–5 ºC). The COP for the different prototypes ranged from 0.4 to 0.6.

Methanolates

Song et al. [104] and Sun et al. [100,101] experimentally studied the systems using calcium chloride ($CaCl_2$) with methanol (CH_3OH). Unfortunately, further description cannot be given since these studies are reported in Chinese.

Methyl-ammoniates

Balat and Spinner [80] obtained also a good performance with the system of $CaCl_2$-expanded graphite with methylamine (CH_3NH_2). The authors obtained a SCP as high as 627 $W \cdot kg^{-1}$ for an evaporator-condenser temperature of 10 ºC a decomposition temperature of 60 ºC and a synthesis temperature of 26 ºC.

Hydrates

The systems based on sorption process between inorganic salt and water, were tested for different purposes. Zondag et al. [77] tested an open sorption system for solar long-term heat storage. The purpose of the system is to fulfil the space heating demand of a building. The reagent used was $MgCl_2$ which was impregnated in cellulose to avoid any problem related to over-hydration. The hydration was carried out using moistened nitrogen with a water vapour pressure of 1.2 kPa and the initial bed temperature was 22 ºC. The temperature lift of the nitrogen flow was about 20 ºC and could be maintained for about 120 min. In an up-scaled reactor (3.6 kg) and not insulated, the authors could reach a maximum temperature lift of about 15 ºC and after 23 hours the temperature lift was around 10 ºC. de Boer et al. [88] developed a prototype (SWEAT) using the reagent of Na_2S-cellulose for cooling applications. The highest SPC obtained was 500 W per kg of Na_2S obtained at evaporating temperature of 20 ºC. The value for COP was 0.57. Lahmidi et al. [165] and Mauran et al. [166] tested a solar powered prototype for heating in winter at

about 35 ºC and refreshing in summer at about 18 ºC using the composite material made of SrBr and expanded graphite. In a first small-scale prototype, the SCP and SHP obtained were 49 $kW \cdot m^{-3}$ and 36 $kW \cdot m^{-3}$, respectively. However, in the up-scaled reactor the SCP and SHP were as low as 15 $W \cdot kg^{-1}$ and 13 $W \cdot kg^{-1}$, respectively. Finally, Stitou et al. [164] tested a heat transformer using the system $MnCl_2$-expanded graphite to produce heat at a temperature level suitable for industrial purposes (160 ºC), from waste heat at 90 ºC (high pressure mode). The mean value of COPA was 1.25.

Chemical reactions

The experimental studies on chemical heat pumps based on solid-gas chemical reaction were mainly focused on the hydration of the magnesium oxide and calcium oxide, and the carbonation of the calcium oxide and lead (II) oxide. The specific heating power of such system were in the range between 100-250 $W \cdot kg^{-1}$. Kato et al. [216] obtained a specific heating power of 119 W per kg of $Mg(OH)_2$ at 200 ºC for 60 min hydration operation with a water vapour pressure of 203 kPa. This prototype of heat pump was designed to store waste heat from exhaust gases at around 250-400 ºC and produce heat at around 100-250 ºC with a water vapour pressure less than 400 kPa [222]. Recently, Kim et al. [224] performed experiment with the composite material of $Mg(OH)_2$ and expanded graphite. However, the performance of the heat pump was only evaluated numerically. Ogura et al. [244] tested a chemical heat pump dryer (CHPD) using the CaO/H_2O system. The CHPD stored heat at 470 ºC and released heat at 80 ºC and 330 ºC heat for hot dry air production and 5 ºC heat for cooling dehumidification continuously by switching the two CHPs. The authors found that the output air temperature could be kept above 80 ºC for 120 min operation and evaporation temperatures ranging from 5 to 60 ºC. Cerkvenik et al. [254] also performed experiments with the system the CaO/H_2O system but for refrigeration applications. Consolidated material made of CaO and expanded graphite was used as the reactive bed. The authors obtained an average SCP of 50 $kW \cdot m^{-3}$ (225 $W \cdot kg^{-1}$) for a cycle time of 1000 s, at water vapour pressure of 0.75 kPa, a heat sink temperature of 200 ºC and a heat source of 400 ºC. Kato et al. [227] also tested a double reactor type of chemical heat pump based on the carbonation of calcium oxide (CaO) and lead (II) oxide (PbO) via carbon dioxide (CO_2). This chemical heat pump was developed to store heat above 800 ºC and upgrade it to higher temperatures. The SHP was of 225 $W \cdot kg^{-1}$ at temperature above 900 ºC for a 60 min operation time with a CO_2 pressure of 304 kPa.

Metal hydrides

Thermally driven metal hydrides heat pumps were studied mainly for air conditioning applications. Generally, the SCP of such systems ranged from 10 to 45 W per kg of desorbing metal hydride, and the COP was ranged from 0.1 to 0.5. However, Lee et al. [56] tested a metal hydride heat pump using $Zr_{0.9}Ti_{0.1}Cr_{0.6}Fe_{1.4}$ / $Zr_{0.9}Ti_{0.1}Cr_{0.9}Fe_{1.1}$ pair for air conditioning applications, which can be operated with waste heat exhausted from automobile and industrial plants. The maximum SCP was obtained with 11 min cycle time, a heat source temperature of 220 ºC, a heat sink temperature of 30 ºC and a cooling temperature of 18 ºC was about 151 W· per kg of desorbing hydride for the whole cycle (continuous operation). The best performance was obtained by Linder et al. [63] with a metal hydride heat pump using $Ti_{0.99}Zr_{0.01}V_{0.43}Fe_{0.09}Cr_{0.05}Mn_{1.5}$ / $LmNi_{4.91}Sn_{0.15}$. A capillary tube bundle reaction bed was applied due to its large heat transfer surface and consequently expected short cycle times. The SCP of the system was 780 W per kg of desorbing hydride obtained with a cycle time in the order of 100-120 s, and at heat source temperature of 130 ºC, a heat sink temperature of 28 ºC and a cooling temperature of 20 ºC.

4 Conclusions

Refrigeration technologies based on inorganic salts and ammonia has progressed considerably over the last 20 years. Consolidated composite materials have shown their potential to increase the cooling performance and currently, specific cooling powers over 700 W per kilogram of desorbing materials can be obtained. In addition, the use of methylamine as an alternative refrigerant to ammonia has shown also a similar performance [80].

The coefficient of performance of the current prototypes is somewhat lower (0.1 - 0.7) compared to commercial ammonia-water (0.25-0.9) and lithium bromide water (0.5-1.7) absorption systems [33]. However, the power output and the COP can be increased with the implementation of heat and/or mass recovery cycle and heat pipe technology [36,39,274]. Further, multi-stage cycles have demonstrated to reduce the driving heat source temperature without a significant reduction on the chemical heat pump performance compared with the basic conventional cycle [189].

Medium-scale and large-scale systems (> 100 kW) with a higher number of modules have not yet been built and tested to prove the same cooling power and COP as with the small-scale system. In addition, long-duration test have not been performed to study the durability of the material. According to Wang et al. [36], problems of expansion, decomposition, deterioration and corrosion in the chlorides salts-ammonia systems are the main drawback for its widespread utilization.

The performance of thermally driven metal hydrides heat pumps for refrigeration applications is lower than the performance of inorganic salts and ammonia or methylamine heat pumps (< 150 $W \cdot kg^{-1}$). The lower performance is mainly related to heat and mass transfer limitations in the hydride bed. However, recently, Linder et al. [63] obtained a SCP of 780 W per kg of desorbing hydride using a capillary bundle reactor with a large heat transfer surface. Muthukumar and Groll [47] have also pointed out the use of composite materials and advanced cycles concepts as future research lines to increase the efficiency and reduce the cost of these systems.

Heating technologies have been studied with sorption process and chemical reactions however, the research on this field is less intensive than in refrigeration technologies. The specific heating power is around 200 to 300 $W \cdot kg^{-1}$. Usually, sorption process based on inorganic salts and ammonia or water are used to produce low temperature heat (< 100 ºC) and medium temperature heat (100 to 400 ºC), while chemical reactions are used to produce medium temperature heat and high temperature heat (> 400 ºC). The potential of heat pumps based on chemical reactions is that can store and produce heat at very high temperature that other heat pumps can not reach. Some of current research is focused on composite materials to increase the heat and mass transfer in the reactive bed, and increase the power output and COP of the system [224].

The research on solid-gas sorption systems or solid-gas chemical reactions systems for seasonal heat storage in the built environment is very limited. So far, only at ECN, an extensively research have been focus to find the optimum working pair for seasonal heat storage to fulfil the heating demand in the winter period. The main challenges in this field is to increase the power output of the material (high energy density) and to be able to deliver 1850 kWh (heat consumption in a low energy building) for the two month in winter without available solar energy [6].

Finally, another important point for its application is that these technologies are operated under a variable waste heat temperature. Therefore, a control strategy of these systems should be optimized in order to obtain a high efficiency, [33].

5 References

[1]. IEA. 2007. Renewables for Heating and Cooling: Untapped Potential - a joint report for the Renewable Energy Technology Deployment Implementing Agreement and the Renewable Energy Working Party of the International Energy Agency. International Energy Agency. (http://www.iea.org).

[2]. Arce P, Medrano M, Gil A, Oró E, Cabeza LF. Overview of thermal energy storage (TES) potential energy savings and climate change mitigation in Spain and Europe. Applied Energy 2011;88:2764-2774.

[3]. Kato Y. Thermal energy storages in Vehicles for fuel efficiency improvement. In: Proc 11th International Conference on Thermal Energy Storage - Effstock 2009 Stockholm, Sweden, 2009.

[4]. Helden Wv. Materials for Compact Seasonal Heat Storage. In: Proc IEA Solar Heating & Cooling Workshop Cape Town, South Africa 2010.

[5]. Dinçer I, Rosen MA. Thermal Energy Storage. Systems and Applications. London: Wiley; 2002.

[6]. Hadorn J-C. Thermal energy storage for solar and low energy building. State of the art. IEA Solar Heating and Cooling Task 32: International Energy Agency; 2005.

[7]. Hadorn J-C. 2004. Storage solutions for solar thermal energy. Swiss Federal Office of Energy. (http://www.viking-house.ie).

[8]. Hadorn J-C. First results of task 32 on advanced heat storage. In: Proc Heat Storage Symposium at Intersolar Freiburg, Germany, 2007. (http://www.preheat.org).

[9]. Bauer D, Marx R, Nußbicker-Lux J, Ochs F, Heidemann W, Müller-Steinhagen. German central solar heating plants with seasonal heat storage. Solar Energy 2010;84:612-623.

[10]. Schmidt T, Mangold D, Müller-Steinhagen H. Central solar heating plants with seasonal storage in Germany. Solar Energy 2004;76:165-175.

[11]. J.-O. Dalenbäck J-O. European Large Scale Solar Heating Network. In: Proc hosted at Institutionen för Installationsteknik Chalmers Tekniska Högskola, Göteborg, Sweden, 2003. (http:///www.hvac.chalmers.se/cshp/).

[12]. Novo AV, Bayon JR, Castro-Fresno D, Rodriguez-Hernandez J. Review of seasonal heat store in large basins: Water tanks and gravel-water pits. Applied Energy 2010;87:390-397.

[13]. Schmidt T, Mangold D. 2008 Solare Nahwärme mit Langzeit-Wärmespeicherung in Deutschland. ERNEUERBARE ENERGIE. [German]. (http://www.solites.de)

[14]. Drück H, Marx R, Bauer D, Nußbicker-Lux J. Central Solar Heating Plants with Seasonal Thermal Energy Storage in Germany. In: Proc Task 45 – Kick-off Meeting (IEA Solar Heating and Cooling Programme) Barcelona, Spain, 2011. (www.iea-shc.org).

[15]. The parabolic trough power plants Andasol 1 to 3. The largest solar power plants in the world – Technology premiere in Europe. Solar Millennium. (http://www.solarmillennium.de).

[16]. Medrano M, Gil A, Martorell I, Potau X, Cabeza LF. State of the art on high temperature thermal energy storage for power generation. Part 2-Case studies. Renewable and Sustainable Energy Reviews 2010;14:56-72.

[17]. Abhat A. Low Temperature Latent Heat Thermal Energy Storage: Heat Storage Materials. Solar Energy 1983;30(4):313-332.

[18]. Lane GA. Solar Heat Storage: Latent Heat Material. Volume I: Background and Scientific Principles. Florida: CRC Press; 1983.

[19]. Lane GA. Latent Heat Material. Volume II: Technology. Florida: CRS Press; 1986.

[20]. Kenisarin M. Energy Storage Using Phase Change Materials. Renewable and Sustainable Energy Reviews 2007;11:1913-1965.

[21]. Zalba B, Marín JM, Cabeza LF, Mehilg H. Review on thermal energy storage with phase change: materials, heat transfer analysis and applications. Applied Thermal Engineering 2003;23(3):251-283.

[22]. Farid MM. A review on phase change energy storage: materials and applications. Energy Conversion and Management 2004;45:1597-1615.

[23]. Tyagi VV, Buddhi D. PCM thermal storage in buildings: A state of art. Renewable and Sustainable Energy Reviews 2007;11:1146-1166.
[24]. Cabeza LF, Heinz A, Streicher W. 2005. Task 32 - Report C2 of Subtask C - Inventory of Phase Change Materials (PCM). IEA Solar Heating & Cooling. (www.iea-shc.org).
[25]. Mehling H, Cabeza LF. Heat and cold storage with PCM. An up to date introduction into basics and applications. Berlin: Springer-Verlag Berlin Heidelberg; 2008.
[26]. Cabeza LF, Castell A, Barreneche C, Gracia Ad, Fernández Ai. Materials used as PCM in thermal energy storage in buildings: A review. Renewable and Sustainable Energy Reviews 2011;15:1675-1695.
[27]. Gil A, Medrano M, Martorell I, Lázaro A, Dolado P, Zalba B, Cabeza LF. State of the art on high temperature thermal energy storage for power generation. Part 1-Concepts, materials and modellization. Renewable and Sustainable Energy Reviews 2010;14:31-35.
[28]. Perino M. 2008. State-of-the-art Review. Vol.2. 2A. Responsive Building Elements. Annex 44. International Energy Agency (IEA) Energy Conservation in Buildings and Community Systems (ECBCS). (http://www.ecbcs.org/).
[29]. Henninger S. 2008. Heat storage technologies. Markets – Actors – Potentials. PREHEAT. Report nr EIE/05/036/SI2.420010. (http://www.preheat.org/).
[30]. Sumathy K, Yeung KH, Yong L. Technology development in the solar adsorption refrigeration systems. Progress in Energy and Combustion Science 2003;29:301-327.
[31]. Demir H, Mobedi M, Ülkü S. A review on adsorption heat pump: problems and solutions. Renewable and Sustainable Energy Reviews 2008;12:2381-2403.
[32]. Wongsuwan W, S. K, Neveu P, Meunier F. A review of chemical heat pump technology and applications. Applied Thermal Engineering 2001;21:1489-1519.
[33]. Deng J, Wang RZ, Han GY. A review of thermally activated cooling technologies for combined cooling, heating and power systems. Progress in Energy and Combustion Science 2011;37:172-203.
[34]. Yu YQ, Zhang P, Wu JY, Wang RZ. Energy upgrading by solid-gas reaction heat transformer: A critical review. Renewable and Sustainable Energy Reviews 2008;12:1302-1324.
[35]. Aristov YI, Vasiliev LL, V.E. N. Chemical and Sorption Heat Engines: State of The Art and Development prospects in the Russian Federation and the Republic of Belarus. Journal of Engineering Physics and Thermophysics 2008;81(1).
[36]. Wang DC, Li YH, Li D, Xia YZ, Zhang JP. A review on adsorption refrigeration technology and adsorption deterioration in physical adsorption systems. Renewable and Sustainable Energy Reviews 2010;14:344-353.
[37]. Wang LW, Wang RZ, Oliveira RG. A review on adsorption working pairs for refrigeration. Renewable and Sustainable Energy Reviews 2009;13:518-534.
[38]. Kim DS, Infante Ferreira CA. Solar refrigeration options – a state of the art review. International Journal of Refrigeration 2008;31:3-15.
[39]. Wang RZ, Oliveira RG. Adsorption refrigeration – An efficient way to make good use of waste heat and solar energy. Progress in Energy and Combustion Science 2006;32:424-458.
[40]. Hauer A. Thermal Energy Storage for Sustainable Energy Consumption - Sorption Theory for Thermal Energy Storage. In: Proc NATO Advanced Study Institute on Thermal Energy Storage for Sustainable Energy Consumption - Fundamentals, Case Studies and Design Izmir, Turkey, 2007. pp 393-408.
[41]. Ruthven DM. Principles of Adsorption & Adsorption Processes: Wiley; 1984.
[42]. Dąbrowski A. Adsorption – from theory to practice. Advances in Colloid and Interface Science 2001;93:135-224.
[43]. N'Tsoukpoe KE, Liu H, Le Pierrès N, Luo L. A review on long-term sorption solar energy storage. Renewable and Sustainable Energy Reviews 2009;13:2385-2396.
[44]. Bales C. 2007. Task 32 - Final Report Subtask B "Chemical and Sorption Storage". The Overview. IEA Solar Heating & Cooling. (www.iea-shc.org).

[45]. Wagner W, Jähnig D, Isaksson C, Hausner R. 2005. MODESTORE. Derivable: Final Report on Austrian Field Test Period (Performance and Evaluation). Gleisdorf, Austria: AEE - Institute for Sustainable Technologies. (http://www.aee-intec.at).

[46]. Schmidt F, Henninger S. Adsorption heat storage. Current status and future developments. In: Proc PREHEAT Symposium at Intersolar Freiburg, Germany, 2007.

[47]. Muthukumar P, Groll M. Erratum to "Metal hydride based heating and cooling systems: A review". International Journal of Hydrogen Energy 2010;35:8816-8829.

[48]. Winsche WE; United States of America, assignee. 1970. Intermittent Power Source. United States of America patent 3,504,494.

[49]. Gruen DM, Sheft I. Metal hydride systems for solar energy conversion and storage. In: Proc NSF-ERDA Workshop on Solar Heating, and Cooling of buildings Charlottesville, Vancouver (USA), 1975.

[50]. Terry LE; United States of America, assignee. 1977. Hydrogen-hydride absorption systems and methods for refrigeration and heat pump cycles. United States of America patent 4,055,962.

[51]. Gruen DM, Sheft I, Lamich GL. 1977. HYCSOS: a chemical heat pump and energy conversion system based on metal hydrides. Argonne National Laboratory. Report nr ANL-77-39

[52]. Gruen DM, Mendelsohn MH, Sheft I. Metal hydrides as chemical heat pumps. Solar Energy 1978;21:153-156.

[53]. Sheft I, Gruen DM, Lamich GL. Current status and performance of the Argonne HYCSOS chemical heat pump system. Journal of the Less-Common Metals 1980;74:401-409.

[54]. Suda S. Recent development of hydride energy systems in Japan. International Journal of Hydrogen Energy 1985;10(11):757-765.

[55]. Murthy SS. Metal hydride based cooling systems with hydrogen as working fluid. In: Proc 1st European Conference of Polygeneration Tarragona, Spain, 2007.

[56]. Lee SG, Kim KY, Lee JY. Operating characteristics of metal hydride heat pump using Zr-based laves phases. International Journal of Hydrogen Energy 1995;20(1):77-85.

[57]. Imoto T, Yonesaki T, Fujitani S, Yonezy I, Hiro N, Nasako K. Development of an F-class refrigeration system using hydrogen-absorbing allows. International Journal of Hydrogen Energy 1996;21(6):451-455.

[58]. Gopal MR, Murthy SS. Experiments on a metal hydride cooling system working with ZrMnFe/MmNi4.5Al0.5 pair. International Journal of Refrigeration 1999;22:137-149.

[59]. Kang BH, Park CW, Lee CS. Dynamic behaviour of heat and hydrogen transfer in a metal hydride cooling system. International Journal of Hydrogen Energy 1996;21(9):769-774.

[60]. Chernikov AS, Izhvanov LA, Solovey AI, Frolov VP, Shanin YI. An installation for water cooling based on a metal hydride heat pump. Journa of Alloys and Compounds 2002;330-330:907-910.

[61]. Klein H-P, Groll M. Development of a two-stage metal hydride system as topping cycle in cascading sorption systems for cold generation. Applied Thermal Engineering 2002;22:631-639.

[62]. Klein H-P. Betriebsverhalten einer zweistufigen Metallhydrid-Sorptionsanlage zur Kälteerzeugung: Universität Stuttgart. 2007. [German]

[63]. Linder M, Mertz R, Laurien E. Experimental results of a compact thermally driven cooling system based on metal hydrides. International Journal of Hydrogen Energy 2010;35:7623-7632.

[64]. Willers E, Groll M. The two-stage metal hydride heat transformer. International Journal of Hydrogen Energy 1999;24:269-276.

[65]. Willers E, Wanner M, Groll M. A Multi-hydride thermal wave device for simulations heating and cooling. Journa of Alloys and Compounds 1999;293-295:915-918.

[66]. Willers E, Groll M. Evaluation of metal hydride machines for heat pumping and cooling applications. International Journal of Refrigeration 1999;22:47-58.

[67]. Ni J, Liu H. Experimental research on refrigeration characteristics of a metal hydride heat pump in auto air-conditioning. International Journal of Hydrogen Energy 2007;32:2567-2572.

[68]. Qin F, Chen J, Lu M, Chen Z, Zhou Y, Yank K. Development of a metal hydride refrigeration system as an exhaust gas-driven automobile air conditioner. Renewable Energy 2007;32:2034-2052.

[69]. Deng S. Sorbent Technology. New York: S. Lee, Marcel Dekker; 2006.
[70]. Weber R, Dorer V. Long-term heat storage with NaOH. Vacuum 2008;82:708-716.
[71]. Hauer A, Lävemánn E. Thermal Energy Storage for Sustainable Energy Consumption - Open absorption systems for air conditioning and thermal energy storage. In: Proc NATO Advanced Study Institute on Thermal Energy Storage for Sustainable Energy Consumption - Fundamentals, Case Studies and Design Izmir, Turkey, 2007. pp 429-444.
[72]. Quinell J, Davidson JH, Burch J. Liquid Calcium Chloride Solar Heat Storage: Concept and Analysis. In: Proc Proceedings of the ASME 2010 4th International Conference on Energy Sustainability (ES2010) Phoenix, Arizona, USA, 2010.
[73]. Bales C, Nordlander S. 2005. TCA Evaluation. Lab Measurements, Modelling and System Simulations. Högskolan Dalarna, Borlänge, Sweden: SERC. Report nr ISRN DU-SERC—91—SE. (www.serc.se).
[74]. Hui L, Le Pierrès N, Lingai L. Seasonal storage of solar energy for house heating by different absorption couples. In: Proc 11th International Conference on Thermal Energy Storage - Effstock 2009 Stockholm, Sweden, 2009.
[75]. Le Pierrès N, Luo L, N'Tsoukpoe KE, Mangin D, Fan L, Marty P, Marvillet C, Paulus C, Lancereau P. Procédé de stokage intersaisonnier de chaleur solaire pour le chauffage du bâtiment par procédé à absorption LiBr-H2O. In: Proc Congrès SFT (Société Française de Thermique) Le Touquet, France, 2010. [French].
[76]. Hui L, N'Tsoukpoe KE, Le Pierrès N, Lingai L. Evaluation of seasonal storage system of solar energy for house heating using different absorption couples. Energy Conversion and Management 2011;52:2427-2436.
[77]. Zondag HA, van Essen VM, Bleijendaal LPJ, Kikkert BWJ, Bakker M. Application of MgCl2.6H2O for thermochemical seasonal solar heat storage. In: Proc Presented at 5th International Renewable Energy Storage Conference IRES 2010 Berlin, Germany, 2010.
[78]. Bertsch F, Mette B, Asenbeck S, Kerskes H, Müller-Steinhagen H. Low temperature chemical heat storage – an investigation of hydration reactions. In: Proc 11th International Conference on Thermal Energy Storage - Effstock 2009 Stockholm, Sweden, 2009.
[79]. Abhat A, Huy TQ. Heat and mass transfer considerations in a thermochemical energy storage system based on solid-gas reactions. Solar Energy 1983;32(2):93-98.
[80]. Balat M, Spinner B. Optimization of a chemical heat pump energetic density and power. Heat Recovery Systems & CHP 1993;13(3):277-285.
[81]. Mauran S, Prades P, L'Haridon F. Heat and mass transfer in consolidated reacting beds for thermochemical systems. Heat Recovery Systems & CHP 1993;13(4):315-319.
[82]. Hun Han J, Kung-Hong L. Gas permeability of expanded graphite-metallic salt composite. Applied Thermal Engineering 2001;21:453-463.
[83]. Visscher K, Veldhuis JBJ, Oonk HAJ, van Ekeren PJ, Blok JG. 2004. Compacte chemische Seizoenopslag Van Zonnewarmte. Energy Research Centre of the Netherlands (ECN). Report nr ECN-C-04-074. [Dutch].
[84]. van Essen VM, Zondag HA, Cot Gores J, Bleijendaal LPJ, Bakker M, Schuitema R, van Helden W, He Z, Rindt CCM. Characterization of MgSO4 Hydrate for Thermochemical Seasonal Heat Storage. Journal of Solar Energy Engineering, Transactions of the ASME 2009;131(3):0410141-0410147.
[85]. van Essen VM, Cot Gores J, Bleijendaal LPJ, Zondag HA, Schuitema R, Bakker M, van Helden WGJ. Characterization of salt hydrates for compact seasonal thermochemical storage. In: Proc Proceedings of the ASME 3rd International Conference on Energy Sustainability 2009 San Fransico, USA, 2009. pp 825-830.
[86]. Balasumbramanian G, Ghommem M, Hajj MR, Wong WP, Tomlin JA, Puri IK. Modeling of thermochemical energy storage by salt hydrates. International Journal of Heat and Mass Transfer 2010;53:5700-5706.

[87]. De Boer R, Haije WG, Veldhuis JBJ. Determination of structural, thermodynamic and phase properties in the Na2S-H2O system for application in a chemical heat pump. Thermochimica Acta 2003;395:3-19.
[88]. De Boer R, Haije WG, Veldhuis JBJ, Smeding SF. 2004. Solid-sorption cooling with integrated thermal storage: The SWEAT prototype. Energy Research Centre of the Netherlands (ECN). Report nr ECN-RX—04-080.
[89]. Ogura H, Haguro M, Shibata Y, Otsubo Y. Reaction Characteristics of CaSO4/CaSO4•1/2H2O Resversible reaction for Chemicals heat pump. Journal of Chemical Engineering of Japan 2007;13:1252-1256.
[90]. Yoshino H, Inaba H, Fujioka K, Hirata Y. Development of Multipurpose Chemical Heat Pump for Cold-heat Generation and Low Temperature Condensation using Hydration Reaction. Nippon Kikai Gakkai Netsu Kogaku Bumon Koenkai Koen Ronbunshu 2001:161-162. [Japanese]
[91]. Fujioka K, Yoshino H, Yamane Y, Hirata Y. Development of Multipurpose Chemical Heat Pump Using Hydration Reaction of CaCl2. Mechanism of Driving Reaction. Nippon Dennetsu Shinpojiumu Koen Ronbunshu 2002;39(3):837-838. [Japanese]
[92]. Goetz V, Elie F, Spinner B. Structure and performance of single effect solid/gas chemical heat pumps. Heat Recovery Systems & CHP 1993;13(1):79-96.
[93]. Chen L, Tan YK. Experimental research on adsorptive performance of metallic halides. Chem Eng 2001;29(5):7. [Chinese]
[94]. Lai H, Li C, Zheng D. Simulation of Dynamic Performance for CaCl2/CH3OH Chemical Heat Pump. Journal of Chemical Engineering of Chinese Universities 1993;02. [Chinese]
[95]. Trudel J, Hossatte S, Ternan M. Solid-gas equilibrium in chemical heat pumps: the NH3-CoCl2 system. Applied Thermal Engineering 1999;19:495-511.
[96]. Nevau P, Castaing J. Solid-Gas Chemical Heat Pumps: Fields of Application and Performance of the Internal Heat of Reaction Recovery Process. Heat Recovery Systems & CHP 1993;13(3):233-251.
[97]. Fadhel MI, Sopian K, Daud WRW. Performance analysis of solar-assisted chemical heat-pump dryer. Solar Energy 2010;84:1920-1928.
[98]. Rivera C, Pilatowsky I, Méndez E, Rivera W. Experimental study of a thermo-chemical refrigerator using barium chloride-ammonia reaction. International Journal of Hydrogen Energy 2007;32:3154-3158.
[99]. Wang L, Chen L, Wang HL, Liao DL. The adsorption refrigeration characteristics of alkaline-earth metal chlorides and its composite adsorbents. Renewable Energy 2009;34:1016-1023.
[100]. Sun L-G, Xu G-Z, He X. The Research Progress on Vapor-Solid Chemical Heat Pump of CaCl2/CH3OH System. Journal of Qiqihar University (Natural Science Edition) 2002;2. [Chinese]
[101]. Sun L-G, Deng YP, Zheng DX, Li CY. Chemical Kinetics of the Demethanolation Reaction of CaCl2/CH3OH. Journal of Yantai University (Natural Science and Engineering) 2002;03. [Chinese]
[102]. Lai H, Cao X, Zhu G. Progress on Vapor-Solid Chemical Heat Pump Technology. Chemical Industry and Engineering Progress 1998;05. [Chinese]
[103]. Zhang X, Kang H, Wang Z. Chemical Kinetics of the Methanolation Reaction of CaCl2/CH3OH. Journal of Beijing Institute of Technology 1994;03. [Chinese]
[104]. Song F, Du W-M, Wu Y-Z, Yan G. Adsorption Bed Characteristic and Dynamic Simulation of Adsorption Heat Pump Using CaCl2/CH3OH Working Pairs. Chinese association of Refrigeration 2005. [Chinese]
[105]. Wang K, Wu JY, Wang RZ, Wang LW. Effective thermal conductivity of expanded graphite-CaCl2 composite adsorbent for chemical adsorption chillers. Energy Conversion and Management 2006;47:1902-1912.
[106]. Han JH, Lee K-H, Kim H. Effective termal conductivity of graphite-metallic salt complex for Chemicals heat pumps. Journal of Thermophysics and Heat Transfer 1999;13:481-488.
[107]. Coste C, Crozat G, Mauran S; Societe Nationale Elf Aquitaine, assignee. 1986. Gaseous-Solid Reaction patent 4,595,774.

[108]. Mauran S, Lebrun M, Prades P, Moreau M, Spinner B, Drapier C; Societe Nationale Elf Aquitaine and Le Carbone Lorraine, assignee. 1994. Active composite and its use as reaction medium patent 5,283,219
[109]. Bou P, Moreau M, Prades P; Elf Aquitaine and Le Carbone Lorraine, assignee. 1999. Active composites with foliated structure and its use as reaction medium patent 5,861,207.
[110]. Olives R, Mauran S. A highly Conductive Porous Medium for Solid-Gas Reactions: Effect of the Dispersed Phase on the Thermal Tortuosity. Transport in Porous Media 2001;43:377-394.
[111]. Dellero T, Sarmeo D, Ph. T. A chemical heat pump using carbon fibers as additive. Part I: enhancement of thermal conduction. Applied Thermal Engineering 1999;19:991-1000.
[112]. Dellero T, Ph T. A chemical heat pump using carbon fibers as additive. Part II: study of constraint parameters. Applied Thermal Engineering 1999;19:1001-1011.
[113]. Oliveira RG, Wang RZ. A consolidated calcium chloride-expanded graphite compound for use in sorption refrigeration systems. Carbon 2007;45:390-396.
[114]. Oliveira RG, Wang RZ, Wang C. Evaluation of the cooling performance of a consolidated expanded graphite-calcium chloride reactive bed for chemisorption icemaker. International Journal of Refrigeration 2007;30:103-112.
[115]. Wank K, Wu YU, Wang RZ, Wang LW. Composite adsorbent of CaCl2 and expanded graphite for adsorption ice maker on fishing boats. International Journal of Refrigeration 2006;29:199-210.
[116]. Li SL, Wu JY, Xia ZZ, Wang RZ. Study on the adsorption performance of composite adsorbent of CaCl2 and expanded graphite with ammonia as adsorbate. Energy Conversion and Management 2009;50:1011-1017.
[117]. Li SL, Wu JY, Xia RZ, Wang RZ. Study on the adsorption isosteres of the composite adsorbent CaCl2 and expanded graphite. Energy Conversion and Management 2011;52:1501-1506.
[118]. Li TX, Wang RZ, Kiplagat JK, Wang LW. Performance study of a consolidated manganese chloride-expanded graphite compound for sorption deep-freezing processes. Applied Energy 2009;86:1201-1209.
[119]. Zhang P, Wang C, Wang R. Composite Reactive Block for Heat Transformer System and Improvement of System Performance. International Journal of Chemical Engineering of Japan 2007;40(13):1275-1280.
[120]. Wang LW, Wang RZ, Wu JY, Wang K. Compound adsorbent for adsorption ice maker on fishing boats. 2004;27:401-408.
[121]. Wang LW, Tamainot-Telto Z, Thorpe R, Critoph RE, Metcalf SJ, Wang RZ. Study of thermal conductivity, permeability, and adsorption performance of consolidated composite activated carbon adsorbent for refrigeration. 2010;36:2062-2066.
[122]. Han JH, Lee K-H. Gas permeability of expanded graphite-metallic salts composite. Applied Thermal Engineering 2001;21:453-463.
[123]. Han JH, Cho KW, Lee K-H, Kim H. Porous graphite matrix for chemical heat pumps. Carbon 1998;36(12):1801-1810.
[124]. Haije WG, Veldhuis JBJ, Smeding SF, Grisel RJH. Solid/vapour sorption heat transformer: Design and performance. Applied Thermal Engineering 2007;7:1371-1376.
[125]. Aidoun Z, Ternan M. Salt impregnated carbon fibres as the reactive medium in a chemical heat pump: the NH3-CoCl2 system. Applied Thermal Engineering 2002;22:1163-1174.
[126]. Zhong Y, Critoph RE, Thorpe RN, Tamainot-Telto Z. Dynamics of BaCl2-NH3 adsorption pair. Applied Thermal Engineering 2009;29:1180-1186.
[127]. Zhong Y, Critoph RE, Thorpe RN, Tamainot-Telto Z, Aristov YI. Isothermal sorption characteristics of the BaCl2-NH3 pair in a vermiculite host matrix. Applied Thermal Engineering 2007;27:2455-2462.
[128]. Sharonov VE, Veselovskaya JV, Aristov YI, Zhong Y, Critoph RE. New composite adsorbent of ammonia "BaCl2 in vermiculate" for adsorptive cooling. In: Proc HPC06 Newcastle, 2006.
[129]. Veselovskaya JV, Tokarev MM, Aristov YI. Novel ammonia sorbents "porous matrix modified by active salt" for adsorptive heat transformation: 1. Barium chloride in various matrices. Applied Thermal Engineering 2010;30:583-589.

[130]. Sharonov VE, Veselovskaya JV, Aristov YI. Ammonia sorption on composites "CaCl2 in inorganic host matrix": isosteres chart and its performance. International Journal of Low-Cabon Technology 2006;1(3):191-200.
[131]. Vasiliev LL, Mishkinis DA, Antukh AA, Vasiliev LL. Solar-Gas Solid Sorption Refrigerator. Adsorption 2001;7:149-161.
[132]. Hirata Y, Fujioka K, Fujiki S. Preparation of fine particles of calcium chloride with expanded graphite for enhancement of diving reaction for Chemicals heat pumps. Journal of Chemical Engineering of Japan 2003;37:827-832.
[133]. Fujioka K, Hatanaka K, Hirata Y. Composite reactants of calcium chloride combined with functional carbon materials for Chemicals heat pumps. Applied Thermal Engineering 2008;28:304-310.
[134]. Fujioka K, Hirata Y. Effects of thermal conductivity of a reactor bed on the reaction of CaCl2/CH3NH2 used for driving chemical heat pump. In: Proc 30th National Heat Transfer Symposium of Japan Yokohama, Japan, 1993. pp 139–141.
[135]. Fujioka K, Katsuhiro S, Kiyomichi O. Enhancement of Heat Transfer in Packed Bed Reactor for Gas-Solid Chemical Heat Pump by Using Graphite Composite Particles. Nippon Dennetsu Shinpojiumu Koen Ronbunshu 2003;40(1):261-261. [Japanese]
[136]. Lee HC, Park SH, Choi SH, Kim YS, Kim SH. Characteristics of non-uniform reaction blocks for chemical heat pump. Chemical Engineering Science 2005;60:1401-1409.
[137]. Zajaczkowski B, Królicki Z, Jeżowski A. New type of sorption composite for chemical heat pump and refrigeration systems. Applied Thermal Engineering 2010;30(11-12):1455–1460.
[138]. Chen H-J, Cui Q, Chen X-J, Tang Y, Yao H-Q. Preparation and water adsorption performance of attapulgite based calcium chloride composite adsorbents for cooling and air-conditioning applications. Gao Xiao Hua Xue Gong Cheng Xue Bao/Journal of Chemical Engineering of Chinese Universities 2009;23(2):290-296. [Chinese]
[139]. Chen H-J, Cui Q, Tang Y, Chen X-J, Yao H-Q. Attapulgite based LiCl composite adsorbents for cooling and air conditioning applications. Applied Thermal Engineering 2008;28(17-18):2187-2193.
[140]. Posern K, Chan K. Calorimetric studies of thermochemical heat storage materials based on mixtures of MgSO4 and MgCl2. Thermochimica Acta 2010;502:73-76.
[141]. Lépinasse E, Spinner B. Production de froid par couplage de réacteurs solide-gaz I: Analyse des performances de tels systèmes. Rev Int Froid 1994;17(5):309-322. [French]
[142]. Lépinasse E, Spinner. B. Production de froid par couplage de réacteurs solide-gaz II: Performance d'un pilote de 1 à 2 kW. Rev Int Froid 1994;17(5):323-328. [French]
[143]. Lépinasse E, Goetz V, Crozat G. Modelling and experimental investigation of a new type of thermochemical transformer based on the coupling of two solid-gas reactions. Chemical Engineering and Processing 1994;33:125-134.
[144]. Goetz V, Spinner B, Lepinasse E. A solid-gas thermochemical cooling system using BaCl2 and NiCl2. Energy 1997;22(1):49-58.
[145]. Lépinasse E, Marion M, Goetz V. Cooling storage with a resorption process. Application to a box temperature control. Applied Thermal Engineering 2001;21:1251-1263.
[146]. Llobet J, Goetz V. Production de froid par transformation thermochimique: expérimentation d'un nouveau système à double effet à contact. International Journal of Refrigeration 2000;23:312-329. [French]
[147]. Nevau P, Castaing J, Mazet N, Meyer P. Performances expérimentales de thermotransformateurs hautes températures et machines à froid à double effet à base d'ammoniacates. In: Proc Symposium Le froid à sorption solide Paris, France, 1992. pp 173-178. [French].
[148]. Wagner A. Systèmes thermochimiques à soprtion solid-gaz à multiples effets, gérés par caloducs: Université de Perpignan. 1996. [French]
[149]. Le Pierrès N, Stitou D, Mazet N. New deep-freezing process using renewable low-grade heat: From the conceptual design to experimental results. Energy 2007;32:600-608.

[150]. Le Pierrès N, Mazet N, Stitou D. Modelling and performance of a deep-freezing process using low-grade solar heat. Energy 2007;32:154-164.
[151]. Le Pierrès N, Mazet N, Stitou D. Experimental results of a solar powered cooling system at low temperature. International Journal of Refrigeration 2007;30:1050-1058.
[152]. Le Pierrès N, Stitou D, Mazet N. Design of a thermochemical process for deep freezing using solar low-grade heat. Chemical Engineering and Processing 2008;47:484-489.
[153]. Mazet N, Amouroux M, Spinner B. Analysis and Experimental Study of the Transformation of a Non-Isothermal Solid/Gas Reacting Medium. Chemical Engineering Communications 1991;99:155.
[154]. Mazet N, Amouroux N. Analysis of Heat Transfer in Non-Isothermal Solid-Gas Reacting Medium. Chemical Engineering Communications 1991;99:175.
[155]. Goetz V, Marty A. A model for Reversible Solid-Gas Reactions Submitted to Temperature and Pressure Constrains. Chemical Engineering Science 1992;47(17-18):4445-4454.
[156]. Nevau P, Castaing-Lasvignottes J. Development of numerical sizing tool for a solid-gas thermochemical transformer- I. Impact of the microscopic process on the dynamic behaviour of a solid-gas reactor. Applied Thermal Engineering 1997;17(6):501-518.
[157]. Castaing-Lasvignottes J, Nevau P. Development of numerical sizing tool for a solid-gas thermochemical transformer-II. Influence of external couplings on the dynamic behaviour of a solid-gas thermochemical transformer. Applied Thermal Engineering 1997;17(6):519-536.
[158]. Lu H-B, Mazet N, Spinner B. Modelling of gas-solid reaction-coupling of heat and mass transfer with chemical reaction. Chemical Engineering Science 1996;51(15):3829-3845.
[159]. Lu HB, Mazet N. Mass-Transfer Parameters in Gas-Solid Reactive Media to Identify Permeability of IMPEX. AIChE Journal 1999;45(11):2444-2453.
[160]. Stitou D, Goetz V, Spinner B. A new analytical model for solid-gas thermochemical reactors based on thermophysical properties of the reactive medium. Chemical Engineering and Processing 1997;36:29-43.
[161]. Goetz V, Llobet J. Testing and modelling of a temperature front solid-gas reactor applied to thermochemical transformer. Applied Thermal Engineering 2000;20:155-177.
[162]. Lebrun M, Spinner B. Simulation for the Development of Solid-Gas Chemical Heat Pump Pilot Plants Part I. Simulation and Dimensioning. Chemical Engineering and Processing 1990;28:55-66.
[163]. Lebrun M. Simulation for the Development of Solid-Gas Chemical Heat Pump Pilot Plants Part II. Simulation and Optimization of Discontinuous and Pseudo-continuous Operating Cycles. Chemical Engineering and Processing 1990;28:67-77.
[164]. Stitou D, Mazet N, Bonnissel M. Performance of a high temperature hydrate solid/gas sorption heat pump used as topping cycle for cascaded sorption chillers. Energy 2004;29:267-285.
[165]. Lahmidi H, Mauran S, Goetz V. Definition, tests and simulation of a thermochemical storage process adapted to solar thermal system. Solar Energy 2009;80:883-893.
[166]. Mauran S, Lahmidi H, Goetz V. Solar heating and cooling by a thermochemical process. First experiments of a prototype storing 60 kWh by a solid/gas reaction. Solar Energy 2008;82:623-636.
[167]. Dutour S, Mazet N, Joly JL, Platel V. Modeling of heat and mass transfer coupling with gas-solid reaction in a sorption heat pump cooled by a two-phase closed thermosyphon. Chemical Engineering Science 2005;60:4093-4104.
[168]. Huang H-J, Wu G-B, Yang J, Dai Y-C, Yuan W-K, Lu H-B. Modeling of solid-gas chemisorption in chemical heat pumps. Separation and Purification Technology 2004;34:191-200.
[169]. Li TX, Wang RZ, Oliveira RG, Kiplagat JK, Wang LW. A combined double-way chemisorption refrigeration cycle based on adsorption and resorption processes. International Journal of Refrigeration 2009;32:47-57.
[170]. Li TX, Wang RZ, Kiplagat JK, Wang LW, Oliveira RG. Thermodynamic study of a combined double-way solid-gas thermochemical sorption refrigeration cycle. International Journal of Refrigeration 2009;32:1570-1578.

[171]. Li TX, Wang RZ, Chen H, Wang LW, Kiplagat JK. Performance Improvement of a Combined Double-Way Thermochemical Sorption Refrigeration Cycle with Reheating Process. AIChE Journal 2010;56(2):477-484.
[172]. Li TX, Wang RZ, Oliveira RG, Wang LW. Performance Analysis of an Innovative Multimode, Multisalt and Multieffect Chemisorption Refrigeration System. AIChE Journal 2007;53(12):3222-3230.
[173]. Bao HS, Oliveira RG, Wang RZ, Wang LW. Choice of Low Temperature Salt for a Resorption Refrigerator. Industrial & Engineering Chemistry Research 2010;49:4897-4903.
[174]. Bao HS, Wang RZ, Wang LW. A resorption refrigerator driven by low grade thermal energy. Energy Conversion and Management 2011;52:2339-2344.
[175]. Xu J, Oliveira RG, Wang RZ. Resorption system with simultaneous heat and cold production. International Journal of Refrigeration 2011;34:1262 – 1267.
[176]. Oliveira RG, Wang RZ, Kliplagat JK, Wang CY. Novel composite sorbent for resorption systems and for chemisorption air conditioners driven by low generation temperature. Renewable Energy 2009;34:2757-2764.
[177]. Wang C, Zhang P, Wang RZ. Investigation of Solid-Gas Reaction Heat Transformer System with the Consideration of Multistep Reactions. AIChE Journal 2008;54(9):2464-2478.
[178]. Wang C, Zhang P, Wang RZ. Performance of solid-gas reaction heat transformer system with gas valve control. Chemical Engineering Science 2010;65:2910-2920.
[179]. Li SL, Xia ZZ, Wu JY, Li J, Wang RZ, Wang LW. Experimental study of a novel $CaCl_2$/expanded graphite-NH_3 adsorption refrigerator. International Journal of Refrigeration 2010;33:61-69.
[180]. Xia ZZ, Li SL, Wu JY, Li J, Wang RZ. Experiment investigation of a novel adsorption deep freezing system using a new type of composite adsorbent. In: Proc International Sorption Heat Pump Conference Hoam Convention Center, Seoul National University, 2008.
[181]. Kiplagat JK, Wang RZ, Oliveira RG, Li TX. Lithium chloride – Expanded graphite composite sorbent for solar powered ice maker. Solar Energy 2010;84:1587-1594.
[182]. Chen H, Wu J-Y, Li TX, Wang RZ. Strontium chloride-expanded graphite consolidated composite adsorbent used in ice-making systems. Kung Cheng Je Wu Li Hsueh Pao/Journal of Engineering Thermophysics 2010;31(4):561-564. [Chinese]
[183]. Chen H, Li T, Wang L, Wang R, Oliveira RG. Sorption performance of consolidated composite sorbent used in solar-powered sorption air-conditioning system. Huagong Xuebao/CIESC Journal 2009;60(5):1097-1103. [Chinese]
[184]. Wang LW, Wang RZ, Wu JY, Wang K, Wang SG. Adsorption ice makers for fishing boats driven by the exhaust heat from diesel engine: choice of adsorption pair. Energy Conversion and Management 2004;45:2043-2057.
[185]. Wang LW, Wang RZ, Lu ZS, Xu YX, WU JY. Split heat pipe type compound adsorption ice making test unit for fishing boats. International Journal of Refrigeration 2006;29:456-468.
[186]. Lu ZS, Wang RZ, Li TX, Wang LW, Chen CJ. Experimental investigation of a novel multifunction heat pipe solid sorption icemaker for fishing boats using CaCl2/activated carbon compound-ammonia. International Journal of Refrigeration 2007;30:76-85.
[187]. Lu ZS, Wang RZ, Wang LW, Chen CJ. Performance analysis of an adsorption refrigerator using activated carbon in a compound adsorbent. Carbon 2006;44:747-752.
[188]. Li TX, Wang RZ, Wang LW, Lu ZS, Chen CJ. Performance study of a high efficient multifunction heat pipe type adsorption ice making system with novel mass and heat recovery processes. International Journal of Journal of Thermal Sciences 2007;46:1267-1274.
[189]. Li TX, Wang RZ, Wang LW, Lu ZS. Experimental investigation of an innovative dual-mode chemisorption refrigeration system based on multifunction heat pipes. International Journal of Refrigeration 2008;31:1104-1112.
[190]. Han JH, Lee K-H, D.H. K, Kim H. Transformation Analysis of Thermochemical Reactor base don Thermophysical Properties of Graphite-MnCl2 Complex. Industrial & Engineering Chemistry Research 2000;39:4127-4139.

[191]. Spoelstra S, Haije WG, Dijkstra JW. Techno-economic feasibility of high-temperature high-lift chemical heat pumps for upgrading industrial waste heat. Applied Thermal Engineering 2002;22:1619-1630.
[192]. van der Paal M, de Boer R, Veldhuis JBJ, Smeding SF. 2009. Thermally driven ammonia-salt type II heat pump: development and test of a prototype. Energy Research Centre of the Netherlands (ECN). Report nr ECN-M—09-059
[193]. van der Paal M, de Boer R, Veldhuis JBJ, Smeding SF. 2011. Experimental setup for determining ammonia-salt adsorption and desorption behaviour under typical heat pump conditions: a description of the setup and experimental results. Energy Research Centre of the Netherlands (ECN). Report nr ECN-M—11-030
[194]. Cerkvenik B, Stitou D, Storkenmaier F, Ziegler F. Measurement results for the novel NH3-NiCl2(NH3)2/6 reaction cooling device. In: Proc 2nd International Heat Powered Cycles Conference Paris, France, 2001.
[195]. Aidoun Z, Ternan M. Pseudo-stable transitions and instability in chemical heat pumps: the NH3-CoCl2 system. Applied Thermal Engineering 2001;21:1019-1034.
[196]. Aidoun Z, Ternan M. The synthesis reaction in a chemical heat pump reactor filled with chloride impregnated carbon fibres: the NH3-CoCl2 system. Applied Thermal Engineering 2002;22:1943-1954.
[197]. Aidoun Z, Ternan M. The unsteady state overall heat transfer coefficient in a chemical heat pump reactor: the NH3-CoCl2 system. Chemical Engineering Science 2004;59:4023-4031.
[198]. Mbaye M, Aidoun Z, Valkov V, Legault A. Analysis of chemical heat pumps (CHPS): Basic concepts and numerical model description. Applied Thermal Engineering 1998;18(3-4):131-141.
[199]. Vasiliev LL, Kanonchik LE, Antuh AA, Kulakov AG. NaX Zeolite, Carbon Fibre and CaCl2 Ammonia Reactors for Heat Pumps and Refrigerators. Adsorption 1996;2:311-316
[200]. Vasiliev LL, Mishkinis DA, Antukh AA, Vasiliev LL. Solar-gas solid sorption heat pump. Applied Thermal Engineering 2001;21:573-583.
[201]. Vasiliev LL, Mishkinis DA, Antukh AA, Vasiliev LL. Resorption heat pump. Applied Thermal Engineering 2004;24:1893-1903.
[202]. Vasiliev LL, Filatova OS, Tsitovich AP. Application of sorption heat pumps for increasing of new power sources efficiency. Archive of Thermodynamics 2010;31(2):21-24.
[203]. Aristov IY, Vasiliev LL. New composite sorbents of water and ammonia for chemical and adsorption heat pump. Journal of Engineering Physics and Thermophysics 2006;79(6):1214-1223.
[204]. Veselovskaya JV, Critoph RE, Thorpe RN, Metcalf S, Tokarev MM, Aristov YI. Novel ammonia sorbents "porous matrix modified by active salt" for adsorptive heat transformation: 3. Testing of "BaCl2/vermiculite" composite in a lab-scale adsorption chillers. Applied Thermal Engineering 2010;30:1188-1192.
[205]. Veselovskaya JV, Tokarev MM. Novel ammonia sorbents "porous matrix modified by active salt" for adsorptive heat transformation: 4. Dynamics of quasi-isobaric ammonia sorption and desorption on BaCl2/vermiculite. Applied Thermal Engineering 2011;31:566-572.
[206]. Hongois S, Kuznik F, Stevens P, Roux J-J. Development and characterization of a new MgSO4-zeolite composite for long-term thermal energy storage. Solar Energy Materials & Solar Cells 2011;95:1831-1837
[207]. Vannoni C, Battisti R, Drigo S. 2008. Potential for solar heat in industrial processes. IEA SHC Task 33 and SolarPACES Task IV: Solar Heat for Industrial Processes.: IEA Solar heating % cooling. (www.iea-shc.org).
[208]. Ervin G. Solar Heat Storage Using Chemical Reactions. Journal of solid state chemistry 1977;22:51-61.
[209]. Kanzawa A, Arai Y. Thermal energy storage by the chemical reaction. Augmentation of the heat transfer and thermal decomposition in the CaO/Ca(OH)2 powder. Solar Energy 1981;27(4):289-294.

[210]. Baker R. The reversibility of the reaction CaCO3 <=> CaO + CO2,. Journal of Applied Chemistry and Biotechnology 1973;23(10):733-742.
[211]. Kato Y, Yamashita N, Kobayashi K, Yoshizawa Y. Kinetic study of the hydration of magnesium oxide for a chemical heat pump. Applied Thermal Engineering 1996;16:853-862.
[212]. Kato Y, Takahashi F, Watanabe A, Yoshizawa Y. Thermal analysis of a magnesium oxide/water chemical heat pump for cogeneration. Applied Thermal Engineering 2001;21:1067-1081.
[213]. Kato Y, Takahashi F, Watanabe A, Yoshizawa Y. Thermal performance of a packed bed reactor of a chemical heat pump for cogeneration. Trans IChemE 2000;78:Part A.
[214]. Kato Y, Yoshizawa Y. Application of a Chemicals heat pump to a cogeneration system. International Journal of Energy Research 2001;25:129-140.
[215]. Kato Y, Minakami A, Li G, Yoshizawa Y. Operability of a Thermally Driven Magnesium Oxide/Water Chemical Heat Pump. The Canadian Journal of Chemical Engineering 2001;79(536-541).
[216]. Kato Y, Sasaki Y, Yoshizawa Y. Magnesium oxide/water Chemicals heat pump to enhance energy utilization of a cogeneration system. Energy 2005;30:2144-2155.
[217]. Kato Y, Kobayashi K, Yoshizawa Y. Durability to repetitive reaction of magnesium oxide/water reaction system for a heat pump. Applied Thermal Engineering 1998;18:85-92.
[218]. Kato Y, Nakahata J, Yoshizawa Y. Durability characteristics of the hydration of magnesium oxide under repetitive reaction. Journal of Material Sciences 1999;34:475-480.
[219]. Kato Y, Saito T, Soga T, Ryu J, Yoshizawa Y. Durable Reaction Material Development for Magnesium Oxide/Water Chemical Heat Pump. Journal of Chemical Engineering of Japan 2007;40:1264-1269.
[220]. Kato Y, Takahashi R, Sekiguchi T, Ryu J. Study on medium-temperature chemical heat storage using mixed hydroxides. International Journal of Refrigeration 2009;32:661-666.
[221]. Kato Y. Development of a Magnesium Oxide/Water Chemical Heat Pump for Efficient Energy Storage and Utilization. In: Proc 5th Minsk International Seminar "Heat Pipes, heat pumps, refrigerators" Minsk, Belarus, 2003. pp 129-140.
[222]. Kato Y. Packed bed reactor demonstration of magnesium oxide/water chemical heat pump. In: Proc Proc 11th International Conference on Thermal Energy Storage - Effstock 2009 Stockholm, Sweden, 2009.
[223]. Ryu J, Takahashi R, Hirao N, Kato Y. Effect of metal mixing on reactivities of Magnesium Oxide for chemical heat pump. Journal of Chemical Engineering of Japan 2003;40:1281-1286.
[224]. Kim ST, Ryu J, Kato Y. Reactivity enhancement of chemical materials used in packed bed reactor of chemical heat pump. Progress in Nuclear Energy 2011;article in press:1-7.
[225]. Kato Y, Saku D, Harada N, Yoshizawa Y. Utilization of high temperature heat from nuclear reactor using inorganic Chemicals heat pump. Progress in Nuclear Energy 1998;32:563-570.
[226]. Kato Y, Harada N, Yoshizawa Y. Kinetic feasibility of a Chemicals heat pump for heat utilization of high-temperature processes. Applied Thermal Engineering 1999;19:239-254.
[227]. Kato Y, Yamada M, Kanie T, Yoshizawa Y. Calcium oxide/carbon dioxide reactivity in a packed bed reactor of a Chemicals heat pump for high-temperature gas reactors. Nuclear Engineering and Design 2001;210:Nuclear Engineering and Design.
[228]. Kato Y, O-shima T, Yoshizawa Y. Thermal performance of a packed bed reactor for a high-temperature Chemicals heat pump. International Journal of Energy Research 2001;25:577-589.
[229]. Ogura H, Miyazaki M, Matsuda H, Hasatani M, Yanadori M, Hiramatsu M. Experimental study on heat transfer enhancement of the solid reactant particle bed in a chemical heat pump using Ca(OH)2/CaO reaction. Kagaku Kogaku Ronbunshu 1991;17(5):916-923. [Japanese]
[230]. Ogura H, Nagura A, Matsuda H, Hasatani M, Yanadori M, Hiramatsu M. Studies on heat transfer augmentation in Chemicals heat pump composed of CaO/Ca(OH)2 reversible reaction and evaporation/condensation of water. In: Proc Proceedings of the International Conference on the Analysis of Thermal and Energy Systems Athens, Greece, 1991. pp 665-676.

[231]. Ogura H, Miyazaki M, Matsuda H, Hasatani M, Yanadori M, Hiramatsu M. Numerial análisis of heat transfer in particle-bed reactor with fins in Chemicals heat pump using Ca(OH)2/CaO reaction. Kagaku Kogaku Ronbunshu 1992;18(5):669-676. [Japanese]

[232]. Ogura H, Nagura A, Matsuda H, Hasatani M, Yanadori M, Hiramatsu M. Studies on improving the efficiency of chemical heat pump using CaO/Ca(OH)2 reversible reaction. In: Proc Proceedings of the 4th World Congress of Chemical Engineering Karlsruhe, Germany, 1991. pp 4.1-4.18.

[233]. Ogura H, Kanamori M, Matsuda H, Hasatani M, Yanadori M, Hiramatsu M. Heat storage characteristics of Chemicals heat pump using Ca(OH)2/CaO reversible reaction. Kagaku Kogaku Ronbunshu 1993;19(3):553-557. [Japanese]

[234]. Ogura H, Kanamori M, Matsuda H, Hasatani M. Generation of low-temperature heat by Chemicals heat pump using CaO/H2O/Ca(OH)2 reaction system. In: Proc Proceedings of the 1st International Thermal Energy Congress Marrakesh, Morocco, 1993.

[235]. Ogura H, Kanamori M, Matsuda H, Hasatani M. Generation of low-temperature heat by use of CaO/H2O/Ca(OH)2 reaction. Kagaku Kogaku Ronbunshu 1993;19(6):941-946. [Japanese]

[236]. Ogura H, Sato S, Iwato I, Kage H, Matsuno Y. Mass transfer augmentation in low-temperature-heat generation by Chemicals heat pump unit using CaO/Ca(OH)2 reaction. In: Proc Proceedings of the International Conference on Fluid and Thermal Energy Conversion Bali, Indonesia, 1994. pp 425-430.

[237]. Ogura H, Sato S, Fujimoto S, Kage H, Matsuno Y. Design and testing of a Chemicals heat pump unit using CaO/Ca(OH)2 reaction for heat storing and high/low-temperature-heat-generating. In: Proc 2nd Interntional Conference on New Energy Systems and Conversions Istanbul, Turkey, 1995. pp 187-194.

[238]. Ogura H, Fujimoto SH, Sato S, Kage H, Matsuno Y. Low-temperature heat-generation by Chemicals heat pump using CaO/H2O/Ca(OH)2 reversible reaction-effect of reactor design and heat-exchange condition. Kagaku Kogaku Ronbunshu 1997;23(3):397-403. [Japanese]

[239]. Ogura H, Fujimoto S, Iwamoto H, Kage H, Matsuno Y, Kanamaru Y, Kitahara T, Awaya S. Basic performance of CaO/H2O/Ca(OH)2 chemical heat pump unit for electric heat storage and medium/low-temperature heat-generation. In: Proc 7th International Conference on Thermal Energy Storage - MEGASTOCK Sapporo, Japan, 1997. pp 895-900.

[240]. Ogura H, Fujimoto S, Iwamoto H, Kage H, Matsuno Y, Kanamaru Y, Awaya S. Basic performance of CaO/H2O/Ca(OH)2 chemical heat pump unit for night-electric heat storage and cold/hot heat-recovering. Kagaku Kogaku Ronbunshu 1998;24(6):856-861. [Japanese]

[241]. Ogura H, Mujumdar AS. Proposal for a novel chemical heat pump dryer. Drying Technology 2000;18(4-5):1033-1053.

[242]. Ogura H, Yamamoto T, Kage H, Matsuno Y, Mujumdar AS. Effects of heat exchange condition on hot air production by a Chemicals heat pump dryer using CaO/H2O/Ca(OH)2 reaction. Chemical Engineering Journal 2002;86(1-2):3-10.

[243]. Ogura H, Yamamoto T, Kage H. Efficiencies of CaO/H2O/Ca(OH)2 chemical heat pump for heat storing and heating/cooling. Energy 2003;28:1479-1493.

[244]. Ogura H, Yamamoto T, Otsubo Y, Ishida H, Kage H, Mujumdar AS. Controllability of a Chemicals heat pump dryer. In: Proc Drying 2004 - 14th International Drying Symposium São Paulo, Brazil, 2004. pp 998-1004.

[245]. Ogura H, Yasuda S, Otsubo Y, Mujumdar AS. Continuous operation of a Chemicals heat pump. Asia-Pacific Journal of Chemical Engineering 2007;2:118-123.

[246]. Ogura H, Abliz S, Kage H. Studies on applicability of scallop material to calcium oxide/calcium hydroxide chemical heat pump. Fuel Processing Technology 2004;85:1259-1269.

[247]. Fujimoto S, Bilgen E, Ogura H. Dynamic simulation of CaO/Ca(OH)2 chemical heat pump Systems. International Journal of Exergy 2002;2:6-14.

[248]. Fujimoto S, Bilgen E, Ogura H. CaO/Ca(OH)2 chemical heat pump system. Energy Conversion and Management 2002;43:947-960.

[249]. Schaube F, Wörner A, Müller-Steinhagen H. High temperature heat storage using gas-solid reactions. In: Proc 11th International Conference on Thermal Energy Storage - Effstock 2009 Stockholm, Sweden, 2009.
[250]. Lin S, Haraka M. CaO Hydration Rate at High Temperature (1023 K). Energy & Fuels 2006;20:903-908.
[251]. Lin S, Wang Y, Susuki Y. High-Temperature CaO Hydration/Ca(OH)2 Decomposition Over Multitude of Cycles. Energy & Fuels 2009;23:2855-2861.
[252]. Darkwa K. Green transport technology. In: Proc 29th International Symposium on Automotive Technology and Automation (ISATA) Florence, Italy, 1996.
[253]. Darkwa K. Experimental studies of a thermochemical store for automobile engines. Journal of Automobile Engineering 1997;211(5):347-360.
[254]. Cerkvenik B, Storkenmaier F, Kato Y. Use of CaO/H2O reversible reaction for cooling. In: Proc 2nd Workshop & Expert meeting, Annex 17 Ljubljana, Slovenia, 2002.
[255]. Cerkvenik B, Satzger P, Ziegler F, Poredos A. High Efficient Cycles using CaO/H2O and LiBr/H2O for Gass Cooling. In: Proc 6th ASME Conference on Renewable and Advanced Energy Systems for the 21th century Maui, Hawaii 1999.
[256]. Cerkvenik B, Poredos A, Ziegler F. Improvement of Topping Cycle Efficiency with Increase in Evaporation Pressure Level. Journal of Mechanical Engineering 2000;46:671-682
[257]. Fuji I, Ishino M, Akiyama S, Murthy MS, Rajanandam KS. Behaviour of Ca(OH)2/CaO Pellet under Dehydration and Hydration. Solar Energy 1994;53:329-341
[258]. Kubota M, Kyaw K, Watanabe F, Matsuda H, Hasatani M. Reaction characteristics of BaO/BaCO3 system for high temperature Chemicals heat pump above 1273 K. Journal of Chemical Engineering of Japan 2001;34(3):326-332.
[259]. Prevost M, Bugarel R. Theoretical and technical aspects of a chemical heat pump: Secondary alcohol-ketone-hydrogen system. In: Proc 2nd World Congress of Chemical Engineering Montreal, Quebec, Canada, 1981. pp 585-590.
[260]. Kato Y, Kameyama H. Study of Catalyst-Assisted Chemical Heat Pump with Reaction Couple of Acetone Hydrogenation and 2-Propanol Dehydrogenation. In: Proc of World Congress III of Chemical Engineering Tokyo, Japan, 1986. pp 676-679.
[261]. Saito Y, Yamashita M, Ito E, Meng N. Hydrogen production from 2-propanol as a key reaction for a Chemicals heat pump with reaction couple of 2-propanol dehydrogenation/acetone hydrogenation. International Journal of Hydrogen Energy 1994;19:223-226.
[262]. KlinSoda I, Piumsomboon P. Isopropanol-acetone-hydrogen chemical heat pump: A demonstration unit. Energy Conversion and Management 2007;48:1200-1207.
[263]. Tanisho S, Fahim MA, Wakao N. Heat transport cycle with methyl alcohol-acetaldehyde chemical reaction. International Journal of Energy Research 1985;9:449-453.
[264]. Fahim MA, Al-Sahhaf TA, Hamam SE. Energy storage using the reaction cycle: Methyl alcohol/acetaldehyde. International Journal of Energy Research 1989;13:289-296.
[265]. Kato Y. Kinetic measurement on the isobutene/water/tert-butanol chemical heat pump; dehydration of tert-butanol. International Journal of Energy Research 1996;20:681-692.
[266]. Kawasaki H, Watanabe T, Kanzawa A. Proposal of a chemical heat pump with paraldehyde depolymerization for cooling system. Applied Thermal Engineering 1999;19:133-143.
[267]. Brennan D. Process Industry Economics: An International Perspective: IChemE; 1998.
[268]. Ma Q, Luo L, Wang RZ, Sauce G. A review on transportation of heat energy over long distance: Exploratory development. Renewable and Sustainable Energy Reviews 2009;13:1532-1540.
[269]. Azpiazu MN, Morquillas JM, Vazquez A. Heat recovery from a thermal energy storage based on the Ca(OH)2/CaO cycle. Applied Thermal Engineering 2003;23:733-741.
[270]. Curran GP, Fink CE, Corin E. CO2 Acceptor Gasification Process. In: Proc 8th Synthetic Pipeline Gas Symposium Chicago, USA, 1976.
[271]. Depta G. Messaparatur fuer Gas-Feststoff-Reaktionen in Waermepumpen. Munich: Technische Universität München. 1994.

[272]. Hartman M, Trnka O, Svoboda K, Kocurek J. Decomposition kinetics of alkaline-earth hydroxides and surface area of their calcines. Chemical Engineering Science 1994;49:1209-1216.
[273]. van der Paal M, Veldhuis JBJ. 2010. Thermodynamic properties of lithium chloride ammonia complexes under heat pump type II working conditions. Energy Research Centre of the Netherlands (ECN). Report nr ECN-M—10-076
[274]. Wang RZ. Performance improvement of adsorption cooling by heat and mass recovery operation. International Journal of Refrigeration 2001;24:602-611.
[275]. Wang W, Qu TF, Wang RZ. Influence of degree of mass recovery and heat regeneration on adsorption refrigeration cycles. Energy Conversion and Management 2002;43:733-741.
[276]. Moroto M, Hiro N, Akashi K, Nasaki K, Yonesaki T, Osumi M. The development of a refrigeration system using hydrogen absorbing alloys. Second ASME-JSES-JSME International Solar Energy Conference. Reno, NV, USA: Solar Engineering ASME; 1991. p 103-108.
[277]. Dantzer P, Meunier F. What materials to use in hydride chemical heat pumps? Materials of Science Forum 1988;31:1-18.

Appendix A. Solid-gas equilibriums of the chlorides salts with ammonia

Reaction	ΔHr (kJ·mol^{-1})	ΔS (J·mol^{-1}·k^{-1})	Cp (J·mol^{-1}·K^{-1})
$BaCl_2 + 8NH_3 \Leftrightarrow BaCl_2 \cdot 8NH_3$	37.665	227.25	75.1
$MnCl_2 \cdot 2NH_3 + 4NH_3 \Leftrightarrow MnCl_2 \cdot 6NH_3$	47.416	228.07	72.86
$NiCl_2 \cdot 2NH_3 + 4NH_3 \Leftrightarrow NiCl_2 \cdot 6NH_3$	59.217	227.75	71.6
$PbCl_2 \cdot 3.25NH_3 + 4.75NH_3 \Leftrightarrow PbCl_2 \cdot 8NH_3$	34.317	223.76	70.05
$MgCl_2 \cdot 2NH_3 + 4NH_3 \Leftrightarrow MgCl_2 \cdot 6NH_3$	55.66	230.63	71.31
$LiCl_2 \cdot NH_3 + 2NH_3 \Rightarrow LiCl_2 \cdot 3NH_3$	43.681(*)	132.62(*)	-
$LiCl_2 \cdot NH_3 + 2NH_3 \Leftarrow LiCl_2 \cdot 3NH_3$	49.098(*)	146.58(*)	-
$LiCl_2 \cdot 3NH_3 + NH_3 \Rightarrow LiCl_2 \cdot 4NH_3$	30.431(*)	109.44(*)	-
$LiCl_2 \cdot 3NH_3 + NH_3 \Leftarrow LiCl_2 \cdot 4NH_3$	36.792(*)	126.59(*)	-
$CaCl_2 \cdot 2NH_3 + 2NH_3 \Leftrightarrow CaCl_2 \cdot 4NH_3$	42.268	229.92	72.52
$CaCl_2 \cdot 4NH_3 + 4NH_3 \Leftrightarrow CaCl_2 \cdot 8NH_3$	41.013	230.3	72.52
$SrCl_2 \cdot NH_3 + 7NH_3 \Leftrightarrow SrCl_2 \cdot 8NH_3$	41.431	228.8	75.53
$CoCl_2 \cdot 2NH_3 + 4NH_3 \Leftrightarrow CoCl_2 \cdot 6NH_3$	53.986	228.1	78.41
$NH_4Cl + 3NH_3 \Rightarrow NH_4Cl \cdot 3NH_3$	26.69(**)	198.46(**)	-
$NH_4Cl + 3NH_3 \Leftarrow NH_4Cl \cdot 3NH_3$	28.98(**)	204.20(**)	-
$NaBr + 5.25NH_3 \Leftrightarrow NaBr \cdot 5.25NH_3$	30.5	-	-

P. Nevau and J. Castaing, Solid-gas chemical heat pumps: field of application and performance of the internal heat of reaction recovery process. Heat Recovery Systems & CHP 13 (1993) 3, 233-251

(*) E.R.T. Bevers, P. J. Van Ekeren, W. G. Haije and H. A. J. Oonk, Thermodynamic properties of lithium chloride ammonia complexes for application in a high-lift high temperature chemical heat pump. Journal of Thermal Analysis and Calorimetry, 86 (2006) 3, 825-832

(**) Bao, H.S., Wang, R.Z., Wang, L.W. A resorption refrigerator driven by low grade thermal energy, Energy Conversion and Management, 52 (2011) 2339-2344